Bianca Leopoldo Gonçalves

Licenciada em Bioquímica

Porous Structures for the Purification of Biopharmaceuticals

Dissertação para obtenção do Grau de Mestre em
Biotecnologia

Orientador: Prof.ª Doutora Ana Cecília Afonso Roque,
Secção de Engenharia Química e Bioquímica, Faculdade
de Ciência e Tecnologias (FCT) da Universidade Nova
de Lisboa (UNL)
Co-orientador: Prof.ª Doutora Ana Isabel Nobre Martins
Aguiar de Oliveira Ricardo, Secção de Engenharia
Química e Bioquímica, Faculdade de Ciência e
Tecnologias (FCT) da Universidade Nova de Lisboa
(UNL)

Júri:

Presidente: Prof. Doutor Carlos Alberto Gomes Salgueiro
Arguente: Doutora Ana Margarida Nunes da Mata Pires de Azevedo

FACULDADE DE
CIÊNCIAS E TECNOLOGIA
UNIVERSIDADE NOVA DE LISBOA

Janeiro 2014

Bianca Leopoldo Gonçalves

Licenciada em Bioquímica

Porous Structures for the Purification of Biopharmaceuticals

Dissertação para obtenção do Grau de Mestre em
Biotecnologia

Orientador: Prof.ª Doutora Ana Cecília Afonso Roque,
Secção de Engenharia Química e Bioquímica, Faculdade
de Ciência e Tecnologias (FCT) da Universidade Nova
de Lisboa (UNL)
Co-orientador: Prof.ª Doutora Ana Isabel Nobre Martins
Aguiar de Oliveira Ricardo, Secção de Engenharia
Química e Bioquímica, Faculdade de Ciência e
Tecnologias (FCT) da Universidade Nova de Lisboa
(UNL)

Júri:

Presidente: Prof. Doutor Carlos Alberto Gomes Salgueiro
Arguente: Doutora Ana Margarida Nunes da Mata Pires de Azevedo

FACULDADE DE
CIÊNCIAS E TECNOLOGIA
UNIVERSIDADE NOVA DE LISBOA

Janeiro 2014

Smart Macroporous Structures for the Purification of Biopharmaceuticals

“Copyright”
Bianca Leopoldo Gonçalves
Faculdade de Ciências e Tecnologia
Universidade Nova de Lisboa

A Faculdade de Ciências e Tecnologia e a Universidade Nova de Lisboa têm o direito, perpétuo e sem limites geográficos, de arquivar e publicar esta dissertação através de exemplares impressos reproduzidos em papel ou de forma digital, ou por qualquer outro meio conhecido ou que venha a ser inventado, e de a divulgar através de repositórios científicos e de admitir a sua cópia e distribuição com objectivos educacionais ou de investigação, não comerciais, desde que seja dado crédito ao autor e editor.

Acknowledgments

This past year has been a real challenge to me. I had the amazing opportunity to work in totally different areas: materials engineering and virology; and so, expand my knowledge and open my scientific horizons. I feel I am stronger, more autonomous, more confident, more knowledgeable. I feel I have grown a lot, and not only as a professional but also as a person. But one thing is for sure, I could not have done it without all the support and encouragement of countless people that I will never forget.

First and foremost I would like to thank my advisors Prof. Ana Cecília Roque and Prof. Ana Aguiar Ricardo, for the opportunity to work with them, in this project and in their labs. It meant a lot, and it was a real honour. Thank you for all the help and thoughtful input that allowed the development of this work, despite the misfortunes faced. Dear Prof. Cecília Roque I want to thank you for all your support, guidance, patience, understanding, exigency, positive mind, constructive criticism, and mostly for your trust and help on making me a more mature person at professional level. Dear Prof. Ana Aguiar Ricardo, I am very thankful for your enlightening and pertinent suggestions that gave me the motivation and guidance to improve this work, and also for your support and exigency. For all stated reasons, I do not have enough words to express my gratefulness.

Then I would like to specially acknowledge Dr. Telma Barroso and Dr. Ana Pina for their fundamental help in the fulfilment of this important stage of my academic and personal life. Dr. Telma thanks for the encouragement, advices, pertinent suggestions, the teachings about materials science, and exigency that contributed for the more confident and autonomous person I have become. Of course I will always remember the awesome periods of unstoppable laughing and relaxation that were crucial for my motivation! Dr. Ana Pina, I want to thank you deeply for all advises and suggestions, cheering and supportive talks, the company in the lab until late, the preoccupation and the rides home. You were very important in this final period of this hard journey! Foremost, thank you both for your availability and meaningful friendship. Working with you was a real pleasure.

Then I would like to acknowledge Claudia for her incomparable company, for the patience and hearing, as well as the advices and encouragement. Thank you Vijaykumar Dhadge for the supportive talks and the strong motivation. Thank you Íris Batalha for the organic chemistry enlightening debates, Dr. Abid Hussain for the pertinent suggestions and Margarida Dias, Susana Palma, Henrique Carvalho and Dr. Ricardo Branco for all the suggestions, smiles and the friendly and fun working environment. Thank you all for the delightful lunches at Caparica and the unbelievably amusing canoeing day group! I miss them already!

From lab 510 I would like to acknowledge all committee for the so pleasant working environment, for the suggestions and for the cake afternoons! Vanessa Correia and Rita Restani a special thanks for your availability on helping me, for the supportive and encouraging talks, for the brainstormings and the funny moments. Vanessa Almeida thank you for the interesting debates, undoubtedly good laughing times and the Ben&Jerry's afternoons!

Thank you Dr. João Canejo for the help with the traction equipment, for the sympathy and willingness to help, and for the enlightening conversations about biomaterials engineering.

I would like to acknowledge also Dr. Cristina Peixoto from IBET and the project PTDC/EBB-BIO/118317/2010.

Thank you my forever friends Catarina Alves, Patrícia Ramos and Joana Gonçalves for the companionship, encouraging supportive talks, for the moments of outburst in times of stress, and foremost for always believing in me. Sofia Pinto your company in the shallow underground where we listened to each other's lab day problems and we talked about genetics and materials engineering all the time, was really important, after the long days of work. Thank you! Thank you also for listening to me and supporting me unreservedly. Thank you to all my friends!

Finally, I would like to acknowledge my family that I love more than anything. Specially my mother, father and sister thank you for everything, thank you for being there all the time. Is in you that I find my inside strength to fight and continue this journey that is life. You are the reason I am here. I do not have enough words to express my deep gratefulness.

All these members contributed and were essential for the fulfilment of this project. Thank you all!

Abstract

This work aimed at the development of a (bio)polymeric monolithic support for biopharmaceuticals purification and/or capture. For that, it was assured that functional groups on its surface were ready to be involved in a plethora of chemical reactions for incorporation of the desired and most suitable ligand. Using cryogelation as preparation method a screening on multiple combinations of materials was performed in order to create a potentially efficient support with the minimal footprint, i.e. a monolithic support with reasonable mechanical properties, highly permeable, biocompatible, ready to use, with gravitational performance and minimal unspecific interactions towards the target molecules, but also biodegradable and produced from renewable materials. For the pre-selection all monoliths were characterized physico-chemically and morphologically; one agarose-based and two chitosan-based monoliths were then subjected to further characterizations before and after their modification with magnetic nanoparticles. These three specimens were finally tested towards adenovirus and the recovery reached 84% for the chitosan-GMA plain monolith prepared at -80°C.

Monoliths based on chitosan and PVA were prepared in the presence and absence of magnetic particles, and tested for the isolation of GFP directly from crude cellular extracts. The affinity ligand A4C7 previously selected for GFP purification was synthesized on the monolith. The results indicated that the solid-phase synthesis of the ligand directly onto the monolith might require optimization and that the large pores of the monoliths are unsuitable for the purification of small proteins, such as GFP.

KEYWORDS: Biopolymers; Cryogelation; Magnetic Nanoparticles; Polymeric Monolith; Purification

Resumo

Este trabalho teve como objetivo desenvolver um suporte monolítico (bio)polimérico para purificação/captura de biofármacos. Para isso, a presença de grupos funcionais na superfície, prontos para intervir em múltiplas reacções químicas como a incorporação do ligando desejado, foi assegurada. Usando a criogelação como método de preparação, foi realizada uma selecção preliminar a partir de múltiplas combinações de materiais, para assim se obter um suporte monolítico potencialmente eficiente com impacto ambiental mínimo, ou seja, um suporte com propriedades mecânicas razoáveis, altamente permeável, biocompatível, com desempenho gravitacional e interacções inespecíficas mínimas entre o alvo e o suporte, mas que seja também biodegradável e produzido a partir de materiais renováveis. Para a pré-seleção todos os monolitos foram caracterizados físico-química e morfologicamente. Em seguida, os três monolitos pré-selecionados - um monolito tendo como biopolímero base a agarose e dois monolitos tendo como biopolímero base o quitosano - foram submetidos a outras caracterizações, antes e depois da sua modificação com nanopartículas magnéticas. Por fim, as três espécies mencionadas, modificadas ou não com nanopartículas magnéticas, foram testadas com uma solução previamente purificada de adenovírus. O valor máximo de recuperação foi de 84% para o monólito quitosano-GMA nativo preparado a -80°C.

Prepararam-se monolitos de quitosano e PVA na presença e ausência de nanopartículas magnéticas. Estes foram testados na isolação de GFP directamente a partir de estratos celulares brutos. O ligando de afinidade A4C7, previamente seleccionado para a purificação de GFP, foi sintetizado na superfície do monólito. Os resultados indicaram que a síntese em fase sólida do ligando directamente no monolito requer optimizações e que os grandes poros dos monolitos preparados não são adequados para a purificação de pequenas proteínas como a GFP.

PALAVRAS-CHAVE: Biopolímeros; Criogelação; Monolito Polimérico; Nanopartículas Magnéticas; Purificação

Table of Contents

Acknowledgments i
Abstract iii
Resumo v
Table of Contents vii
Index of Figures ix
Index of Tables xv
List of Abbreviations xvii

1 LITERATURE REVIEW 1
  1.1. Monoliths in Bioseparation 3
    1.1.1. Methods to Produce Monoliths 8
    1.1.2. Surface Modification in Monoliths 13
  1.2. Motivation and Aim of the Work 14
2 EXPERIMENTAL 17
  2.1. Materials 19
    2.1.1. Chemical Compounds 19
    2.1.3. Equipment 20
  2.2. Methods 21
    2.2.1. Monolith Preparation 21
      2.2.1.1. Smart Monolith Preparation 23
    2.2.2. Monoliths Characterization – Chemical Properties 25
    2.2.3. Monolith Characterization – Morphological and Mechanical Properties 26
    2.2.4. Screening of Non-Functionalized Monoliths with Ad5 Virus 28
    2.2.5. Production of GFP Containing-Crude Extracts 29
      2.2.5.1. Preparation of LB Medium and LB Agar Plates with Ampicillin 29
      2.2.5.2. Transformation of pET-21c Plasmid in NZY5α Competent Cells 30
      2.2.5.3. Isolation and Purification of pET-21c pDNA 30
      2.2.5.4. Spectrophotometric Quantification of pET-21c pDNA 31

2.2.5.5. Agarose Gel 32
2.2.5.6. Large Scale Expression of GFP 32
2.2.6. Chitosan-based Monoliths Fuctionalization Towards GFP Protein........ 35
2.2.6.1. Monoliths Amination by Plasma Technology 35
2.2.6.2. Aldehyde Groups on the Surface of Previously Aminated Monoliths 37
2.2.6.3. A4C7 ligand Solid-Phase Synthesis on Monolith Platform 38
2.2.7. Screening Assays with GFP and Ligand Leaching Tests 40
2.2.7.1. SDS-PAGE Analysis 40
3 DEVELOPMENT OF MONOLITHS FOR VIRAL PARTICLES PURIFICATION 43
3.1. Introduction 45
3.2. Preparation of Monoliths by Freeze-Drying 51
3.3. Monoliths Architecture and Analysis of its Properties through Characterization54
3.3.1. Materials Employed: an Overview 54
3.3.2. Monoliths Characterization 59
3.3.3. Magnetic Field Responsive Monoliths 70
3.4. Testing for Non-Specific Binding of Ad5 78
3.5. Concluding Remarks 79
4 AFFINITY MONOLITHS FOR GFP PURIFICATION 83
4.1. Introduction 85
4.2. Results and Discussion 87
4.2.1. GFP Expression and Production 87
4.2.2. Preparation of Affinity Monolith towards GFP Purification 90
4.2.2.2. Evaluation of Affinity Monoliths for GFP Purification 97
4.4. Concluding Remarks 102
5 GENERAL CONCLUSIONS AND RECOMMENDATIONS FOR FUTURE WORK. 105
6 REFERENCES 111

Index of Figures

Figure 1.1.- Classification of chromatography stationary phases according to their morphology[4,5]. Micropores size correspond to values below 2 nm, mesopores size to values between 2-50 nm, macropores size to values between 50-5000 nm, and super-macropores to values between 5000-105 nm[6–9]..3

Figure 1.2.- Schematic depiction of research approaches followed in present work. 15

Figure 2.1. – Reaction mechanism in the base of Magnetite Method. 24

Figure 2.3. – Layout of Amination apparatus used for monolithic samples: argon gas bottle (1), gas 2 manometer (2), vacuum pumb (3), plasma chamber (4), high frequency generator (5), heat gun (6), stirrer hot plate (7), 1,6-diaminohexane vessel (8), gas 1 manometer (9)..36

Figure 2.4. – Kaiser test reaction. Compound 1 absorbs at 570 nm.......................................37

Figure 2.5. – Plasma amination[104] followed by Ugi reaction onto monolith. "X" denotes oxygen, nitrogen or carbon atoms. 39

Figure 3.1. – Adenoviral particle external (A) and internal (B) structure. Structures based on Martín[118] and Russel[116] works respectively..46

Figure 3.2. – General scheme for Ad downstream purification. Black spheres represent possible applicable unit operations (most common ones); numbering represents sequential steps (most common ones. The diagram was based on Prazeres work[114]. On capture step AEC is the only method present once it is the most commonly applied one, however Ad can also be separated based on size, hydrophobicity, and metal affinity. AEC: anion-exchange chromatography; SEC: size exclusion chromatography; IPRPC: ion-pair reversed phase chromatography; IMAC: immobilized-metal affinity chromatography.....48

Figure 3.3. – Cryogelation process: The initial system comprising a reaction mixture rich on gel-forming units is frozen; despite looking as a whole firm block, the system is essentially heterogeneous containing an unfrozen liquid micro-phase (UFLMP) together with crystals of frozen solvent; the gel-forming units concentrated in UFLMP allows cryo-concentration occurance with gel formation; solvent acts as porogen leaving cavities when sublimated; the surface tension between solvent and gel phase guarantees the round smooth shape of pores. Green ribbons represent polymers, blue dots represent solvent molecules and the red ones represent the low-molecular weight solutes (e.g. monomers, initiators). Schem based on[138,139]........52

Figure 3.4. - Whole dextran-based monolith (A) and the three samples in which it was sliced (B). 53

Figure 3.5. – Polymers (blue) and monomers (orange) used in monoliths preparation towards a novel, green and virus purifying support. 54

Figure 3.6. – Polymer scale arrangement of composites into monoliths. Structure of chitosan blended with PVA monolith (C/P) (A). Hydrogen bonds are established between polymer chains; and MBAAm polymerizes and imprisons the H-bonding stabilized chains improving. Structure of semi-IPN C-G monolith (B). Here MBAAm crosslinks poly-GMA imprisoning chitosan at some regions. Structure of agarose and dextran-based monoliths (C) where the closed (no loose ends) AAm-GMA copolymer entangles and imprisons agarose/dextran. Orange ribbon represents chitosan; blue ribbon represents PVA molecule; black piece represents MBAAm monomer; black ribbon represents polymerized MBAAm imprisoning H-bonding stabilized C/P chains; green shadow highlights the H-bonding. Purple chains represent poly-GMA; brown sticks represents intra-chain covalent bonds. Pink chain represents agarose/dextran; green chain represents poly(AAm-GMA) chains. 57

Figure 3.7. – Cyclical swelling analysis: variation of percent swelling degree (W) with time (t). Each monolith (frozen at -20°C) is alternately plunged into two different pH buffers (pH7 and 5) over time. C2.9% (a); C2% (b); C-G (c) C/P(50:50) (d); C/P(33:67) (e). All samples are presented in duplicate. 62

Figure 3.8. – Variation of percent swelling degree (W) with time (t). Each monolith (frozen at -80°C) is alternately plunged into two different pH (pH 7 and 5) solutions over time (t). C2.9% (a); C2% (b); C/P(50:50) (c); C/P(33:67) (d). All samples are presented in duplicate. 64

Figure 3.9- Swelling kinetics of A-AAm-G(58:12:30), C-G and C/P(50:50). 70

Figure 3.10.- Digital pictures from C-G monoliths: dry monolith embedding MNPs (A, on the left) and native monolith (A, on the right); hydrated magnetic monolith (B, on the left) and native monolith (B, on the right); sequential squeezing of hydrated magnetic monolith (C1-6) and native monolith (D1-3). Both recover its original shape after deformation. 71

Figure 3.11. – Permanent magnets used for field response testing. 74

Figure 3.12.– Magnetic-field response of Agarose (A-AAm-G (58:12:30)) and chitosan-based monoliths (C/P (50:50), C-G) to different magnetic-flux densities: 0.25T, 0.50T, 0.53T and 1.5T. The first five points plotted no each graph corresponds to deformation under external magnetic-field, the following five corresponds to matrix behaviour after external field removal (when reached the initial length no more points were plotted). Data was obtained from duplicated measurements. 75

Figure 3.13. – SEM micrographs of non-magnetic (A,C,E) and magnetic (B,D,F) chitosan and agarose-based monoliths at x300 magnification: Ag-Am-G(58:12:30) corresponds to A and B; C/P(50:50) to C and D; and C-G to E and F. For C-G monoliths a micrograph with lower magnification (x100 (left) x150 (right)) is shown. 77

Figure 3.14. – SEM micrograph of C/P(50:50) native monolith at a magnification of x500. Notice the peculiar pendant polymer strings..78

Figure 4.2. – pET-21c isolation and purification was successfully achieved as agarose gel electrophoresis (0.8%(w/v) agarose, stained after running) can prove (A): marker, 1st elution, 2nd elution (lanes 1, 2, 3 from left to right). First and second elutions recovered through NZYminiprep kit for DNA purification were quantified and analysed by NanoDrop spectrophotometer (B). 87

Figure 4.3. – Monitoring of Cells growth and GFP expression through OD_{600nm} (A) and fluorescence intensity measurements (B), respectively. A correlation between phenomena can be seen (conversion of nearly all cell's resources towards GFP gene expression[209]). 88

Figure 4.4. – Time course SDS-PAGE gel (12.5% acrylamide gel stained with Coomassie Blue R-250). GFP mass production can be visualized. M represents protein marker; PRE corresponds to sample collected at $t_{induction}$=0; all following lanes matches the GFP profile at different times of induction (2h, 4h, 5h and 18h). The band of GFP is expected to be placed at ~29 kDa[101,201]. The loading volume of each sample was normalized to a constant specific optical density value (1.2). 89

Figure 4.5. – Fluorescence monitoring during induction time and fractionation (A): 0h-18h represents the time after induction; Sc corresponds to supernatant obtained after centrifugation; Pc to pellet obtained after centrifugation; Su to supernatant obtained from ultracentrifugation; Pu to pellet obtained from ultracentrifugation. Cellular fractionation analysis by SDS-PAGE was performed (B): M represents protein marker; PRE corresponds to sample collected just before induction; POS corresponds to sample collected after 18h induction...89

Figure 4.6. – Silver mirror test on aldehyde functionalized monoliths: non-magnetic and non-functionalized monolith (NC, negative control); non-magnetic and functionalized monolith (NL); magnetic and functionalized monolith (ML); Glutaraldehyde as positive control (C+); and magnetic and non-functionalized monolith (MC, negative control) (from left to right)..........92

Figure 4.7. – Pyrene presence at the surface of NL and ML monoliths: non-magnetic monolith functionalized with A4C7 (NL) (A,E); non-magnetic and non-functionalized monolith (NC) (B,F), magnetic monolith functionalized with A4C7 (ML) (C,G), magnetic non-functionalized monolith (MC) (D,H) (from left to right). Pictures were taken on the fluorescence microscope under bright field filter (A,B,C,D) and fluorescence filter (E,F,G,H) at x40 magnification. All supports were regenerated before analysis. 93

Figure 4.8. – SEM micrographs of NC monolith with x300 magnification kindly provided by Barroso et al.[27] (A), MC monolith with x300 magnification (B), NL monolith with x1000 magnification (C), and ML monolith with several magnifications: x30 (D), x500 (E) and x1000 (F)..........95

Figure 4.9. – Visual comparison between stages of monolith surface modification. C/P(50:50)80 native just lyophilized monolith (A), after aldehyde functionalization (B), after A4C7 solid-phase synthesis (C) (from left to right)..........95

Figure 4.10. – Magnetic-field response of magnetic C/P (50:50)80 monolith at various modification stages at its dry (square) and wet states (diamond): without any modification (A); after aldehyde functionalization (B); after stability test in 100%(v/v) MeOH during 48h (C); C/P(50:50)80 after A4C7 functionalization. First five points plotted no each graph corresponds to deformation under external magnetic-field (1.5T), the following five corresponds to matrix behaviour after external-field removal (when reached the initial length no more points were plotted). Data obtained from duplicated measurements..........96

Figure 4.11. – Ligand Leaching assays. A4C7 leaching for NL and ML monoliths at 0.1M glycine-NaOH pH 9 (E1) and 0.1M glycine-NaOH pH 9, 50%ethylene glycol (E2 97

Figure 4.12. – Selectivity of ligand A4C7 towards GFP at different pH values: pH7.4 (A) and pH9 (B). Results refer to a batch system where the protein is incubated with the support for 15 minutes. TP denotes for total protein..........98

Figure 4.13. – Selectivity of A4C7 towards GFP at different times of incubation: 0 minutes or continuous system (A), 15 minutes (B) and 60 minutes (C) batch system. Binding condition: pH7.4. 100

Figure 4.14. – SDS-PAGE analysis of GFP screening on magnetic functionalized (ML) monoliths: Continuum assay (A); 15 minutes batch assay (B); 60 minutes batch assay. M corresponds to protein marker and lanes 1, 2, 3, 4, 5, 6, 7, 8, 9 denotes for: loading, flow-through, 1st wash, 2nd wash and 1st elution for ML and loading, flow-through, 1st wash, 2nd wash and 1st elution for MC, respectively. GFP bands position (~29kDa) is highlighted.101

Figure 4.15. – Magnetic-field response of ML monolith before and after screening assay.102

Index of Tables

Table 1.1.- Benefits and limitations of each chromatographic media type used in bioseparation. The present comparison of generalized structures of porous beads, stacked membranes, and monoliths is not drawn to scale. Black arrows show the bulk convective flow, and shaded orange areas the diffusion regions. Green curling arrows show turbulent flow (eddies) with consequent counter-current between laminar flow and eddy flow (shear). In case of beads media green arrows represent inter-particles eddies[20,21,5,2]. 6

Table 1.2.- Examples of the application of monoliths in bioseparation. 7

Table 1.3.- Methods for preparation of monoliths to be applied in separation science[12,54,48].9

Table 1.4.- Benefits and limitations associated with each type of monolith structure.[80,81,79,54]12

Table 2.1.- Casting solutions processed for monoliths preparation. All casting solutions were formulated with 3 mL of distilled water per monolith. Polymers and/or monomers content in every 2.9%(w/w) casting solution is 90mg. Conversely in PVA:GMA 79:21%(w/w) casting is 101mg), AAm:MBAAm:GMA 95mg/210mg, agarose:AAm:GMA and dextran:AAm:GMA 142 mg/172 mg. 22

Table 2.2. – Required volumes to prepare one 12.5% Acrylamide gel. 34

Table 3.1. – Traditional methods used in Ad purification. 47

Table 3.2.- Summary of possible combinations of chromatographic steps in Ad purification steps. 50

Table 3.3. – Monoliths prepared for screening tests accompanied by the respective monomeric/polymeric ratios...56

Table 3.4.– Stability Tests performed at pH3, 7 and 11 with different monoliths prepared at -20°C/-80°C. Monoliths were macroscopically analysed during fourteen days. 59

Table 3.5.– Stability Tests performed at pH 3, 7 and 11 of different chitosan-based monoliths prepared at -20°C Monoliths behaviour was analysed during fourteen days, having the first picture being taken at day three. 60

Table 3.6. – Morphological and mechanical properties of all monoliths prepared at -20°C. All data was obtained from duplicated measurements (in case of water flux measurements each one of the two samples was measured three times). 65

Table 3.7. – Morphological and mechanical properties of all monoliths prepared at -80°C. All data was obtained from duplicated measurements (in case of water flux measurements each one of the two samples was measured three times). 68

Table 3.8. – Morphological and mechanical comparison between non-magnetic and magnetic monoliths with MNPs at two different concentrations for each specimen. All data was obtained from duplicated measurements (in case of water flux measurements each one of the two samples was measured three times). M_C/P(50:50) denotes magnetic C/P(50:50), the same is true for the others. 72

Table 3.9. – Pore volume and density values for magnetic and non-magnetic (native) monoliths. All data was obtained from duplicated measurements. M_C/P(50:50) denotes magnetic C/P(50:50), the same is true for the others. 73

Table 3.10. – Comparative analysis of different monolithic supports for recovery of adenovirus vectors. 79

Table 4.1. – Comparative analysis on the efficiency of amination through three different approaches: traditional preliminary epoxyactivation, non-thermal plasma treatment followed by amination out-of-chamber, and non-thermal plasma with direct amination inside chamber. MC denoted for magnetic non-functionalized monolith and NC for non-magnetic non-functionalized monolith. 91

Table 4.2. – Morphological and mechanical properties of functionalized and non-functionaliized monoliths. All data was obtained from duplicated measurements (in case of water flux each one of the two samples was measured three times). 94

Table 4.3. – Flow analysis through ML monolith after different times of exposure. Monolith is kept inside magnet during different periods of time. All data was obtained from duplicated measurements (in case of water flux each one of the two samples was measured three times..99

List of Abbreviations

AAm	Acrylamide
Ad	Adenovirus
AEC	Anion Exchange Chromatography
Ad5	Adenovirus type 5
APS	Ammonium Persulphate
CEC	Capillary electrochromatography
DLS	Dynamic light scattering
E1	Elution condition 1: 0.1M glycine-NaOH pH9
E2	Elution condition 2: 0.1M glycine-NaOH pH 9, 50%(v/v) ethylene glycol
EMA	European Medicines Agency
GFP	Green Fluorescent Protein
GCE	GFP crude extract
GMA	Glycidyl Methacrylate
HPLC	High performance liquid chromatography
IPTG	Isopropyl β-D-1-thiogalactopyranoside
NC	Plain C/P(50:50) monolith
NL	C/P(50:50) monolith non-modified with MNPs, functionalized with A4C7
MAbs	Monoclonal antibodies
MBAAm	N,N'-methylene-bis-acrylamide
MC	C/P(50:50) monolith modified with MNPs, non-functionalized in any way
MCR	Multicomponent reactions
ML	C/P(50:50) monolith modified with MNPs, functionalized with A4C7
Mw	Molecular weight
PBS	Phosphate Buffer Saline
PDB	Protein Data bank
pDNA	Plasmid DNA
PVA	poly(vinyl alcohol)
rAd	Recombinant Adenovirus
SEM	Scanning Electron Microscopy
SDS	Sodium Dodecyl Sulphate
SPOS	Solid Phase Organic Synthesis
TEMED	N,N,N,N – Tetramethylethylenediamine

1 LITERATURE REVIEW

1.1. Monoliths in Bioseparation

Adsorption chromatography can be performed using distinct solid phase media, namely porous beads, membranes, and monoliths (Figure 1.1.). Porous particle-based supports are currently the most widely employed stationary phases for purification of biomolecules, particularly proteins[1]. However, due to present research and market evolution towards large biomolecules (virus, DNA, intact cells, complex proteins) in (bio)pharmaceutical industry, and particle-based media inadequacy to purify this types of molecules, monoliths arise as a promising alternative[1–3].

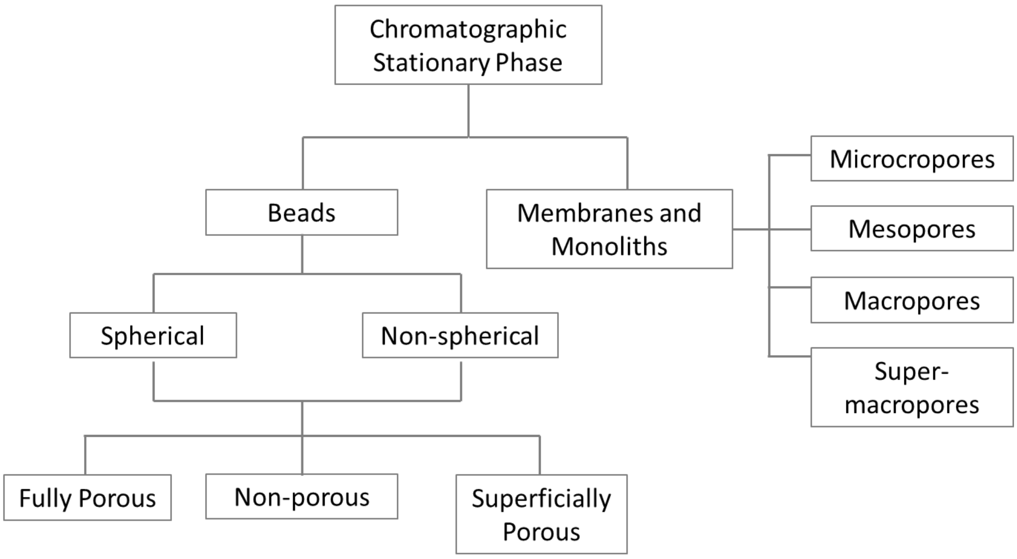
Chromatographic Stationary Phase
Beads
Membranes and Monoliths
Microcropores
Mesopores
Macropores
Super-macropores
Spherical
Non-spherical
Fully Porous
Non-porous
Superficially Porous

Figure 1.1.- Classification of chromatography stationary phases according to their morphology[4,5]. Micropores size correspond to values below 2 nm, mesopores size to values between 2-50 nm, macropores size to values between 50-5x10^{5} nm, and super-macropores to values between 5x10^{3}-1x10^{5} nm[6–9].

Monolith is defined as a continuous and porous stationary phase moulded as a column and inserted in a chromatography housing[2,5]. Their *"format can be compared to a single large particle"*[10], and include *"compressed hydrophilic gels, macroporous polymer discs, columns, tubes and silica rods"*[10].

Beyond the possibility of being prepared through several procedures and distinct chemistries, monoliths can also be tailored to present differences at microstructural level (e.g. pore size and geometry)[11,12]. However, they are all characterized by high porosity and pore interconnection, leading to the formation of a network of channels[5]. This single structure allows mobile phase to flow through these channels by convection, minimizing mass transport resistance (low backpressure) and increasing separation speed, independently of molecular size or diffusion coefficient[5]. These flow-through pores characterized by convective transportation of mass are thus responsible for the flow independent chromatographic properties of monoliths, such as dynamic binding capacity and resolution, and consequently for the efficient high speed assays[13,14]. In fact, monoliths exhibit plate efficiencies that compete with finest bead-packings[14].

This constitutes a totally different picture compared to diffusion, the representative driving force of mass transfer between solid surface and bulk liquid phases on porous packed-beads separation media, a slow phenomenon dependent on molecular weight[5,2]. This phenomenon takes place due to the adsorption surface shallow dead-end pores with 10–100 nm large, where neither convective transport can be achieved nor big molecules like virus, DNA and cells can have access[5,15]. The mass transport dependence on molecular weight of analytes comprises the speed of the assays and can only be overcome with resolution and binding capacity commitment. The independence of dynamic binding capacity and resolution from flow-rate can be achieved with non-porous micrometerized small beads (<5μm) made of silica or synthetic polymers. However due to its low porosity compared to monoliths, only short column lengths can be used to avert high backpressures and achieve attractive assay speeds[13]. Moreover in particulate-bead packings there are preferential paths for the solution – interparticle void volumes (~40% of total bed volume[1]) – where flow vortices (eddies) are created due to differential friction between particle surfaces and inter-particle void areas. This eddies origin turbulent mixing that reduce resolution, broaden peaks, and may cause shear forces that can harm sensitive/unstable molecules, lowering yields. Perfusive particles, with channels transecting them, allow a little increase on convective mass transport together with an increment on bio-nanoparticles accessible area, however this type of beads are not free from the undesired void volumes, where fluid flows preferentially and eddies occur[1].

Conversely to packed beads, and equally to monoliths, membranes are designed particularly to take the maximum advantage of convective transport. In fact, a membrane can even be almost equalized to a monolith, once it is cast as a single continuous unit provided with large channels rather than pores. Nevertheless, their exceedingly flat bed height, their usually smaller channels width (generally not surpassing 1μm[1] against ~100μm for monolithic cryogels[9,16]), together with the different physical arrangements in which they are applied (e.g. stacked membranes, pleated cartridge) make them distinct from monoliths in terms of operating features[17,1]. In fact all these differences together render membrane arrangement less effective compared to the monolith one. Inside membrane housings there is an uncontrolled and uneven distribution of flow-rates (inlet side of membrane), together with turbulent mixing between membrane layers forming the dead or void volumes; all this is due to the discontinuity of channels, consequence of the discontinuous character of the whole format (discontinuous pore distribution) and the characteristic inlet arrangement itself[5]. As the turbulent mixing occurring in these void volumes can be compared to eddy dispersion in porous bead supports[1], the threat of shear forces presence as consequence of eddies formation is a possibility, and so it is product integrity commitment. The flow aberrations located on the outlet side of the membrane generate dispersion decreasing process performance[5]. So the flow uneven distributions and undesired behaviours are thus responsible for a slight decrease on capture efficiency and strong reduction on elution efficiency (unwell resolved peaks).

In turn, monoliths not only exhibit a binding capacity three times wider than membranes[14] but also lack the dead volumes. In fact the laminar flow through all monolith avoid eddies, decrease shear, and guarantees immediate response to variations in buffer composition, maximizing elution kinetics and contributing to sharper, better resolved and more concentrated elution peaks, and high functional recoveries. They offer *"the selectivity of particulate resins and the throughput of membrane absorbers"*[18], suggesting that monoliths should be more efficient, especially when it comes to larger biomolecules purification[14,2].

Table 1.1. presents a comparison between the three main chromatographic media available.

Monoliths that can be prepared in multiple ways and also find diverse applications, are usually easy to prepare in various sizes and shapes from different materials and through different methods. Monoliths surface can then be or not chemically modified with multiple molecules and applied in the capture/purification of large biomolecules, as they present fast performance at low pressures and room temperature, and a high productivity due to their flow-independent properties[2,13].

The retention of target molecule can be performed through selective electrostatic, hydrophobic, affinity or pseudo-affinity interactions; and nature of the matrix has potential to vary widely; however either commercially available monoliths or lab developed ones are mostly composed by silica, acrylamide or methacrylates[6,3,19].

Table 1.1.- Benefits and limitations of each chromatographic media type used in bioseparation. The present comparison of generalized structures of porous beads, stacked membranes, and monoliths is not drawn to scale. Black arrows show the bulk convective flow, and shaded orange areas the diffusion regions. Green curling arrows show turbulent flow (eddies) with consequent counter-current between laminar flow and eddy flow (creating shear). In case of beads media green arrows represent inter-particles eddies. Table based on [20,21,5,2].

	Beads	*Membranes*	*Monoliths*
Chromatographic Media	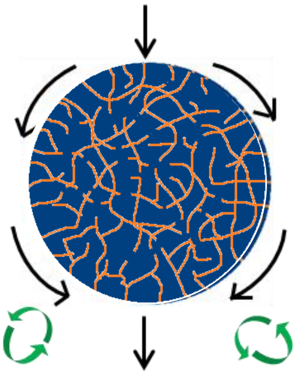	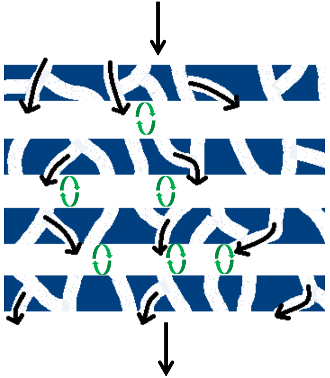	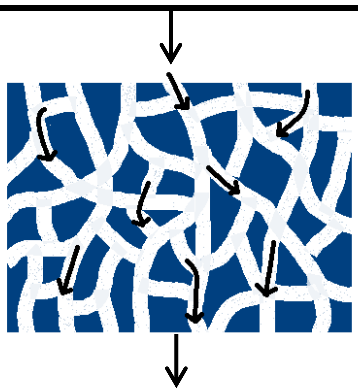
Advantages	• High product purity (SM); • Consistency and safety; • Industrial scale well known; • High adsorption and elution efficiency (SM); • High surface area and high binding capacity (SM); • Multiple column chemistries and HPLC column dimensions are commercially available; • Validated applications/assays.	• Low pressure drop; • high flow rates; • Small footprint; • Inexpensive; • Disposable; • Moderate resolution; • High hydraulic permeability; • Rapid mass transfer (convection), allowing high flow rates with high productivity and major decrease in separation times.	• High porosity; • Large interconnected channels with rapid mass transfer (convection), allowing high flow rates with major increase crease in separation times; • High productivity; • No void volumes and laminar flow, so no eddies are formed, neither shear; • High purity products; • Ease of preparation and processing in various volumes and shapes (PM); • Flexible surface chemistry for ligand attachment, due to plethora possible usable materials; • High hydraulic permeability; • Inexpensive; • Moderate-high resolution; • Low-moderate pressure drop; • High binding capacity (BM); • Mechanically robust;
Limitations	• High pressure drop; • Weak mechanical properties; • Eddy dispersion and shear forces due to voids compromising productivity; • Extensive footprint; • Moderately expensive; • Low binding capacity (BM); • Peak broadening, resolution and recovery worsens with flow rate (BM); • Low mass transfer (diffusion) with consequent low flow-rates • High backpressure; • Extra machinery required for sample solution to cross media; • Air incursion into column destroys bed integrity.	• Low binding capacity; • Limited available surface area; • Shear forces due to eddies; can compromise productivity • Flow aberrations compromise performance; • Fouling; • Broad peaks due to eddies (desirable in situations where neither high purity nor high eluted product concentration is required); • Accumulated bubbles difficult to displace without breaking system sterility.	• Scale-up difficult; • Low specific surface area per unit volume, and so low binding capacity for SM and medium large proteins as monoclonal antibodies; • Extensive footprint; • Low efficiency (SM) and HPLC column to column reproducibility; • Limited column chemistries and dimensions commercially accessible; • Constrained use in routine analysis due to few commercial suppliers available.

PM: Polymeric Monolith; **BM:** Big Molecules; **SM**: Small Molecule

Currently, this new category of porous media has been extensively applied in analytical chemistry, mainly in separation science areas. Through liquid chromatography, namely high performance liquid chromatography (HPLC) and capillary electrochromatography (CEC)[22], monolith stationary phase has been used to capture, purify, enrich and analyse diverse bio-nanoparticles, from plasmidic and genomic nucleic acids to organelles, inclusion bodies, virus and other macromolecular assemblies[2,23]. The specific interactions between the target macro-biomolecule and the adsorptive matrix allow their isolation from related small molecules[24]. Table 1.2. shows some applications of monoliths as sorbents for isolation of macro-biomolecules.

Table 1.2.- Examples of the application of monoliths in bioseparation.

Monolith Material	*Mode*	*Ligand*	*Application/Target(s)*	*Pore Size (µm)*	*Surface Area (m^2/g)*	*Capacity*	*Recovery (%)*	*Purity*	*Ref*
GMA-EDMA	CEC	Acetic Acid	Purification and simultaneous renaturation of rhIFN-γ	0.4-2.0 (>80%)	n.a.[a]	n.a.	n.a.	93%	25
(Hybrid silica) TEOS-AEAPMDMS	AEC	Amine groups	Extraction of genomic DNA from blood	≤6.0	n.a.	9.3 ng/cm	52.1	n.a.	26
Chitosan-PVA cryogel	Affinity	(Artificial protein A) ligand 22/8	Capture of pure IgG, and direct capture and recovery of mAb from a non-clarified homogenate	~45	2.3	150 mg/g	90, 48	98%	27
CIM	AEC	Q	Isolation of bacterial ribosomes from crude cell lysates	0.6-5.0	~40	n.a.	n.a.	< sucrose gradient centrifugation	28
			Concentration and purification of rubella virus from a complex biological suspension	0.6-5.0	~40	n.a.	~100	High	29
Aam-AGE-MBA	IMAC	IDA-Cu^{2+}	Direct capture of enzyme (His)6-LDH from non-clarified crude cell homogenate	0.01-100	n.a.	0.13 mg/ml	70-90	Need to be improved	9
			Chromatography of *E. coli* cells	0.01-100	n.a.	n.a.	80	Reasonable	30
Aam-DMAEMA-MBAAm	AEC	DEAE	Chromatography of *E. coli* cells	0.01-100	n.a.	n.a	70–80	Need to be improved	30
LMA-EDMA-VPBA	CEC and HIC	Boronic acid and C_{12} chain	Analysis and identification of *cis*-diol biomolecules/TRF	$5x10^{-3}$–$50x10^{-3}$	43.5-54.8	n.a.	n.a.	Need to be improved	31
Aam-MBAAm-GMA	Affinity	Streptavidin	Single-step capture of chemically biotinylated MoMuLV	0.01-100	n.a.	$2x10^5$ cfu/mL	<8	High	32,9
PHEMAH cryogel	Pseudo Affinity	MAH	purification of pDNA	10–100	n.a.	13,350 µg/g	90	Reasonable	33

CEC: Cation-exchange chromatography; **AEC**: Anion-exchange chromatography; **IMAC**: Immobilized methal affinity chromatography; **HIC**: Hydrophobic interaction chromatography; **rhIFN-γ**: Recombinant human interferon gamma (growth factor); **TRF**: Transferrin; **MAH**: N-methacryloyl-(l)-histidine methyl ester; **PHEMAH**: Poly(hydroxyethyl methacrylate-Nmethacryloyl-(L)-histidine methyl ester). **MoMuLV:** Moloney Leukemia virus; cfu: colony forming units

a) Data no available on the literature as far as we are concerned.

Besides their wide applicability in bioseparation (liquid chromatography, capillary separations, capillary electrochromatography (CEC), thin-layer chromatography, gas chromatography)[9,29,32,27,25,34,22] as adsorbent matrices, monoliths have also found usefulness in sample pre-treatment[21,23], catalysis[35,36] (mainly towards micro-scale protein mapping or proteomic analysis[36,37]), solid phase and combinatorial chemistry[38,39], scavenging[40], as static mixers[41], drug delivery, in vitro cell cultivation, and tissue engineering[42,43].

1.1.1. Methods to Produce Monoliths

Despite the possibility of monoliths to be miniaturized into capillaries, microfluidic devices or microarrays, they are usually prepared on an analytical scale: in a conventional large column/rod, tube or disk format, in a multi-well plates format for screenings assays[44,2], in a thin-layer format for planar chromatography[34,2], or with a tip geometry[45,2].

Monoliths can be divided into organic polymer monoliths, inorganic silica monoliths and hybrid organic-silica monoliths. Inorganic silica monoliths can be fabricated by (i) fusion of porous silica beads through thermal sintering, (ii) cementing/immobilizing silica beads in a packed bed by cross-linking/entrapping them through sol-gel process, or (iii) polymerization of sol-gel precursors (silicon alkoxide). The latter, a waste-free method, is the most commonly used[46].

Recently a review on what authors called 'exotic monoliths', shows that beyond the famous silica gel-based monoliths inorganic monoliths can be prepared from both a 'pure' metal or a metal-oxide, and be applied in separation science[47].

In turn organic polymer monoliths can be prepared from i) solely a polymer, ii) a blend of polymers, iii) a polymerization of monomers in presence or not of one or more polymers, or (iv) co-polymerization of monomers in presence or not of one or more polymers; using a variety of possible methods[12,48,49] (Table 1.3.). Generally they are produced by in situ polymerization of a mixture containing monomer(s) (commonly acrylamides, methacrylates, or styrene[50,6]), crosslinker, porogenic solvent(s) and an initiator, using a simple moulding procedure executed inside a mould such as a chromatographic column, capillary or micro-channel (see figure 2 on Nordborg *et al.* work[51]). The most employed method is the free radical polymerization, more precisely the thermally and UV irradiation photo-initiated approaches[48]. Other approaches have been explored, such as microwave or γ radiation initiated polymerizations[51,12,52]. Recently 1-vinyl-3-octylimidazolium (ViOcIm+) ionic liquid-based monoliths were prepared via thermal free radical copolymerization and used to separate a mixture of standard proteins (BSA, quine myoglobin, lysozyme and cytochrome c)[53].

Table 1.3.- Methods for preparation of organic monoliths to be applied in separation science[12,54,48]**.**

Preparation Method	*Materials*	*Initiator/ Porogen/ Other*	*Pore Size (μm)*	*Application*	*Obs.*	*Ref*
Thermally initiated free radical polymerization (TIFRP)	PA:PDA (50:50 %w/w)	AIBN / 2-propanol, THF	0.22	Separation of proteins and oligo-deoxynucleotides	• 1^{st} method used for preparation of rigid polymer-based monoliths; • Very simple; • Process origin can be traced down to techniques generally applied in preparation of porous beads by suspension polymerization; • High reproducibility; • Assembled by irregular micro-globules forming aggregated clusters, leading to some limitations (e.g. permeability) (all FRP).	54,55, 12,56
Photo-initiated free radical polymerization (UV rays)	GMA: EGDMA: BMA (51:40:5 %v/v)	AIBN / 1-dodecanol, cyclohexanol	0.5-3	High throughput sample clean-up throughput. Roscovitine and lidocaine in plasma samples used as model substances.	• Faster than TIFRP; • Can lead to columns with lower backpressure, and better chromatographic performance than TIFRP (comparing columns of same pore size); • Reaction can be stopped when irradiation source is removed and column is flushed; • Limited by use of UV transparent molds with a small size in one dimension and UV transparent monomers, exclusion of aromatic monomers, and wavelength of maximum absorbance of initiator;	57,54, 12,58, 59
Photo-initiated free radical polymerization (visible light)	St:DVB (50:50 %v/v)	mixture of CQ, EDAB, MPPB / ACN, 1-propanol, 1-decanol	n.a.[a]	Separation of mixture of standard proteins: ribonuclease A, cytochrome c, myoglobin and ovalbumin	• Performed at room temperature, allows less common porogens usage, including those with low boiling point.	58
Radiation initiated free radical polymerization (y-rays)	DEGDMA: GMA	No initiator / t-butanol or methanol or ethanol or propanol or acetone or THF or ethylpropionate	~3	Diagnostics and purification	• Faster than TIFRP; • Greater penetration depth of radiation than UV-initiated polymerization, allowing preparation of any volume monoliths; • No initiator needed; • Pore volume and pore size distribution tuning in a broad range through process variables as irradiation dose and dose rate, non-available in other polymerization processes.	60,61
Radiation initiated free radical polymerization (microwaves)	St:DVB: MAA (33.3: 33.3:33.3 %v/v)	AIBN / toluene, isooctane	0.28 -8.88	pCEC, CEC, LPLC of neutral compounds (thiourea, benzene, toluene, ethyl benzene, biphenyl, naphthalene)	• Polimerization time shortened from 24h (TIFRP) to 15min; • Lower expense than TIFRP and UV-ligth initiated FRP.	62

(Continued)

Table 1.3. ***(Continued)***

Preparation Method	*Materials*	*Initiator/ Porogen/ Other*	*Pore Size (μm)*	*Application*	*Obs.*	*Ref*
Radiation initiated free radical polymerization (electron beam)	EMA: TMPTA (50:50 %w/w)	No initiator / 2-propanol, 1-dodecanol	0.08-0.11	Separation of proteins: lysozyme, ribonuclease, insulin, cytochrome c, andalbumin; heterogeneous catalysis	• No initiator needed; • Successful column scale up reported; • Fastest separation with sufficient peak resolution, in comparison to ROMP prepared monoliths.	52
Polymerization by high internal phase emulsions (polyHIPE)	GMA: EGDMA (77:23 %w/w)	Potassium persulfate / Emulsified water droplets / calcium chloride hexahydrate (electrolyte) and Synperonic PEL 121 (surfactant)	~0.1 (holes size 1 -10)	Separation of standard protein mixture of myoglobin, conalbumine and trypsin inhibitor	• Good separation in a very short time, comparable to separation achieved by commercial methacrylate monoliths (FRP); • Monoliths characterised by high porosity (>70%) and large spherical hollows interconnected by ''windows''; • Possible drawback: monoliths present low specific surface area, restraining its use in separation science.	63,12, 64
Cryogelation	HEMA: MAH (PHEMAH)	APS / Water crystals / TEMED (catalyst)	10–100	Purification of pDNA	• Freezing temperature define pore size; • Due to large produced pores (1–100μm) and high porosity (≤90%), hydrodynamic cryogels properties are exceptional.	12,65, 33
Living Polymerization Nitroxide Mediated (SFRP)	St:DVB (50:50 %w/w)	Benzoyl peroxide / PEG 400, 1-decanol / 3-carboxy-PROXYL or 4-carboxy-TEMPO (promoter)	≤0.01-1	separation of mixture of myoglobin, cytochrome c, and lysozyme	• Slower kinetics characterizing TEMPO-mediated polymerizations avoids significant shifts in pore size distribution; • TEMPO-capped dormant radicals usable for grafting pore surface and tailoring its chemistry; • Initiator remains on or within the material, enabling post-polymerization modifications. • Least versatile (against ATRP, and RAFT)	12,66
Living Polymerization (TERP)	MBAAm	AIBN / PEO (phase-separator) / BTEE (promoter)	0.5 -2	Aqueous phase applications (bioseparation, support for catalysis)	• A recent strategy lacking preparation of columns and chromatographic evaluation of their performance; • High surface areas attained may ease separation of small molecules in isocratic mode; • High temperatures employed.	67
Living Polymerization (ATRP)	VC:EDMA (50:50 %v/v)	CCl4 / dodecyl alcohol / $FeCl_2$ (catalyst)	0.85	Separation of: IgG from human plasma, lysozyme from egg white, and mixture of papain, snailase, IgG.	• Control over rate of monomer combination with growing polymer chain (chains similar in length) (all LP); • Highly homogeneous crosslinking due to isotropic spinodal decomposition promotion possibility (ATRP, TERP); • Popular in general polymer chemistry, but poorly explored in monoliths preparation.	68,12
Living Polymerization (RAFT)	MAA: EDMA	AIBN / Toluene, dodecanol / DBTTC (chain transfer)	n.a.	Extraction of clenbuterol from biological samples	• Surface functionalization eased (all LP); • Control over polymerization kinetics, structure morphology and surface functionality (all LP).	69,70

(Continued)

Table 1.3. ***(Continued)***

Preparation Method	*Materials*	*Initiator/ Porogen/ Other*	*Pore Size (μm)*	*Application*	*Obs.*	
Living Polymerization (ROMP)	NBE: DMN-H6 or COE:CL (50:50 %w/w)	$[RuCl_2(PCy_3)_2(CHPh)]$ or $[RuCl_2(Py)_2(IMesH_2)CHPh]$ / 2-Propanol, toluene	0.006 -~0.04	Separation of Ribonuclease A , carbonic Anhydrase, insulin, cyctochrome C, albumin	• Restricted range of possible monomers; • Noticeable irregularities in the porous structure with increasing ratio of pore size to the capillary diameter.	71,12
Poly-condensation	polyglycerol-3-glycidyl ether	$BF_3{\cdot}Et_2O$ in dioxane / Toluene, t-butyl methyl ether	22	Capture of Gram-negative bacteria	• Oxygen insensitive reaction, rendering unnecessary the careful de-aeration required for FRP; • Produces attractive morphological structures for separation; • Mild reaction conditions and possibility of room temperature employment avoids pore structure heterogeneities in contrast to FRP.	72
Thermally induced phase separation	Polyamide	No initiator needed / Benzyl alcohol	~0.01- ~0.02	n.a.	• Structures produced present uniform architecture. Exceptionally simple method (thermally controlled dissolution and phase segregation process) for preparing monoliths with attractive chemical, physical and porous properties.	73
Non-solvent induced phase separation	Polycarbonate	No initiator needed / Cyclohexane	0.45-3.2	Adsorption ofmetal ions and purification of proteins	• Easy and clean process, so morphology tailoring is easy.	74

THF: Tetrahydrofuran; **PA**: Phenyl Acrylate; **PDA**: 1,4-Phenyl Diacrylate; **BMA**: Butyl Methacrylate; **EDMA**: Ethylene Glycol Dimethacrylate; **St**: Styrene; **DVB**: Divinyl Benzene; **MAA**: Methacrylic Acid; **PEO**: Poly(ethylene oxide); **TEMPO**: 2,2,6,6-Tetramethyl-1-piperidyloxy **VC**: Vinyl Carboxylate; **SFRP**: Stable Free Radical Polymerization **TERP**: Organotellurium-mediated living Radical Polymerization; **ATRP**: Atom Transfer Radical Polymerization; **NMP**: Nitroxide-Mediated Polymerization; **RAFT**: Reversible Addition-Fragmentation Chain Transfer; **ROMP**: Ring-Opening Metathesis Polymerization; **polyHIPE**: Polymerization by High Internal Phase Emulsion; **LP**: Living Polymerization; **FRP**: Free radical Polymerization.

a) Data no available on the literature as far as we are concerned.

Another attractive method for the preparation of monoliths is cryogelation. This versatile technique allows the preparation of elastic and sponge-like structures with a broad range of porosities, and gives rise to highly interconnected supermacroporous matrices with 100μm sized pores. Moreover its green character does not go unnoticed[75,12,65,33].

A 2010 review from Svec[12] gathers all different polymerization methods that could be used to prepare polymeric monolith structures, so far. However since that comprehensive publication, several developments in this area have been made, with some breakthrough approaches reported[48], namely, the growing incorporation of nanostructures into monoliths like nanoparticles of silica, gold, silver, metal oxides, hydroxiapatite, and polymers, or carbon nanotubes[76]. This strategy aims to tailor surface characteristics, incorporating nanostructures features into monoliths, what increases surface area-to-volume ratio, and consequently offers an extended surface for biomolecules adsorption, possibly facilitating mass transfer and improving separation efficiency[76,77]. The incorporation of particles can be performed by embedding them into the matrix, which includes simply its dispersion (entrapment) or polymerization of their dispersions into polymerizing mixture (co-/polymerizing monomers attached by functionalized nanoparticles), or by immobilizing them on surface of manufactured monoliths through surface coating[76,78]. To our knowledge, up to now, just a recent unpublished work accomplished the embedding of iron oxide MNPs into monoliths to be used in analytes separation (IgG), more specifically an external magnetic field aided separation[79].

Table 1.4.- Benefits and limitations associated with each type of monolith structure.[80–82,54]

Monolith Nature	*Advantages*	*Limitations*
Organic/Polymeric	• Broad pH working range (2-13); • Simplicity of preparation; • Inertness to biomolecules; • Absence of adverse effects from silanol; • Easy to be modified; • Wide range of choices in terms of surface chemistry resulting from diverse pre-polymerization conditions; • Easily preparable under mild and facile conditions via inexpensive machineries (e.g.an oven and a water aspirator); • Swelling/shrinkage in some solvents can help in chromatographic separation; • More suited for macromolecules separation.	• Limited mechanical stability due to swelling/shrinkage in some organic solvents; • Presence of micro-pores on polymer surface have an adverse effect on separation efficiency of small molecules as well as peak symmetry • More trouble in controlling skeletal structure comparing to silica monoliths.
Inorganic Silica	• Resistance to swelling/shrinkage; • Great mechanical properties; • High column efficiency for small molecules (≥ 100 000 N/m) • Wide variety of highly characterized monoliths commercially available, together with distinct chemistries accessible for surface modification and ligand attachment • Bimodal pore structure (large surface area: ≤300 m^2/g) • More suited for small molecules separation	• Difficult and time consuming fabrication procedures; • Trouble to control full preparation process; • Time consuming post modification once silica monolith generally cannot be used directly • Limited pH working range (2-8)
Hybrid silica-based	• Ease preparation process compared to silica monolith; • Less shrinkage during fabrication; • High column efficiency (≤267 000 N/m).	• Difficult to control full preparation process; • Possible deficient hydrolysis of Si-O-Si-C bonds; • Close pH working scope (pH 2–8); • Poor reproducibility and time-consuming preparation.
Hybrid polymer-based	• Functional groups at the surface, so modification can be avoided (more suitable for separation applications than silica hybrids); • Improved organic solvent resistance and mechanical properties.	• Swelling in organic solvents, with unwanted changes in pore architecture; • Mechanical instability mainly after repeated use.

Hybrid organic-silica monoliths, can be further split in hybrid silica-based and hybrid polymer-based monoliths, being the former (the one attracting more attentions) usually prepared by sol–gel process from silica precursors containing organic groups, and the latter, prepared by polymerizing monomers. So, generally they can be prepared by i) covalent bonding, ii) non-covalent bonding between organic and inorganic portions, or iii) modifications on pure inorganic based-monoliths[82,80]. Despite hybrid monolith flexibility, service longevity, exceptional biocompatibility, mechanical stability, ease of preparation and design at molecular level, the limitations they entail (Table 1.4.) have slowed its preferential use process[82,80].

1.1.2. Surface Modification in Monoliths

Multiple approaches have been developed over the years, and are now accessible for the preparation of various functionalised monoliths[48,83,12,84]. The simplest, and possibly the most straightforward methodology to tailor monoliths' surface chemistry is just by choosing the suitable monomers that possess the desired functional groups (ionic, polar, non-polar, zwitterionic, etc.), once these groups are going to be exposed on the surface of the monolith after its preparation[48,83]. Nevertheless, every time a new monomer system is employed there is a need of polymerization process *de novo* optimization so that a monolith with the desired properties is attained; however this could end in a dull experimental procedure. Moreover as both monomers and crosslinkers become part of the final structure part of functional monomers added will be buried on the polymer bulk and not exposing its functional groups on the surface of the monolith for reaction[48,12]. Additionally proteins attachment on surface is virtually impossible through this strategy due to proteins denaturation into casting solution. Thus besides this simple but limited approach, plethora strategies were developed to make possible the tailoring of monolith surface functionality as user pleases[48,83,12,84]. One approach, less direct but perhaps more convenient, comprises the functionalization of a pre-formed monolith by post-preparation modification of reactive groups protruding from its surface. This type of modification, where each single reactive site provides one new functionality, allows the non-dependent optimization of bulk monolith properties and surface chemistry, enabling a onetime optimization of the monolith in question. The post-preparation modifications comprise the reaction of functional reagents with material surface groups (in case of silica-based monoliths it is first required the introduction of reactive sites or anchor groups for further incorporation of functionality to be accomplished); monomer/polymer chains grafting to or from monolith surface; dynamic or static coating in case of polymeric monoliths, and permanent or semi-permanent coating in case of silica-based monoliths. It is noteworthy that grafting strategy is frequently used to increment the ligand density (thus binding capacity) and also to improve hydrophilicity of column surface, to minimize non-specific interactions between analyte and monolithic media[48]. However beyond copolymerization and post-preparation modifications (covalent immobilization) monoliths can also be modified by entrapment or bio-specific adsorption of ligand[85]. These methodologies are reviewed in some comprehensive works[51,12,83].

To these traditional methodologies used to tailor monolith surface chemistry, new surface functionalities can be afforded via attaching nanoparticles with a broad range of properties on monolith surface. These nanostructures (silica, silver, gold, metal oxides or polymers-based particles, or even carbon nanotubes) have been employed to enhance parameters as selectivity, chemical stability, and efficiency of 3D monolithic structure in gas and liquid chromatography, electrophoresis, and solid-phase extraction[77,76].

1.2. Motivation and Aim of the Work

Monoliths show an attractive potential towards separation, especially of biomolecules. Moreover the astonishing growth of biopharmaceutical industry over the last decade denounce the urge for the development of novel, productive and efficient methods of purification, namely chromatographic matrices, once chromatography is the most widespread used and efficient purification approach nowadays.

The present work can be divided in two main parts. In a first approach a screening of materials processed by cryogelation was made in order to develop suitable monolithic structures for adenovirus purification. All structures were characterized physically and chemically. In the end three monolithic materials were elected, analysed morphologically and tested for binding adenovirus type 5 (Ad5).

In a second approach a monolithic structure was used for the first time as solid-phase platform for the synthesis of a small synthetic ligand specific for Green Fluorescent Protein (GFP). For this it was used an existing monolith previously developed in our lab by cryogelation. The matrix was characterized physically, chemically and morphologically before and after each step of the synthesis protocol to evaluate the presence or not of significant changes on the support during the process. Finally the functionalized affinity support was tested towards the target.

In the two approaches iron oxide magnetic nanoparticles (MNPs) were synthesized and embedded in the selected monoliths. The respective physical and morphological characterization was performed and compared with the respective plain supports in order to analyse the changes triggered. The MNPs modified monoliths were analysed regarding its performance on bioseparation of the protein in study upon external field exposure or not.

In brief, this work objective is the preparation of a biocompatible, biodegradable, robust, and efficient monolithic material, with minimal environmental footprint, to purify biomolecules.

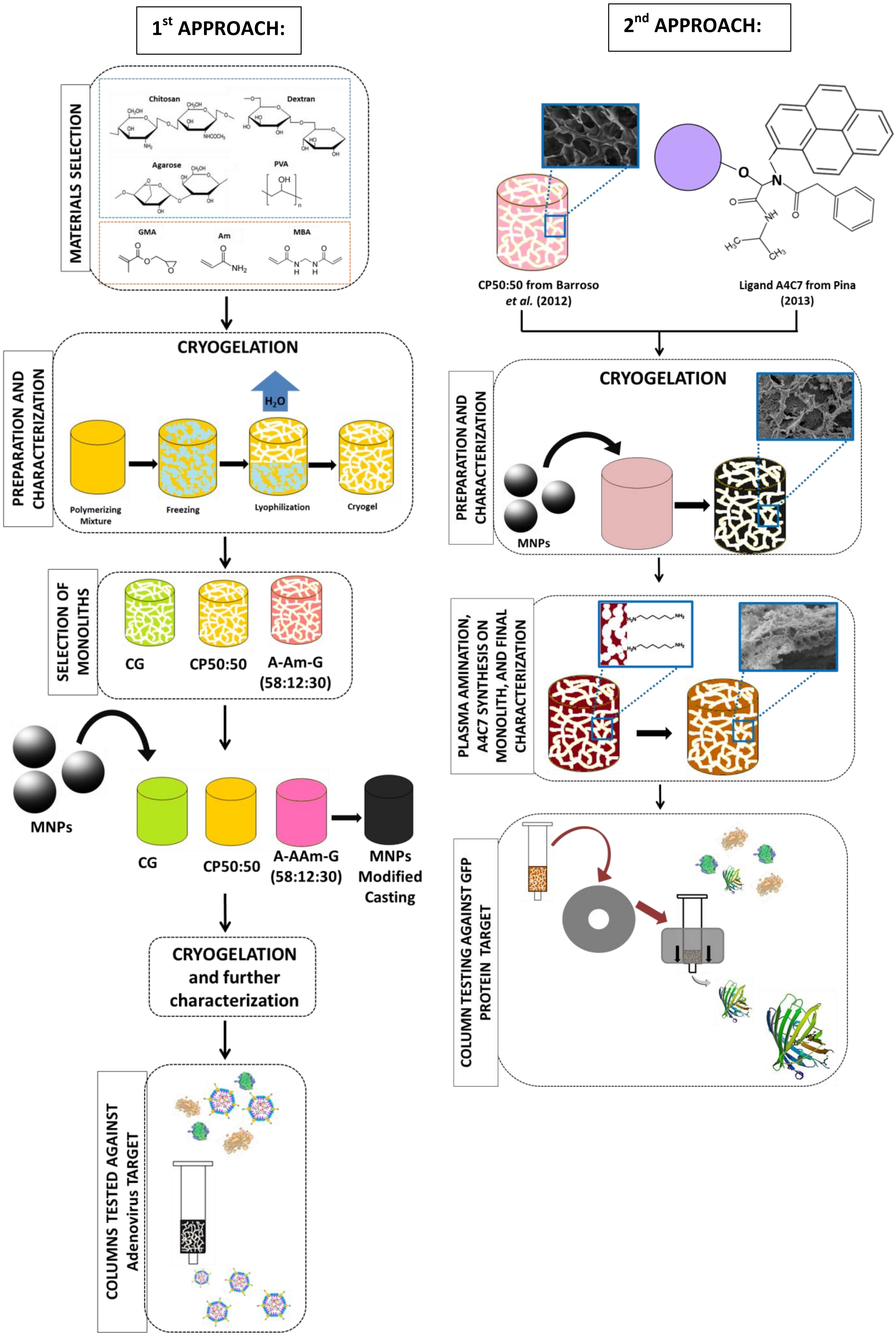
1st APPROACH:
2nd APPROACH:
MATERIALS SELECTION
Chitosan
Dextran
Agarose
PVA
GMA
Am
MBA
CRYOGELATION
PREPARATION AND CHARACTERIZATION
H2O
Polymerizing Mixture
Freezing
Lyophilization
Cryogel
SELECTION OF MONOLITHS
CG
CP50:50
A-Am-G (58:12:30)
MNPs
CG
CP50:50
A-AAm-G (58:12:30)
MNPs Modified Casting
CRYOGELATION and further characterization
COLUMNS TESTED AGAINST Adenovirus TARGET
CP50:50 from Barroso et al. (2012)
Ligand A4C7 from Pina (2013)
CRYOGELATION
PREPARATION AND CHARACTERIZATION
MNPs
PLASMA AMINATION, A4C7 SYNTHESIS ON MONOLITH, AND FINAL CHARACTERIZATION
COLUMN TESTING AGAINST GFP PROTEIN TARGET

Figure 1.2.- Schematic depiction of research approaches followed in present work.

2 EXPERIMENTAL

2.1. Materials

2.1.1. Chemical Compounds

Chitosan (75-85% deacylated, medium Mw), dextran (from *Leuconostoc mesenteroides*, Mw ≈150,000), acrylamide (AAm, for electrophoresis, purity ≥99%), poly(vinyl alcohol) (PVA, 99.0-99.8%(mol) hydrolysed, Mw 89,000-98,000), glycidyl methacrylate (GMA, 97%), 1,6-hexanodiamine 98%, N,N-dimethyl formamide (DMF, purity ≥99.8%) , phenylacetic acid 99%, iron (III) chloride hexahydrate (purity ≈98.0-102%), iron (II) chloride tetrahydrate (purity ≥99.0%), β-mercaptoethanol (purity ≥99.0%), phenol (unstabilized, purity ≥99%), potassium cyanide (purity ≥96.0%), pyridine (purity ≥99%), glutaric dialdehyde solution 50 wt% in water, silver nitrate (purity ≥99.0%), 1-pyrenemethylamine hydrochloride (purity 95%), isopropyl isocyanide (purity ≈97%), glycerol (purity ≥99.5%), ethylenediaminetetraacetic acid (EDTA) (purity ≥98.5%), bichinchoninic acid (BCA) kit and phosphate buffered saline tablet (PBS) were supplied by Sigma-Aldrich.

Ammonium persulphate (APS, purity ≥98%) and N,N,N′,N′-tetramethylethylenediamine (TEMED, purity ≈99%), methanol (purity ≥99%), bromophenol blue sodium salt and 2-propanol were purchased from Roth.

N,N′-Methylenebisacrylamide (MBAAm, purity ≥98%), ninhydrin (purity ≥99%), ammonium hydroxide (purity ≈25%), maleic acid (purity ≥98%) and 1,10-phenanthroline 1-hydrate (purity ≥99.0%) were acquired from Fluka.

Glacial acetic acid (purity ≥99,7%) was purchased from Fisher Chemical.

Bacteriological Agar powder was acquired from HIMEDIA.

β-D-1-Thiogalactopyranoside (IPTG), luria broth (LB), agarose (electrophoresis grade), ampicillin, glycine ultrapure for molecular biology, NZYMiniprep kit, tris(hydroxymethyl)aminomethane (Tris) Base ultrapure for molecular biology, and Greensafe were acquired from NZYTech.

Sodium citrate dihydrate (purity ≥99%) was supplied by Merk.

Absolute ethanol (purity ≥99.9%) was purchased from Scharlau.

Glycine (98% purity) and hydroxylamine hydrochloride (97% purity) were obtained from Acros.

Sodium hydroxide, hydrochloric acid 37%, ethylene glycol and sodium chloride were supplied by Panreac.

The 30% acrylamide/bisacrylamide solution 37:5:1, sodium dodecyl sulphate solution 10% (SDS, 161-0416) and the Silver Stain Plus Kit (fixative enhancer concentrate, silver complex solution, reduction moderator solution, image development reagent and development accelerator reagent) were purchased from BIO-RAD.

The Coomassie Plus (Bradford) assay kit was supplied by Thermo Scientific.

Nitrogen and argon were provided by Air Liquide.

2.1.2. Biochemical Reagents

Albumin from bovine serum (BSA, purity ≥98%) was purchased from Sigma. Recombinant green fluorescent protein rTurboGFP (FP552-Evrogen) was acquired from Biocat GmbH. The plasmid pET-21c containing the DNA fragment encoding for GFP was synthesized and subcloned by Geneart™ (Germany). Competent cells NZY5α and BL21(DE3), DNA marker ladder III and low molecular weight protein marker were purchased from NZYTech.

DNaseI was aquired from Roche.

Ad5 virions 10 times concentrated and 5 times diafiltrated (21st February DM/CP) was kindly produced and manipulated by Dr Cristina Peixoto's laboratory on ITQB-UNL/IBET, Portugal.

2.1.3. Equipment

Stirring of the casting solutions was performed using Dragon LAB MS-H-Pro stirring plates.

The lyophiliser used was a Telstar cryodos-50.

For the swelling tests, growing assays, GFP expression, A4C7 ligand synthesis, and BCA assays it was used an IKA KS 4000 i control incubator shaker.

The uniaxial compression measurements were attained using the compressive mode of tensile testing equipment (MINIMAT firmware v.3.1).

An Hitachi S 2400 equipment was used for SEM micrographs acquisition.

The amination of monoliths was performed in a Plasma system FEMTO, version 3, Diener Electronics.

Hydrodynamic diameter and Zeta Potential measurements of MNPs samples were accomplished in a Malvern Dynamic Light Scattering (DLS) Zetasizer Nano ZS.

For magnetite assays the pH of solutions was adjusted in a Hanna Instruments microprocessor-based pH/mV/°C bench meter.

Flux measurements with and without magnet, non-specific interactions column testing with Ad5 and GFP, and screening assays between A4C7 ligand functionalized monolith and GFP were achieved in 0.9x6.5 cm Varian columns. On virus assays all columns were equipped with a frit from Varian.

The Fluorescence Microscope Olympus BX51 with an objective U-RFL-T (40x amplification) and U-MWB (λ_{exc}= 460-490 nm; λ_{em} = 515-570 nm), an U-RFL-T lamp, an objective Uplam FLN, and Cell F software was employed to confirm the presence of the ligand into the functionalized supports.

The isolation of pET-21c plasmid was fulfilled with Sigma 3-18K centrifuge. The plasmid DNA (pDNA) was evaluated through agarose gel electrophoresis, by using a BIO-RAD electrophoresis chamber with BIO-RAD PowerPac Basic power supply. Gel visualization was possible with KODAK 1D 3.6 software through UVITEC Transilluminator. For pDNA concentration determination samples were introduced in NanoDrop ND-1000 v3.5.2 spectrophotometer.

E.coli cells grown were collected with Herceus Multifuge X3R centrifuge (Thermo Scientific), lysed with Thermo Scientific French press and ultracentrifuged in a Beckman Optima LE-80 (rotor 45TI). For the SDS-PAGE gels electrophoresis it was used the BIO-RAD Mini-Protean Tetra System, for gel revelation it was used the KODAK 1D 3.6 software through UV UVITEC Transilluminator.

Absorbance readings were performed in Greiner 96-well UV half area, or Sarstedt 96 well flat transparent microplates (colorimetric assays), and fluorescence readings were performed in brand black immunograde 96-well microplates (VWR). The spectrophotometric and spectrofluorometric measurements were conducted on a Tecan's microplate reader Infinite F200 with respective brand filters (λ_{exc}=485–505 nm; λ_{em}=535-560 nm, 492 nm and 560 nm) with exception for E. coli growth monitoring once it was used a spectrophotometer PerkinElmer Lambda 35 UV/Vi Spectrometer (600 nm).

Nanosight nanoparticle tracking analyser was used toanalyse samples from virus screening assays.

Length measurements were performed with a SOMET vernier caliper or a ruler.

2.2. Methods

2.2.1. Monolith Preparation

Monoliths preparation by cryogelation process accompanied by freeze-drying method involved the former brewing of distinct casting solutions, with different composites and compositions. Table 2.1. shows in detail the composition of the casting solutions that were prepared.

Table 2.1.- Casting solutions processed for monoliths preparation. All casting solutions were formulated with 3 mL of distilled water per monolith. Polymers and/or monomers content in every 2.9%(w/w) casting solution is 90mg. Conversely in PVA:GMA 79:21%(w/w) casting it is 101mg, in AAm:MBAAm:GMA 95mg/210mg, and in agarose:AAm:GMA and dextran:AAm:GMA 142 mg/172 mg.

Materials	*Proportions %(w/w)*	*Concentrations %(w/w)*	*Freezing Temperature (°C)*
Chitosan	100	2.9	-20 and -80
		2.0	-20 and -80
Chitosan:PVA	50:50	2.9	-20 and -80
	33:67	2.9	-20 and -80
Chitosan:GMA	89:11	2.9	-20 and -80
PVA:GMA	79:21	3.3	-20 and -80
	89:11	2.9	-20 and -80
AAm:MBAAm:GMA*	78:17:5	3.1	-20
		6.5	-20
Agarose:AAm:GMA	56:7:37	4.5	-20
	58:12:30	5.4	-20
Dextran:AAm:GMA	56:7:37	4.5	-20 and -80
	49:14:37	4.5	-80
	58:12:30	5.4	-20 and -80
	52:17:30	5.4	-80
PVA	100	2.9	-20 and -80

*MBAAm is used not only as a "crosslinker" but also as a monomer.

Chitosan-based casting solutions were prepared based on a recent work[27] with little increment on "crosslinker" (from 2%, in relation to polymers and/or monomers mass, to 5.6%). In case of sole chitosan-based solutions two types were prepared, based on the polysaccharide concentration in the 3 mL final solution (2.0 and 2.9%(w/w)). Blended solutions of chitosan with GMA and PVA in various ratios were also brewed. Chitosan was varied in a range of 33-89% (w/w), PVA in a range of 0-67%(w/w) and GMA in a range of 0-11%(w/w). It is noteworthy that all chitosan-based casting solutions were prepared with 3 mL of acetic acid acidified water 1%(v/v), all the remaining solutions are prepared with 3 mL of distilled water.

Regarding PVA:GMA-based solutions PVA varied between 79-89%(w/w) and GMA between 11-21%(w/w). A 100%(w/w) PVA casting solution was also prepared and maleic acid was used as the crosslinker in 2%(w/w).

For the preparation of supermacroporous polymeric matrices acrylamide, agarose and dextran-based castings were also elaborated. With respect to acrylamide monoliths two casting types were prepared varying composites content in solution from 3.1-6.5%(w/w). Monomers and crosslinker ratios for both casting types are based on a previously described work[9]. For Agarose-based monoliths acrylamide content varied from 7-12%(w/w), GMA from 30-37%(w/w) and agarose from 56-58%(w/w). For Dextran-based monoliths acrylamide content varied between 7-17%(w/w), GMA between 30-37%(w/w) and dextran in a range of 49-58%(w/w).

All casting solutions were formulated into individual 1.4x4.9 cm plastic tubes where they were submitted to different temperatures and stirring velocities, depending on their viscosity and solubility in water. PVA-based solutions were subjected to stirring rates of ~500 rpm and temperatures of 85-90°C. Chitosan-based solutions, depending on their chitosan content, have been submitted to different stirring rates. In fact, the ones with uppermost chitosan fraction required a superior rate and a higher stirring temperature (70-85°C) due to casting higher viscosity. Dextran and acrylamide-based solutions were stirred at room temperature and in contrast agarose-based solutions were subjected to a stirring temperature of 40°C. The objective of stirring was to efficiently homogenize the casting solutions for further freezing and lyophilisation procedures. Thereunto globally the stirring rate varied between 300-800rpm, the stirring temperature between 20-90°C and stirring time between 1-3 days. When homogenized initiator (APS (42 µl)) and catalyst (TEMED (23 µl)), were added to promote the "crosslinking" and/or polymerization process (all solutions were ressuspended or mingled to assure the maximum contact of TEMED and APS with solutions composites). While the "crosslinking" process were performed at 0°C during 30 minutes for chitosan-based and PVA:GMA solutions, for dextran ones it occurred during 30/45 minutes. In case of agarose-based and AAm:MBAAm:GMA solutions this process occurred for 30 minutes under stirring, but at room temperature. For 100%(w/w) PVA the initiator and catalyst are added under stirring at 90°C and the reaction was continued for 90 minutes.

Finally all solutions were frozen at -20°C and/or -80°C during 24h and then lyophilized for another 24h or until dry state.

2.2.1.1. Smart Monolith Preparation

Some specimens from **2.2.1.** were prepared in the presence of magnetic nanoparticles. The same quantity of "crosslinker", polymers and/or monomers was dissolved not on 3 mL distilled water but on 2 mL. The remaining 1 mL was added as MNPs solution (24-67 mg/mL). Complete homogenization took 3-4 days to be accomplished.

2.2.1.1.1. MNPs Synthesis

Magnetic nanoparticles were synthesized at room temperature by co-precipitation method of $FeCl_3$ and $FeCl_2$ salts with a molar ratio of 2:1, as described elsewhere[86]. The procedure implies mixing 115 mL of distilled water with 60 mL of ammonia hydroxide 25% and further nitrogen gas inertization of vessel cell (~15 minutes) under stirring (1500 rpm). Hereafter a freshly prepared iron solution (5.438g of $FeCl_3.6H_2O$ plus 2.0g of $FeCl_2.4H_2O$ in 25 mL of distilled water) was added dropwise to the N_2 purged ammonium solution. Then the reaction was extended for 2 hours under maximum stirring (2000 rpm) and inert atmosphere (N_2 ongoing bubbling). Once completed the synthesis, ammonium hydroxide traces were completely removed from MNPs solution by washing several times with distilled water using magnetic field for separation. MNPs solution concentration was measured by subtracting the weight of empty flask from a flask with overnight dried MNPs solution.

2.2.1.1.1. 1. MNPs Characterization

MNPs physico-chemical properties (hydrodynamic diameters, polidispersity and zeta potential) were determined by DLS. For these analysis samples with a concentration of 0.05 mg/mL in distilled (pH5.8) water were prepared.

2.2.1.1.2. MNPs Leaching Assessment

The amount of iron-oxide particles released during the A4C7 ligand synthesis or during screening assays was determined by a colorimetric assay, the magnetite test. Its principle relies on magnetite ionization to Fe^{3+} ions under acidic conditions, then its reduction to Fe^{2+} by hydroxylamine hydrochloride and finally its reaction with 3 molecules of 1,10-phenantroline with $Fe(o\text{-}Phen)_3^{2+}$ complex formation, a characteristic orange-red coloured complex absorbing at 509nm[87]. Colour intensity is directly proportional to Fe^{2+} amount present in solution (Figure 2.1.). The sample analysis procedure to estimate iron release involved, as described elsewhere[88], the addition of 100 µl sample, 500 µl of concentrated HCl and 500 µl of 1.44M hydroxylamine to a test tube and solutions rest in the dark (15 minutes). Then 1 mL of 0.0126M o-phenanthroline and 250 µl of 12M NaOH were added, and finally the pH was adjusted to ~4.0 with 0.5M sodium citrate buffer. The absorbance of 200 µl samples was read at 492 nm. A calibration curve was constructed with several concentrations of Fe_3O_4 in distilled water subjected to same treatment.

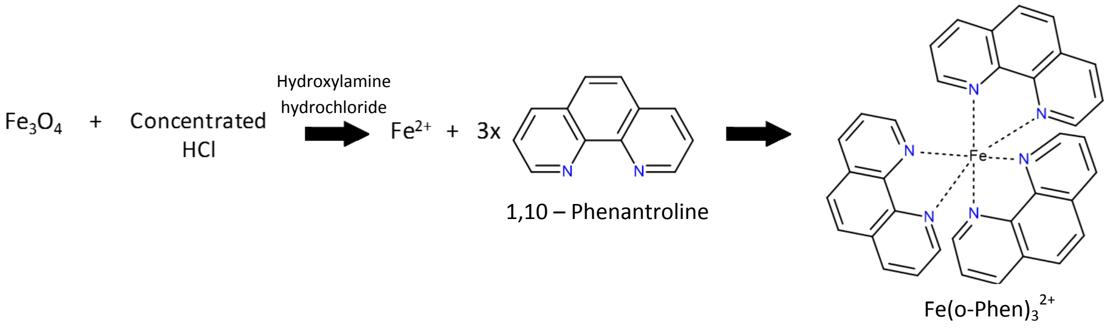

Figure 2.1. – Reaction mechanism in the base of Magnetite Method.

2.2.2. Monoliths Characterization – Chemical Properties

Each one of three chopped samples from each specimen with ~0.7 cm height was immersed in 30 mL flasks, with 10 mL of distinct pH solutions: pH 3, 7.4, or pH 11. The submerged sample behaviour and macroscopic modifications were recorded and registered during two whole weeks.

To determine the water uptake ability of materials at different pHs, swelling tests with dynamic character were performed. Dry samples of each monolith specimen were weighted (w_{dry}) and immersed in 30 mL flasks with 10 mL of PBS. At specific time intervals, each sample was removed from swelling medium, slightly wiped with soft tissue to remove excessive water at the surface, and weighted (w_{wet}). Following 24 hours, the scaffold samples mass have reached a plateau value and were conveyed to acetate buffered saline solution 0.1M, pH5. After further 24 hours, the polymeric matrix mass have reached another plateau value, and samples were then transferred to a new PBS solution. After another 24 hours one more plateau value was reached and each sample was conveyed to the last swelling medium, a fresh pH5 acetate buffer, and was left for the last 24 hours to reach the last plateau of the study. Therefore during one week the dynamic swelling and shrinking was studied. The procedure occurred at ~28°C under stirring (100rpm). Hereupon, the swelling degree or swelling ratio (W) of the studied monoliths was defined as the ratio of weight increase to initial weight, as stated by the following equation (1):

$$W(\%) = \left(\frac{w_{wet}-w_{dry}}{w_{dry}}\right) \times 100 \qquad (1)$$

Where w_{wet} denotes weight of monoliths after immersion onto swelling medium, and w_{dry} stands for weight of monoliths before immersion onto swelling medium[89,90].

Swelling kinetic analysis was made by measuring water uptake capacity over time (≈25°C) through a conventional gravimetric procedure[91]. Monolith sections were dried in the oven (60°C), weighted and plunged in deionized water. Samples were weighted at the first two halves a minute and then per minute weightings were executed until 10 minutes completion. The water uptake capacity was finally determined (2)[91]:

$$W_u(\%) = \left(\frac{w_t-w_{dry}}{w_e}\right) \times 100 \qquad (2)$$

Where w_u denotes water uptake capacity, w_t the wet weight at particular time intervals, and w_e the water weight into the swollen gel at swelling equilibrium.

2.2.3. Monolith Characterization – Morphological and Mechanical Properties

The water fluxes were determined at ~22°C under atmospheric pressure. All samples were mounted in a 0.64 cm^2 effective area and 6 cm height chromatography column. This column in turn is seized by a clamp added by a holder and supported in a stand. The dry sample inside the column is wetted with 1 or 2 mL of distilled water depending on its swelling capacity, and then the time that 1 mL of clean distilled water lingers to cross the column all the way out is recorded three times with each three samples of the same specimen[27].

Regarding dry and wet apparent densities, their values were determined through the ratio of dry and wet weight respectively with respect to the corresponding volume[92]. Regarding monolith true and relative densities, they were determined by equations (3) and (4) as described elsewhere[93]. Height (100%) was set as 2 cm. Equation (5) gives information about pore volume[94].

$$\rho_{true} = \frac{mass_{monolith}}{volume_{polymer}} = \frac{mass_{monolith}}{\left(\frac{m_{pol\,1}}{\rho_{pol\,1}} + \frac{m_{pol\,2}}{\rho_{pol\,2}} + \cdots\right) \times \, height\, fraction} \tag{3}$$

$$\rho_{relative} = \frac{\rho_{apparent}}{\rho_{polymer}} = \frac{\rho_{apparent}}{\left(f_{pol\,1} \times \rho_{pol\,1} + f_{pol\,2} \times \rho_{pol\,2} + \cdots\right) \times height\, fraction} \tag{4}$$

$$V_p = \frac{1}{\rho_{apparent}} - \frac{1}{\rho_{true}} \tag{5}$$

The density corresponds to ρ (g/cm^3), polymer fraction to f_{polx} (%(w/w)), and total pore volume to V_P (cm^3/gsupport). Regarding densities and V_P, although the method used is simple and fast, it comprises a rough estimation of its value as significant errors can be made during determination of monolith volume[92]. For monoliths designed for GFP protein purification, density was measured in PBS solution. Weighings were done at room temperature.

Specimens' porosity was estimated applying a fluid displacement measurement method, a modified Archimedes principle technique based on published methods[95,92]. First the volume of cylindrical samples (~0.5 cm height) was registered ($V_{monolith}$). Then each individual sample was immersed in a graduated cylinder filled with ~10 mL ethanol (displacement liquid), previously weighted (w_1). Then a series of brief evacuation-repressurization cycles were performed to force ethanol into monolith pores. This cycling is continued for ~15 minutes and then the sample is kept under vacuum until it reaches the bottom of the graduated cylinder, no air bubbles are seen emerging from the support neither in its surface. The procedure can take just one hour or few days depending on monolith specimen. At last, the ethanol-impregnated scaffold is removed from graduated cylinder and the weight of ethanol left in the cylinder is set as w_2. See equation (6).

$$Porosity\ (\%) = \frac{pore\ volume}{monolith\ volume} \times 100 = \left[\frac{\frac{w_1 - w_2}{\rho_{ethanol\ 20°C}}}{V_{monolith}}\right] \times 100 \qquad (6)$$

To examine and study the mechanical response of supports, all specimens were subjected to macro-scale mechanical experiments, specifically uniaxial compression. Those analyses were conducted at room temperature using tensile testing equipment. Unhewn prepared monoliths are sliced in cylindrical chops with 0.75-1.20 cm in diameter. The distance between clamps is determined by specimens' length (0.53-1.30 cm). The motor speed was set at 1 mm/min and the maximum displacement of compression varied between 5-13 mm depending on sample width, a full scale load of 20N was used. These measurements were performed with dry and hydrated samples. As such, for testing wet supports, samples of each specimen are soaked in distilled water (or PBS in case of monoliths towards GFP purification) for 5 minutes, rinsed and then set on the apparatus.

It is obtained an assembly of load versus compression charts, which are converted to stress versus strain curves applying equations (7) and (8)[27]:

$$Stress = \sigma = \frac{F}{A} \qquad (7)$$

$$Strain = \varepsilon = \frac{\Delta l}{L} \qquad (8)$$

Here F corresponds to the applied force, A to the cross-sectional area, Δl to the change in length and L to clamps distance. The compression modulus is then calculated as the slope of the initial linear portion of the stress-strain curve.

Monolithic morphology was accessed by scanning electron microscopy (SEM). An accelerating voltage was set to 15 kV. All samples were frozen and fractured in liquid nitrogen for cross-sectional analysis, mounted on aluminium stubs using carbon discs (D-400, Neubaeur Chemikalien), and gold-coated by sputtering before analysis.

Then micrographs were examined using the image analyser software ImageJ® 20 to determine the average pore size diameter[96].

In case of magnetic monoliths, to evaluate their magnetic response ability, two monolith cylindrical pieces were chopped and its distortion and shape recovery were monitored during 1 hour with a ruler help. Four different magnetic fields were tested: 0.25T, 0.5T, 0.53T and 1.5T.

2.2.4. Screening of Non-Functionalized Monoliths with Ad5 Virus

To check for non-specific interactions between Ad5 virions and the different monolithic materials screenings assays were performed in ITQB-UNL/IBET, Portugal, under Dr. Cristina Peixoto supervision. All columns were first washed and regenerated alternating five times 2 mL of regeneration buffer (1M NaOH 30% isopropanol) with 2 mL of distilled water, then they were equilibrated with 20mM Tris-base 150mM NaCl pH8 buffer (5 mL) and stored in the same buffer. The assay itself compromised the loading of each column with 1 mL of previously 3x diluted Ad5 particles (~1.45×10^{11} TP/mL) followed by its washing with 2 mL of elution buffer (20mM Tris, 150mM NaCl, pH8). Virus recovery was calculated (9)[97].

$$Recovery\ (\%) = \frac{Eluted\ Sample}{Loading} x100 \qquad (9)$$

2.2.5. Production of GFP Containing-Crude Extracts

The standard procedure used for large scale production of GFP is deeply summarized on Figure2.2. and is explained in detail in the following sections.

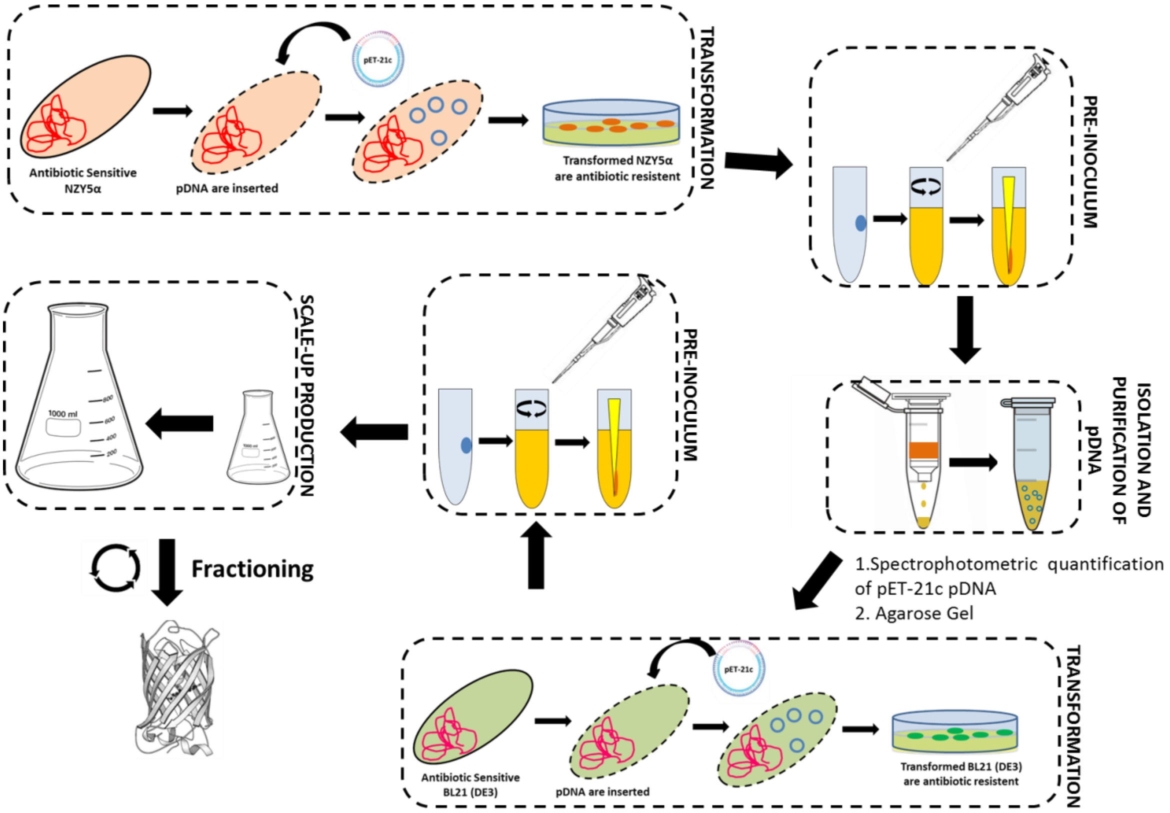
pET-21c
Antibiotic Sensitive NZY5α
pDNA are inserted
Transformed NZY5α are antibiotic resistent
TRANSFORMATION
PRE-INOCULUM
ISOLATION AND PURIFICATION OF pDNA
1.Spectrophotometric quantification of pET-21c pDNA
2. Agarose Gel
pET-21c
Antibiotic Sensitive BL21 (DE3)
pDNA are inserted
Transformed BL21 (DE3) are antibiotic resistent
TRANSFORMATION
PRE-INOCULUM
SCALE-UP PRODUCTION
1000 ml
Fractioning

Figure 2.2. – Diagram of summarized GFP large scale production protocol.

2.2.5.1. Preparation of LB Medium and LB Agar Plates with Ampicillin

For the bacterial culture it was prepared the LB medium by adding 20 g to 800 mL MiliQ water. The LB agar involved the dissolution of 7.5 g of LB and 4.5 g agar in 300 mL of MiliQ water in a Schott flask. Afterwards, the LB and LB agar were autoclaved (120°C, 20 minutes). Later, LB agar medium was cooled to ~50°C (avoiding medium solidification) and 500 µl of 100µg/mL ampicillin were added under sterile conditions. The importance of cooling down LB agar medium before antibiotic addition is connected to its degradation at high temperatures[98]. After ampicillin addition, the medium was spread in sterile Petri dishes (~20 mL of medium per Petri dish) under sterile conditions. After solidification all plates were kept at 4°C wrapped in aluminium foil[98]. LB liquid medium was kept at room temperature.

2.2.5.2. Transformation of pET-21c Plasmid in NZY5α Competent Cells

The pET-21c plasmid, synthesized by Geneart™ carries the gene that encodes for GFP protein. For transformation of the *E. coli* NZY5α competent cells with pET-21c supplier instructions (NZYTech) were followed. So first NZY5α cells (60 µl) were thawed on ice, and then mingled with 10 µl of plasmid solution, gently mixed and incubated on ice for 30 minutes. Subsequently, cells endured a 30 second and 42°C heat-shock in a water bath followed by an immediate plunge on ice for 2 minutes. Afterwards, 940 µl of LB medium were added to the cells and the final solution was shaken during 1 hour (210rpm, 37°C). Later 50 µl and 100 µl of the transformed cells volume were spread on LB agar plates containing ampicillin antibiotic. In order to concentrate the cells, the remaining volume (860 µl) of cell culture was centrifuged (1850*xg*, 5 minutes) and 700 µl of the supernatant medium was discarded. The concentrated cells were ressuspended in the remaining supernatant volume and spread on LB agar plates that were incubated overnight (37°C). Regarding negative and positive controls they were prepared with 20 µl of NZY5α cells and without any plasmid addition or adding 1 µl of pNZY28 plasmid (0.1ng/µl), respectively.

2.2.5.3. Isolation and Purification of pET-21c pDNA

The isolation and purification of pET-21c pDNA whole procedure began with the drawing up of three pre-inoculum test tubes: 2x pET-21c and a negative control. Each tube held 6 µl of ampicillin (100 µg/mL), 6 mL of LB medium and a single isolated colony of transformants (**2.2.5.2.**). For the negative control test tube no colony was included. All tubes were incubated overnight (210rpm, 37 °C). The isolation and purification itself was executed using NZYMiniprep kit and the supplier instructions were followed. As pET-21c is a low-copy number plasmid, showing low basal expression levels[99], cells and lysis buffers volumes were doubled for a more effective process. Thus procedure began with cell harvest after overnight growth: 6 mL of NZY5α cells culture were centrifuged (1850*xg*, 2 minutes) and then the supernatant was discarded. This was followed by a step of cell lysis: the obtained pellet was ressuspended with 500 µl of buffer A1 (RNase A) by vigorous vortexing, then 500 µl of buffer A2 (SDS, NaOH) were added, the solution was mingled gently by inverting the tubes ~8 times, and was then incubated at room temperature (4 minutes). After incubation, 600 µl of buffer A3 was added and solution was mixed by gently inverting the tubes ~8 times. Then to clarify the lysate the tubes were centrifuged (1850xg, 10 minutes*)* and the supernatant was poured onto a NZYTech spin column placed in a 2 mL collection tube to allow pDNA binding. The column was centrifuged (1850xg, 2 minutes) and the flow-through was forgone. Then it was time for silica membrane washing: 500 µl of pre-warmed (50°C) buffer AY were added into the column and centrifuged (1850xg, 2 minutes). The obtained flow-through was discarded. Then it was added 600 µl of buffer A4 (with previous ethanol addition) into the column and another centrifugation step followed (1850xg, 2 minutes). Once more the flow-through was discarded. Before pDNA elution silica membrane had to be dried. So NZYTech column was inserted into a new empty 2 mL collecting tube and centrifuged (1850xg, 3 minutes). Once dried the NZYTech column was placed into a clean 1.5 mL microcentrifuge tube for the first elution step to begin: addition of 30 µl of pre-warmed (65°C) MilliQ water at the central part of the tube, further incubation in a 37°C water bath (1 minute) and centrifugation (1850xg, 2 minutes) at room temperature. The first fraction of the eluted pDNA was then maintained at 4°C. This procedure was repeated for the second elution step although 50 µl of MilliQ water were added. Then the two eluted fractions were kept at -20°C for further usage.

2.2.5.4. Spectrophotometric Quantification of pET-21c pDNA

Through spectroscopic analysis it is possible to quantify the pDNA present in each eluted fraction obtained (**2.2.5.3.**) and to ascertain its purity. For that 1µl sample of 1st and 2nd elutions was placed onto the receiving fiber of NanoDrop Spectrophotometer. Then a spectrum scan between 220-280nm was realized with the direct obtainment of sample concentration and Abs_{260nm}/Abs_{280nm}, Abs_{260nm}/Abs_{230nm} ratios. In fact determination of DNA concentration is related with absorbance at 260nm, where for 1 cm path length the absorbance at 260nm equals the unit for 50µg/mL of double stranded DNA (dsDNA), as is stated by equation (10), being D the dilution factor[100]:

$$[dsDNA] = 50\,\mu g/ml\,xAbs_{260nm} \times D \qquad (10)$$

The DNA purity is given by the ratio Abs_{260nm}/Abs_{280nm} that should be ~1.8 in case of a pure DNA samples. Abs_{260nm}/Abs_{230nm} ratio is used as a secondary measure of nucleic acid purity; its values generally vary between 1.8-2.2[100].

2.2.5.5. Agarose Gel

For further examination of the two eluted fractions of pET-21c plasmid agarose gel electrophoresis was employed. This analysis comprised evaluation of DNA in terms of its conformation. In fact DNA can assume three different conformations: closed circle supercoiled form (SC), nicked circular form (NC) and linear form (LF) that will determine its mobility in the gel[101]. The DNA form that presents a higher electrophoretic mobility is SC followed by LF and finally NC. A 0.8% agarose gel was prepared by addition of 0.80 g of agarose to 100 mL of 1x TAE (Tris-acetate-EDTA) buffer pH8.5. For a 50x TEA buffer it was added 121g of Tris, 28.55 mL of glacial acetic acid, 50 mL of 0.5M EDTA (pH8.0) and distilled water up to 500 mL, pH was adjusted to 8.5, then the respective dilution was made for a 1x buffer. The Agarose and TAE buffer mixture was microwave heated (~2 minutes) until complete agarose dissolution. Then, the solution was shed in a proper container with a comb allowing complete solidification of agarose with creation of the desired number of wells. Samples were prepared adding 2 µl of each elution fraction in distinct eppendorfs plus 5 µl of loading buffer blue juice (65%(w/v) sucrose, 10mM Tris-HCl (pH 7.5), 10mM EDTA, and 0.3%(w/v) bromophenol blue). Same treatment was executed for DNA marker. After a spin down samples were added to the gel and the running was extended for 60 minutes, 100 V. Gel staining was performed within a solution of 11 µl of GreenSafe in 100 mL of 1x TAE buffer under gentle agitation (1h). Later the gel was photographed.

2.2.5.6. Large Scale Expression of GFP

2.2.5.6.1. Transformation of E. coli BL21(DE3) Competent Cells with pET-21c

E. coli competent BL21(DE3) cells were transformed with positive pET-21c clone as outlined in **2.2.5.2.** using the pDNA isolated and purified on **2.2.5.3.**. The negative control was performed without plasmid addition and the positive one by adding 1 µl of pUC19 plasmid to 20 µl of cells.

2.2.5.6.2. Cell Growth and Expression of GFP

The large scale production of GFP requires two inocula. First 1L of LB medium was formulated (**2.2.5.1.**) in a 2L erlenmeyer. Then a pre-inoculum was prepared in a sterile test tube by addition of 6 mL LB, 6 µl ampicillin (100µg/mL) and a single colony from the recently transformed BL21(DE3) cells (**2.2.5.6.1.**). Negative control received no colony. Both preparations were kept for 7 hours (37 °C, 210 rpm) in orbital shaking.

Later 50 mL LB, 50 µl of ampicillin (100µg/mL) and 1 mL of pre-inoculum were added to a 250 mL erlenmeyer with posterior overnight incubation (37°C, 210 rpm) (inoculum was prepared). Then the large scale expression began by adding to the 1L of LB medium prepared, 1 mL of ampicillin (100µg/mL) and 10 mL of inoculum, keeping it with orbital shaking (220 rpm, 37°C). As according to small scale studies reported by Dr. Ana Pina[102] the optimal conditions for GFP production comprises addition of 1mM IPTG (inductor) at OD_{600nm} 0.6-0.8, and orbital shaking (220 rpm, 37°C) during 22 hours, the large scale expression was conducted with the mentioned conditions. So, after preparation of the last inoculum (in 2L shaken flask) cellular growth was monitored by optical density measurements. Once reached an OD_{600nm} 0.6-0.8, GFP expression was induced with 1 mL IPTG. So during growth and expression, ~5 mL aliquots of cell culture after 2 hours, 2h45min, 3h15min, 3h30min, 3h50min, 4h05m, 6h05min, 8 hours, 9h05 and 22h30m inoculation were taken and analysed optically and/or fluorimetrically and by SDS-PAGE. The induction occurred after 4h05min growth.

2.2.5.6.3. SDS-PAGE Analysis for Evaluation of GFP Production

To evaluate GFP amount produced during time course there was a need to normalize sample volumes in order to introduce a fair quantity of cells in each one. Normalization was applied according to the ratio between 1.2 and respective optical density value of each sample. Then normalized volume samples were centrifuged (1850*xg*, 5 minutes). Supernantant was thrown out and 15 µl of sample buffer (5 mL of 0.5M Tris-HCl pH 6.8, 2 mL of 100% glycerol, 4 mg Bromphenol blue sodium salt, 8 mL of 10% SDS, 1 mL β-mercaptoethanol and distilled water up to a final volume of 20 mL) was used to ressuspend the pellet. After spun down samples were dipped in a boiling water bath (2 minutes). The protein marker (5 µl) was subjected to the same treatment but 5 µl of sample buffer were added. After this procedure all samples, including marker were placed in a 12.5% acrylamide gel. This whole gel assembles two different gels: a bottom one (running gel) and a top one (stacking gel). Each gel was prepared according to a standardized protocol (table 2.2.).

After addition of running gel solution to the glass plates casting moulding ~1 mL of 2-butanol 99% was added on top of it promoting a flat surface generation. Then the gel was polymerized for 30 minutes. When finished the butanol solution was removed and the gel washed with distilled water. Afterwards the 5% stacking gel was formulated and polymerized (30 minutes) on the top of the former along with the moulding wells comb. The running apparatus was then assembled, electrophoresis buffer (0.25M Tris Base, 1.92M Glycine, 0.1% SDS pH 8.3, 10x diluted) added and 15 µl samples were pipetted to each well to finally run at 150 V, 250 mA (1h). The staining (1 g Coomassie Blue, 15 mL glacial acetic acid, 90 mL methanol and distilled water up to 200 mL) was 30 minutes long and destaining (75 mL glacial acetic acid, 450 mL of methanol and distilled water up to 1L) occurred overnight.

Table 2.2. – Required volumes to prepare one 12.5% Acrylamide gel.

Reagents	*Running Gel Volume (ml)*	*Stacking Gel Volume (ml)*
Solution I (3M Tris-HCl, pH 8.8)	0.75	-
Solution II (0.5M Tris-HCl, pH 6.8)	-	0.45
Solution III (Acrylamide/Bisacrylamide) (30:0.8)	2.08	0.3
10% SDS	0.05	0.018
Distilled Water	2.1	0.94
10% APS	0.038	0.0135
99% TEMED	0.0025	0.002

2.2.5.6.4. Evaluation of GFP Amount by Fluorescence Measurements

The GFP flurescence of each sample collected at a precise time after induction was measured through addition of 200 µl of sample in each microplate well. The fluorescence was evaluated using $\lambda_{excitation}$=485 nm and $\lambda_{emission}$=535 nm and a gain of 41.

2.2.5.6.5. BL21(DE3) Cells Fractionation

Aiming the acquirement of a soluble GFP crude extract from the large scale expression, cells were crumbled and further subjected to some centrifugation steps. So, once protein expression is terminated cells culture was centrifuged (11000*xg*, 20 minutes, 4°C). Supernatant was disposed and pellet ressuspended on 10 mL PBS (10mM sodium phosphate, 150mM NaCl, pH7.4), the binding buffer required for screening assays. Then ressuspended cells underwent a series of freeze/thaw cycles weakening its membrane to consequently improve fractionation effectiveness. The disruption was a mechanical step executed by a French Press in which cells passes three times through a narrow valve under outer 1280 psi. Afterwards the lysate sample made contact with DNaseI (15 minutes) in order to reduce its viscosity, and was centrifuged at 4°C (11000*xg*, 15 minutes). The pellet fraction was ressuspended in 15 mL PBS and 500 µl stored for further SDS-PAGE and fluorimetric analysis. An aliquot of supernatant was also collected and the remaining further ultracentrifuged (42000rpm, 1h30m, 4°C). The resultant pellet was ressuspended in 26 mL PBS and 500 µl stored for further SDS-PAGE (**2.2.4.6.3.**) and fluorimetric analysis (**2.2.4.6.4.**). However, in the present case the aliquots volumes used for SDS-PAGE analysis were normalized according to the final volume of the samples after each step. Then, the normalized aliquot volumes from each step of cells disruption were mixed with 5 µl of sample buffer and then transferred to the respective well.

2.2.5.6.6. Soluble Crude Extract Quantification in terms of GFP and Total Protein Content

The quantification of GFP and total protein was assessed by GFP fluorescence and BCA colorimetric assay. GFP fluorescence enabled the quantification of GFP protein through fluorescence intensity measurements as described in **2.2.5.6.4.**. It is noteworthy that mentioned measurements required a calibration curve obtained through the measurement of different pure GFP concentrations within the range 10^{-6}-10^{-1}mg/mL. The quantification of total protein through BCA assay involved the creation of a calibration curve using BSA as standard protein. The range of concentrations was 0.2-1.0mg/mL. To perform the BCA assay, 25 μl of each sample (calibration curve and crude extract) was pipetted to each microplate well. Then, 200 μl of light green BCA working reagent formulated with mixing of 50 parts of reagent A with 1 part of reagent B was added to each wells. Then follows a 30 minutes incubation (37°C) finalized by samples absorbance measurement at 560nm.

2.2.6. Chitosan-based Monoliths Fuctionalization Towards GFP Protein

2.2.6.1. Monoliths Amination by Plasma Technology

The objective of this step was to fill the utmost surface of monolith with amine free groups. Thus, an oil bath was heated up (140-150°C) under stirring to ensure a 1,6-diaminohexane temperature on the whole flask of ~130°C. As 1,6-diaminohexane have a reduced vapour pressure (0.12 mmHg at 25°C[103], 1 mmHg at 43°C)[104] and only boils at 204-205°C at 1 atm[103] a proper preheating and system isolation were strongly required. Therefore aluminium foil was used to fully isolate all system i.e., the 1,6-diaminohexane flask and the tubing connecting the flask and plasma chamber. A heat gun was used (~180°C) to maintain the connecting tubing at a minimum temperature of ~160°C thereby assuring the entrance of 1,6-diaminohexane into the chamber at gas state. All samples were placed in wire lace made boxes and then introduced into the plasma chamber. The vacuum bomb was turned on, assuring a negative pressure on the chamber, and later an inertization step with a continuous flow of argon gas was conducted (~2 minutes). This was accomplished in order to minimize all trace amounts of air and moisture inside the chamber. Finally, the reaction was performed (33 minutes). During the first 3 minutes of treatment, argon gas flow was adjusted to keep a constant pressure of 0.3 Torr inside the chamber and a power of 60 W was applied to the equipment ensuring the formation of radicals at the surface. After those 3 minutes argon entrance is sealed and 1,6-diaminohexane enters the chamber reacting for 30 minutes at the same power. Once finished the experiment, the plasma chamber was ventilated and the samples withdrawn and stored. The apparatus is schematically shown on figure 2.3. This method is based on a recent work[79].

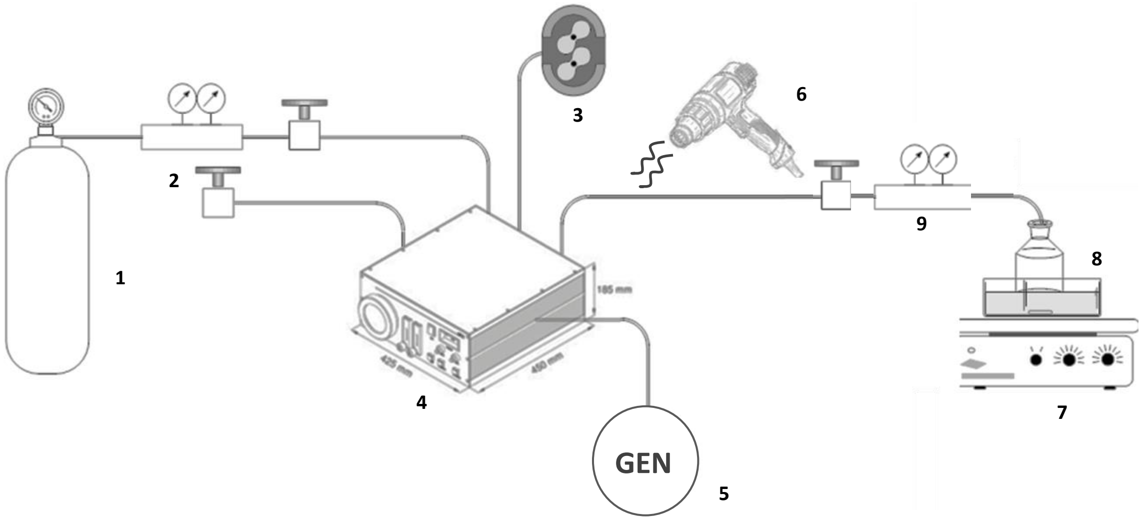

Figure 2.3. – Layout of Amination apparatus used for monolithic samples: argon gas bottle (1), gas 2 manometer (2), vacuum pumb (3), plasma chamber (4), high frequency generator (5), heat gun (6), stirrer hot plate (7), 1,6-diaminohexane vessel (8), gas 1 manometer (9).

2.2.6.1.1. Evaluation of Amine Groups Content by Kaiser Test

The amount of free amine groups at monoliths surface was ascertained through a colorimetric assay, Kaiser test. This test is a qualitative one and is based on ninhydrin reaction with primary amines that origins an intensely blue/purple pigment (figure 2.4.). The monolith is soaked in 1.5 mL distilled water and then 50 µl of each following solutions are pipetted over the sample: 80% crystalline phenol in ethanol (w/v), 2%(v/v) 0.001M aqueous solution of potassium cyanide in pyridine and 5% ninhydrin in ethanol (w/v). Then follows a 5 minutes plunge on a boiling water bath (100°C). The calibration curve was realized by measuring the absorbance (560nm) of standard solutions of glycine (0–5µmoL/mL).

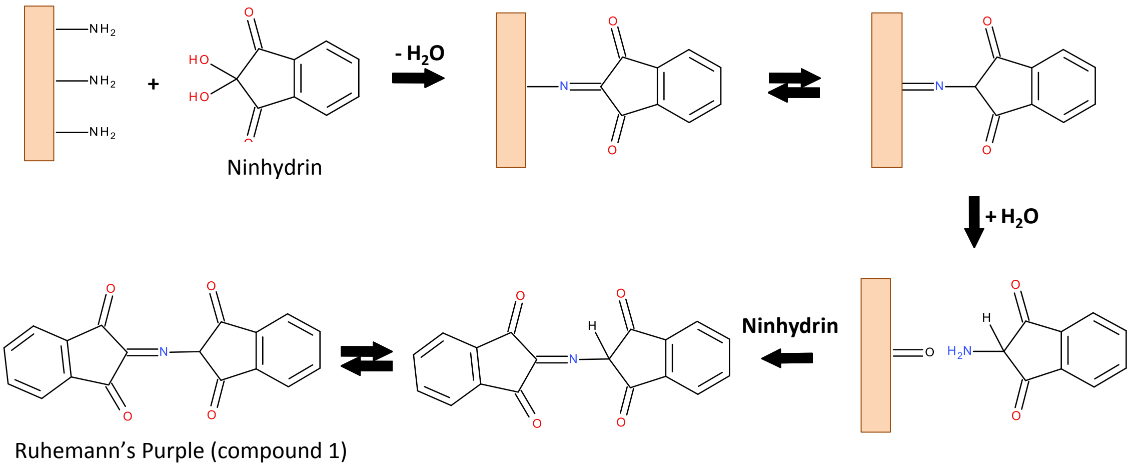

Figure 2.4. – Kaiser test reaction. Compound 1 absorbs at 570 nm.

2.2.6.2. Aldehyde Groups on the Surface of Previously Aminated Monoliths

In order to move from an aminated surface to an aldehyde one, a reaction between the free amine groups and an aldehyde containing compound must occur. Glutaraldehyde was chosen as aldehyde containing compound, leading to a nucleophilic addition reaction with imine formation to take place. First it was prepared a 5%(v/v) glutaraldehyde solution to which was added 1M NaOH in order to respect a glutaraldehyde/NaOH ratio of 50/3. Then the monolith was added to the yellowish solution and the reaction was sustained for 1 hour (200 rpm, 30°C). At the end the monolith was washed with distilled water until clear water achievement.

2.2.6.2.1. Qualitative Analysis over Aldehyde Functionalization

The silver mirror test that is performed by Tollens' reagent reveals the presence of aldehyde groups through a silver mirror or a brown precipitate. Tollen's reagent, an alkaline solution of ammoniacal silver nitrate, contains a weakly oxidizing ion ($[Ag(NH_3)_2]^+(aq)$) which precipitates out metallic silver in the form of a silver mirror, that covers the inner surface of the receptacle. An aldehyde is oxidized to a carboxylic acid while the Ag^{1+} ion is reduced to silver metal. To prepare Tollens' reagent first a flask was cleaned with 3M NaOH, then it was added 2 mL of 0.2M $AgNO_3$ followed by a drop of 3M NaOH and afterwards 2.8% NH_4OH was added dropwise under stirring until almost all precipitate of silver oxides has dissolved. To totally remove the precipitate, 8.8% NH_4OH was added dropwise. The freshly prepared Tollens' reagent was ready to use, being 1 mL then added to each monolith sample. The positive control was performed with 1 mL of glutaraldehyde and the negative control with unmodified monolith samples. After Tollens' reagent addition solution was vigorously stirred and heated with a lighter.

2.2.6.3. A4C7 ligand Solid-Phase Synthesis on Monolith Platform

The ligand with affinity towards GFP was developed in Dr. Cecília Roque's laboratory by Dr. Ana Pina and is reported in her PhD thesis[102]. The ligand is denominated A4C7 and was obtained by solid-phase (agarose) combinatorial synthesis of a library of affinity ligands based on Ugi reaction. This type of reaction is a one-pot multicomponent reaction involving four different components: an aldehyde, an amine, an isocyanide and a carboxylic acid. In case of A4C7 ligand the amine component is 1-pyrenemethylamine hydrochloride (A4), the carboxylic acid is phenylacetic acid (C7), the aldehyde is the already functionalized glutaraldehyde and the isocyanide is isopropyl isocyanide. So in order to perform the Ugi reaction and synthesize the ligand the Ugi-components had to be prepared: for A4 solution preparation, 9.4 or 14 mg A4 were mingled with 2,5 mL 100%(v/v) methanol and 35.26 or 52.8 μl of 1M NaOH for neutralization; for C7 preparation, 4.8 or 7.20 mg C7 were mixed with 2.5 mL 100%(v/v) methanol (all referred quantities are per monolith and depending on type of monolith: native or magnetic, respectively). Afterwards, each ready and washed monolith containing the aldehyde component on its surface (**2.2.6.2.**) was placed into a 30 mL flask and then 5 mL of 100%(v/v) methanol and 2.5 mL A4 were pipetted into the flask for a 2 hours reaction to go on (60°C, 220 rpm) with another C=N bond formation. The following added compound was isopropyl isocyanide (3.33 or 3.66 μl per native or magnetic monolith, respectively), along with 2.5 mL C7 and 5 mL 100%(v/v) methanol and the reaction was protracted for 48 hours (60°C, 200 rpm).

Each compound used presented a 5 molar excess in respect to average amine content on monolith surface.

After reaction conclusion each monolith was washed with the following solutions (at room temperature, 170 rpm, 10 minutes with each solution): first 100%(v/v) methanol followed by 50%(v/v) DMF in methanol, destilled H_2O, 0.1M HCl, H_2O again, 0.2M NaOH in 50%(v/v) isopropanol, again 2x H_2O and finally 20%(v/v) ethanol.

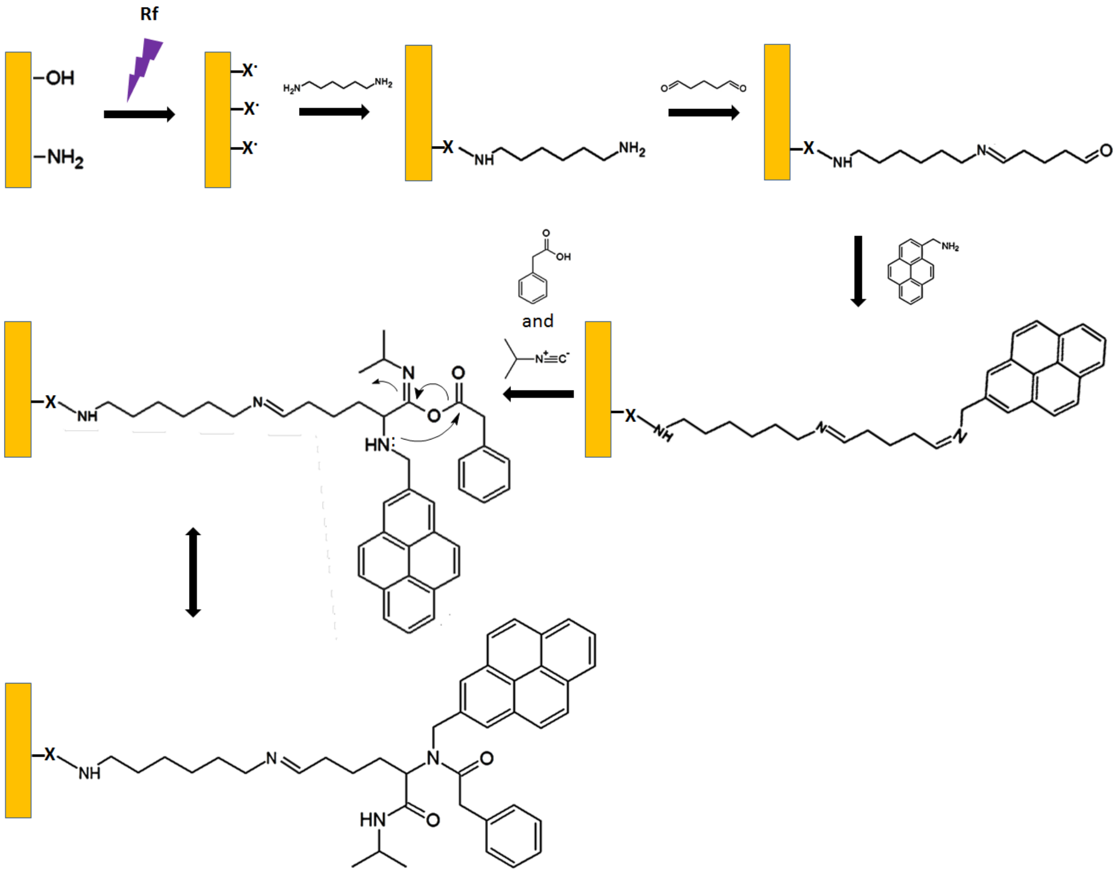

Figure 2.5. – Plasma amination[79] followed by Ugi reaction onto monolith. "X" denotes oxygen, nitrogen or carbon atoms.

2.2.6.3.1. Presence of A4C7 on Functionalized Monoliths Accessed by Fluorescence Microscopy

In order to verify the presence of A4C7 ligand on the monolith surface, samples of regenerated functionalized monoliths were crushed, placed on a microscope blade, moistured with distilled water and covered with a lamella. Then the samples were analysed by fluorescence microscopy (40x amplification). Three different photographs of the samples field were taken under bright field and filtered light appropriate for excitation and emission ($\lambda_{excitation}$=460-490 nm and $\lambda_{emission}$ =520 IF), and recorded with Cell F software. The negative control was performed with a totally non-functionalized monolith either with or without MNPs modification.

2.2.7. Screening Assays with GFP and Ligand Leaching Tests

Each screening assay encompassed regeneration, equilibration, loading, washing and an elution stages performed with the monolith functionalized with A4C7 in column. The regeneration was carried out by first adding 2x 1 mL distilled water followed by 1 mL regenerated buffer (0.1M NaOH, 30%(v/v) isopropanol) alternated with 1 mL of distilled water in a total of 2x; regeneration is finalized with 2x 1 mL distilled water. Then 5x 1 mL of elution buffer (0.1M Glycine-NaOH pH9 or 0.1M Glycine-NaOH pH9 in 50%(v/v) ethyleneglycol) were added and finally equilibration stage was conducted by adding 6 x equilibration buffer (PBS buffer (**2.2.5.6.5.**)). Each 1 mL added to the column was collected and 200 µl aliquots were tested for ligand and MNPs leaching (**2.2.1.1.2.**). The later only in case of MNPs modified monoliths. In case of ligand leaching the fluorescence was measured with $\lambda_{excitation}$=485 nm and $\lambda_{emission}$=535 nm and a gain of 62. Once ready to load, the crude extract produced and containing GFP target was added to the column. Incubation times of 0, 15 and 60 minutes were tested at 4°C except 0 minutes (tested at room temperature), however all collected samples were immediately plunged into ice and covered in aluminium foil. The flow-through was collected as well as the following 8 washes with PBS buffer and 5 elutions (with one or the other of the two referred elution conditions). After the screening all columns were regenerated with alternating volumes (1 mL) of regeneration buffer and distilled water (3x) finalized with 3 additions of 1 mL of 20%(v/v) ethanol. Monoliths were stored at 4°C embedded on PBS. Once more, all fractions were collected and 200 µl samples were quantified by the BCA assay (**2.2.5.6.6.)** and GFP fluorescence (**2.2.5.6.4.**). The enrichment of the target by the lead ligand A4C7 was also evaluated by SDS-PAGE analysis.

All stages were carried out under gravitational force excluding the regeneration one and the volume added at each step of a stage was 1 mL. Negative controls with plain monoliths passed through the same steps and analysis.

2.2.7.1. SDS-PAGE Analysis

The presence and enrichment of the GFP was evaluated by SDS-PAGE analysis according to **2.2.5.6.3.** in which the gel concentration as well as samples preparation procedure was maintained, although volume pipetted from each aliquot collected and sample buffer were 10 µl and 5 µl, respectively, and 2.5 µl of the protein marker used. The gel runned for 75 minutes (130V, 250 mA). The samples analysed were the flow-through, the two first washes and the first elution. Gels staining were performed with

Silver Stain Plus Kit. The fixative step was conducted by immersing the gel into 200 mL fixative enhancer solution (100 mL 100%(v/v) methanol, 20 mL 100%(v/v) glacial acetic acid, 20 mL fixative enhancer concentrated solution and 60 mL distilled water) for 20 minutes under gentle unrest. The solution was discarded and gels 2x cleaned with 200 mL of distilled water during 10 minutes under mild turmoil. Rinsing water was disposed. Then the gels were immersed in a staining solution (distilled water (35 mL), silver complex solution (5 mL), reduction moderator solution (5 mL), image development reagent (5 mL) and room temperature development accelerator solution (50 mL)) and were kept during 20 minutes under gentle unrest to be revealed. When the gels were ready, the staining reaction was stopped by adding 5%(v/v) acetic acid solution, followed by gently agitation (15 minutes). Finally, the gels were rinsed with 100 mL MiliQ water (5 minutes) and photographed.

3

DEVELOPMENT OF MONOLITHS FOR VIRAL PARTICLES PURIFICATION

3.1. Introduction

The global biopharmaceutical market is an on growing market expected to worth 185.7 billion Euros in 2017[105]. From the three main relevant segments in which biopharmaceuticals can be divided (therapeutic proteins, monoclonal antibodies and vaccines), therapeutic proteins are the section forecasted to present the highest market share (83.6 billion Euros), followed by monoclonal antibodies (MAbs) and finally by vaccines (36.1 billion Euros) with the second higher growth rate[106]. In fact, vaccines are the second segment with more products in Phase I and II clinical trials after MAbs, covering approximately the same number of products on Phase III as the latter, and covering even more products under review by FDA[107]. The majority of commercialized vaccines are viral-based vaccines[108].

Gene-therapy is another on-growing area, where viral particles are the key elements. The approval of first drug[109] set the beginning of a relevant and expected growth[109,110], mainly due to this area immense growth potential[110,111] and number of drugs in clinical trials or awaiting approval[109,111]. Adenoviruses (Ad) are the preferred platform for gene therapy[111], and a very attractive choice in vaccination[112]. Furthermore a rise on R&D concerning adenovirus vaccines has experienced a significant growth in last decade[108]. The vogue of Ad as extremely appealing platforms is explained by its production in high titers (10^{10} pfu/mL), capacity to embrace an insert up to 37kb, and non-integration into host cell genome, etc.[113,114,111]. Moreover further developments on Ad vectors as gene delivery vehicles allowed significant progress on issues as long-term transgenes expression and immunogenicity[113], rendering Ad even more attractive.

Ad are $2x10^8$ Da non-enveloped virus, composed by 26-45kb linear double-stranded genomic DNA protected by a capsid. With a 60–110 nm diameter and an icosahedral architecture, its proteic capsid comprises 240 hexon capsomeres covering the 20 triangular faces of the icosahedron, and 12 vertex penton capsomeres provided with one/two protruding spike-shaped fibers (Figure 3.1.)[114,113,115]. The hexon capsomer protein is a homotrimer of polypeptide II and the penton protein is a pentameric structure composed by polypeptide III that together with polypeptide IV trimers composes the penton complex. Fiber protein binds non-covalently to penton base through its N-terminal tail, and is connected to cell recognizable globular knob domain by a rigid rod[114]. Referred proteins assemble into capsid proteins however, inside protein shell coexist minor proteins connected with capsid, and core proteins associated to viral genome. At virion core there is also a key protease playing a vital role in viral particle assembly. Core proteins are involved in genome replication and packaging, whereas minor proteins are involved in maturation, stability, assembly of capsid proteins[116,117,114].

As the charge of each major capsid protein monomer (hexon) in Ad5 is −23.8, the capsid is endowed of highly negativity, its overall surface charge exceeds −17,000[114].

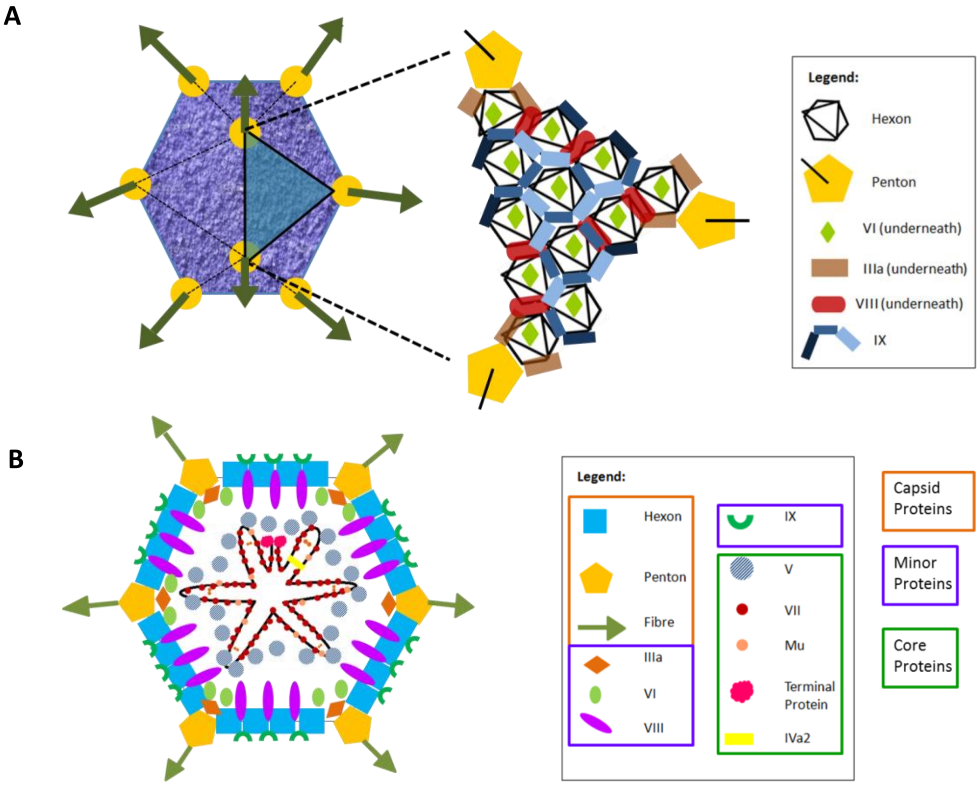
A
Legend:
Hexon
Penton
VI (underneath)
IIIa (underneath)
VIII (underneath)
IX
B
Legend:
Hexon
Penton
Fibre
IIIa
VI
VIII
IX
V
VII
Mu
Terminal Protein
IVa2
Capsid Proteins
Minor Proteins
Core Proteins

Figure 3.1. – Adenoviral particle external (A) and internal (B) structure. Structures based on Martín[118] and Russel[116] works respectively.

The blockbuster development of virus-based biopharmaceutical drugs for its application on vaccination and gene therapy areas demands for: fast-tracking and fairly efficient purification; conservation of virus infectivity; great recovery of infectious particles; and contaminating DNA and host cell proteins clearance, allowing at the same time viral product concentration for minimization of validation requirements and final delivery[119]. Clinical-grade Ad-based vectors, sometimes demanded to achieve 10^{13} total particles/patient or 10^{11} infectious particles/patient claims for robust production and purification protocols at a large scale meeting regulatory pharmaceutical requirements compliant with clinical specifications - current Good Manufacturing Practices (cGMPs)[120]. Great quality analytics applied throughout upstream and downstream processes to monitor protocol employed are the key to guarantee desired final product properties[121].

The traditional methods for adenovirus purification are listed in Table 3.1. CsCl method is the most applied one due to its simplicity with extremely pure yields of Ad preparations. However the method is limited to small-scale viral lots and CsCl toxicity renders imperative the extensive dialysis of Ad preparations. Moreover it presents variable quality of viral preparations, substantial loss of infectivity and aggregation during storage[115]. The tendency however is to design more complex purification schemes composed of several steps, and based on chromatography (Figure 3.2.).

Table 3.1. – Traditional methods used in Ad purification.

Purification Steps	*Target*	*Purity(%)*	*VP/IU ratio*	*Recovery (%)*	*Ref*
CsCl density gradient ultra-centrifugation	rAd5	High	23:1, 8:1	-	[122,123]
Sucrose gradient ultra-centrifugation	rAd5	CsCl Comparable	-	-	[124]
PEG precipitation[a]	rAd5	-	6:1	90	[125]
Ammonium sulphate precipitation[a]	rAd5	-	17:1	84	[125]
Two-phase Extraction (PEG-salt)	rAd5	High	n.a.	80	[126]

[a] Precipitation methods are mainly used for recovery of viral particles present in cell-culture medium, and which are frequently discarded (~47% of total virus amount). It constitutes an alternative path to CsCl method to be used together with it; a Scheme is outlined by Schagen et *al.*[125]

In a primary isolation, cells are harvested generally by centrifugation or microfiltration, and afterwards Ad particles are separated from cells together with most abundant impurities (cell debris, proteins, DNA and metabolites, media components and liquid) through cell lysis by chemical, mechanic or thermal means, followed, generally, by solid-liquid separation. The cleared lysate is then typically digested with nucleases towards minimization of cellular DNA and RNA cargo. This step improves product purity (safer viral product), and decreases Ad particles agglomeration. Alternatively selective precipitation of cellular DNA can be achieved during lysis with cationic detergents reducing or even eliminating DNA removal steps, like nuclease treatment or anion exchange chromatography. The nucleic acids-free Ad particles solution is then typically filtered, concentrated, and conditioned for subsequent final purification[114]. Concentration of Ad guarantees high titer viral stocks decreasing the handling volume, and reducing the number of steps[119]. During intermediate purification a solvent/detergent step should be pertinent to guarantee inactivation of enveloped viruses that might have been co-amplified. Final purification, where recalcitrant impurities are removed, comprises a capture step, and is usually performed by a combination of liquid chromatography and filtration steps. Countless chromatography-based methodologies have been reported, exploring properties as size, charge, hydrophobicity, and metal affinity; however anion exchange chromatography (AEC) is the most popular approach[119,114,115].

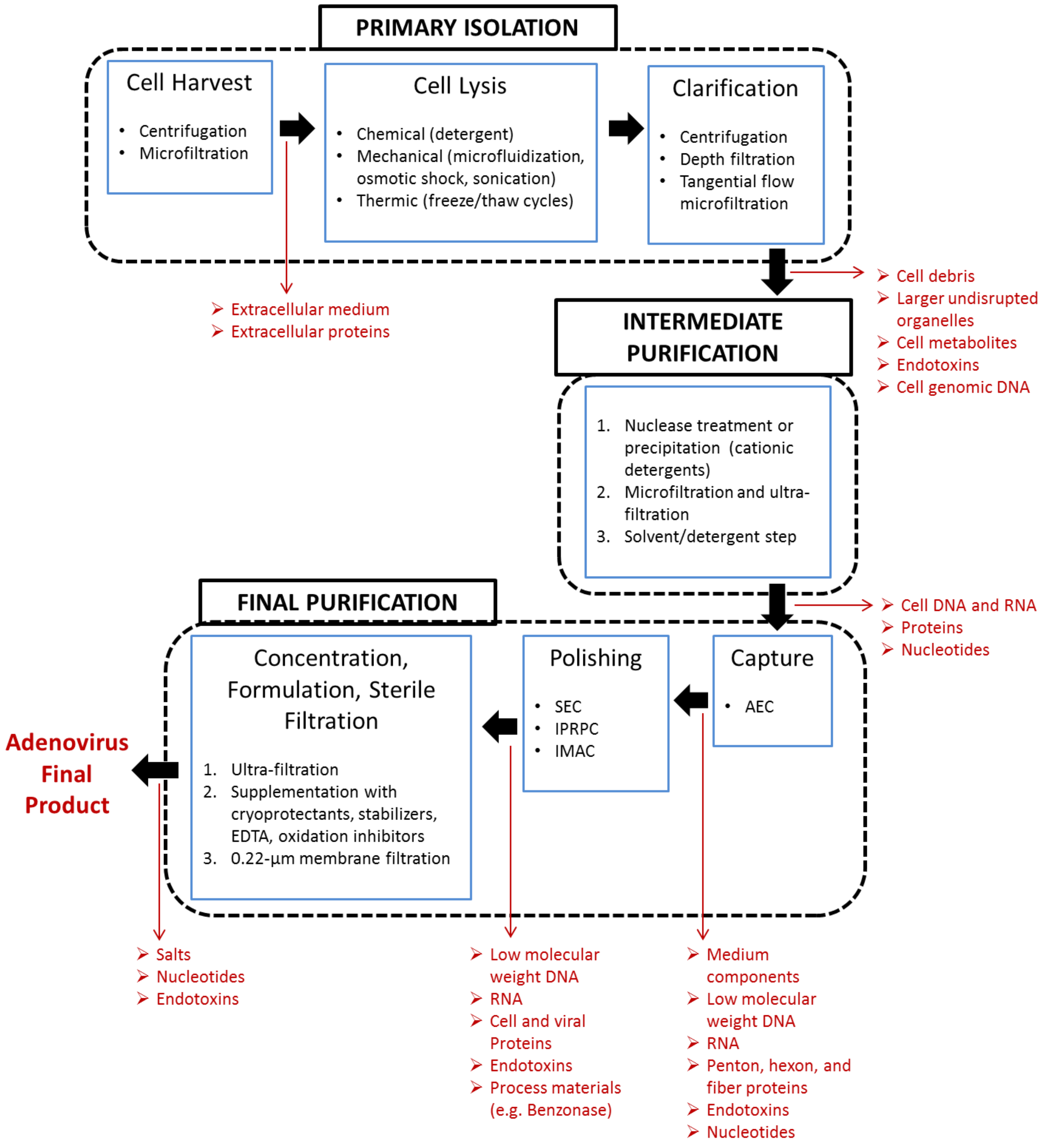
PRIMARY ISOLATION
Cell Harvest
Centrifugation
Microfiltration
Cell Lysis
Chemical (detergent)
Mechanical (microfluidization, osmotic shock, sonication)
Thermic (freeze/thaw cycles)
Clarification
Centrifugation
Depth filtration
Tangential flow microfiltration
Extracellular medium
Extracellular proteins
Cell debris
Larger undisrupted organelles
Cell metabolites
Endotoxins
Cell genomic DNA
INTERMEDIATE PURIFICATION
1. Nuclease treatment or precipitation (cationic detergents)
2. Microfiltration and ultra-filtration
3. Solvent/detergent step
Cell DNA and RNA
Proteins
Nucleotides
FINAL PURIFICATION
Concentration, Formulation, Sterile Filtration
1. Ultra-filtration
2. Supplementation with cryoprotectants, stabilizers, EDTA, oxidation inhibitors
3. 0.22-µm membrane filtration
Polishing
SEC
IPRPC
IMAC
Capture
AEC
Adenovirus Final Product
Salts
Nucleotides
Endotoxins
Low molecular weight DNA
RNA
Cell and viral Proteins
Endotoxins
Process materials (e.g. Benzonase)
Medium components
Low molecular weight DNA
RNA
Penton, hexon, and fiber proteins
Endotoxins
Nucleotides

Figure 3.2. – General scheme for Ad downstream purification. Black spheres represent possible applicable unit operations (most common ones); numbering represents sequential steps (most common ones. The diagram was based on Prazeres work[114]. On capture step AEC is the only method present once it is the most commonly applied one, however Ad can also be separated based on size, hydrophobicity, and metal affinity. AEC: anion-exchange chromatography; SEC: size exclusion chromatography; IPRPC: ion-pair reversed phase chromatography; IMAC: immobilized-metal affinity chromatography.

AEC alone seems to be insufficient to guarantee an Ad-based product with the demanded purity, so a chromatographic polishing step is required. Afterwards product is concentrated, formulated and subjected to sterile filtration. It is noteworthy that different chromatographic modes combinations have been applied over time in order to capture and polish Ad particles (Table 3.2.). Monoliths are now being also employed.

Most chromatographic matrices used on virus purification are bead-based, however they comprise pore dimensions known to exclude viral vectors, and diameters known to limit viral adsorption due to low binding capacities. This issue can be addressed by using membrane adsorbers or monolithic columns as tentacle supports, once diffusion limitations are surpassed with faster volumetric throughput rates and an increment in speed and productivity. However, membranes flow aberrations creates shear forces that can compromise performance and productivity of labile Ad products, not an issue for monolith platform[120,127].

This chapter aimed at the development of a porous cryogel structure able to capture Ad particles from a pre-clarified crude extract, with potential to fulfil all virus purification process requirements. This support will be prepared in accordance with green chemistry principles.

Table 3.2.- Summary of possible combinations of chromatographic steps in Ad purification steps. Monolith-based virus separation is starting to emerge.

Chromatographic Steps	*Column type*	*Ligand*	*Column material*	*Pore Size (nm)*	*Target*	*Scale*	*Surface Area*	*Flow Rate (mL/min)*	*Capacity*	*Purity*	*VP^e Yield*	*IU^f Yield*	*VP/IU ratio*	*Ref*
1. AEC [a]	Fractogel DEAE-650M	DEAE	Methacrylate-based	> 80	rAd5	10^{14} VP input	n.a.	2 cm/min	$5.0x10^{12}$ vp/ mL	High	73%	75%	3:1	128
2. IPRPC [b]	PolyFlo	n.a. [d]	n.a.	n.a.			n.a.	2 cm/min	$1.0x10^{13}$ VP/g	High	84%	94%	n.a.	
Final product										>CsCl	55%	57%	1:1	
1. AEC	Streamline Q XL	Q	6% Agarose, quartz core, dextran extender	n.a.	rAd5	10^{12} input of VP (2L bioreactor bulk)	n.a.	20	n.a.	CsCl Comparable	70%	45%	13:1	123
Final Product										CsCl Comparable	n.a.	32%	n.a.	
1. AEC	Q Sepharose XL	Q	6% Agarose with dextran	12	rAd5	30 mL scale suspension culture	n.a.	1.0;4.0	n.a.	96%	<~87%	(98%)	n.a.	129
2. IMAC [c]	Sartobind IDA75	IDA-Zn^{2+}	Cellulose	>3000			75 cm^2/2.1 mL	1.0;4.0	n.a.	97.20%	~87%	2.5 x10^8 IU/mL	n.a.	
Final Product										CsCl Comparable	n.a.	n.a.	n.a.	
1. AEC	CIM QA	Q	poly(GMA-co-EGDMA)	1000-5000	rAd5	n.a.	~40 m^2/g	3.0	$3x10^{12}$ VP/mL	High (≥CsCl)	57.9% (can be >90%)	66.70%	n.a.	130,131
Final Product										n.a.	n.a.	n.a.	n.a.	
1. HIC	Fractogel EMD propyl (S)	Propyl	Methacrylate based	> 80	rCAV2	10^{11} pp [g]	n.a.	0.5	$0.45 x10^{12}$ vg/mL	High	88%	n.a.	n.a.	132
2. AEC	CIM DEAE	DEAE	poly(GMA-co-EDMA)	600 - 750			~40 m^2/g	2.0	$0.7x10^{12}$ vg^e/mL	High	58-69%	n.a.	n.a.	
Final Product										High	38–45%	n.a.	16:1	

a) Anion-exchange chromatography; b) Ion-paired reversed-phase chromatography; c) Immobilized methal affinity chromatography; d) n.a. data no available on the literature as far as we are concerned; e) VP viral particles; f) IU infective units; g)Physical particles e) viral genome copy number

3.2. Preparation of Monoliths by Freeze-Drying

Porous supports for virus separation must possess a robust character, fast flow rates and resistance to leachables, but also should have an easy-to-validate direct flow use, should involve a low infective titer reduction allied to high recovery yields, should be scalable, and comprise a low protein binding with efficient contaminant removal, always meeting regulatory standards for safety[133–135]. These requirements can be assured by proper hydrophilicity of the support, chemical and mechanical resistance, narrow pore size distribution, and enough reactive surface area, as well as proper porosity, interconnectivity, and morphology: stationary phase features that play crucial roles in bioseparation procedures[27,17,5,136]. Freeze-drying, also known as lyophilization, has already been employed in the preparation of monoliths[27,137,136]. Prior to lyophilization the homogenized casting solutions were cooled to 0°C and then polymerized and/or netted, by addition of the initiator APS and catalyst TEMED (a redox pair), in a process named cryopolymerization[49,138]. Cryogelation that can or not involve cryopolymerization relies on the generation of a polymeric structure in a semi-frozen system (Figure 3.3.).

The time the polymerizing solution is exposed to the 0°C environment during monolith preparation is not enough to form robust and completely nucleated crystals[139]. Indeed as studied by Wilson et al.[140] the presence of solute species in an aqueous solution is responsible for a nucleation temperature decrease (below -2°C[139]). This decreasing does not depend on the ionic specimen but on its concentration in solution[139,140]. So, the low concentration of casting solutions used in this work is thought to have little impact on nucleation temperature, i.e. -2°C.

This reticulation 0°C period, provided with slow agitation was directed to: guarantee maximum spread possible of initiator/catalyst pair, avoiding disruption of newly forming net and ensuring later creation of a homogeneous structure, and guarantee following solution stabilization, with time and temperature decrease until 0°C. Moreover freezing driving force of castings transferred from a 0°C environment to respective freezer (-20°C/-80°C) is less pronounced than from a room temperature environment. This allows a better organization of the system in: polymeric structure and ice crystal lattices[141].

After this initial phase, cryogelation continues at negative temperatures (-20°C and/or -80°C depending on the desired monolithic specimen), where growth of crystals takes place.

Apart from the freezing temperature applied or composites nature, it is known that in both cases a nucleation phenomenon starts, immediately followed by crystal growth. Indeed there is a competition between these two phenomena, which determines the features of originated crystals. That is, if one is in presence of a rapid freezing (in this case -80°C) several nuclei will be formed, and the time for growth is minimal; this lead to the formation of countless small ice crystals. On the other hand, if one is in presence of a slow freezing (in this case -20°C), it will be formed a smaller amount of crystals, but with higher dimensions[139,140,27]. Actually it is these fast and slow freezing phenomena (different rates of crystal growth) that were used in this work to tune crystal dimensions, and so monolith microstructure, once the crystals define each pore dimensions and shape. Indeed further sublimation of ice then empties the pores leading to different macroporous structures, depending on the freezing temperature applied. Moreover it is this 3D microstructure that will define the properties of the monoliths prepared and so its applicability in the desired area.

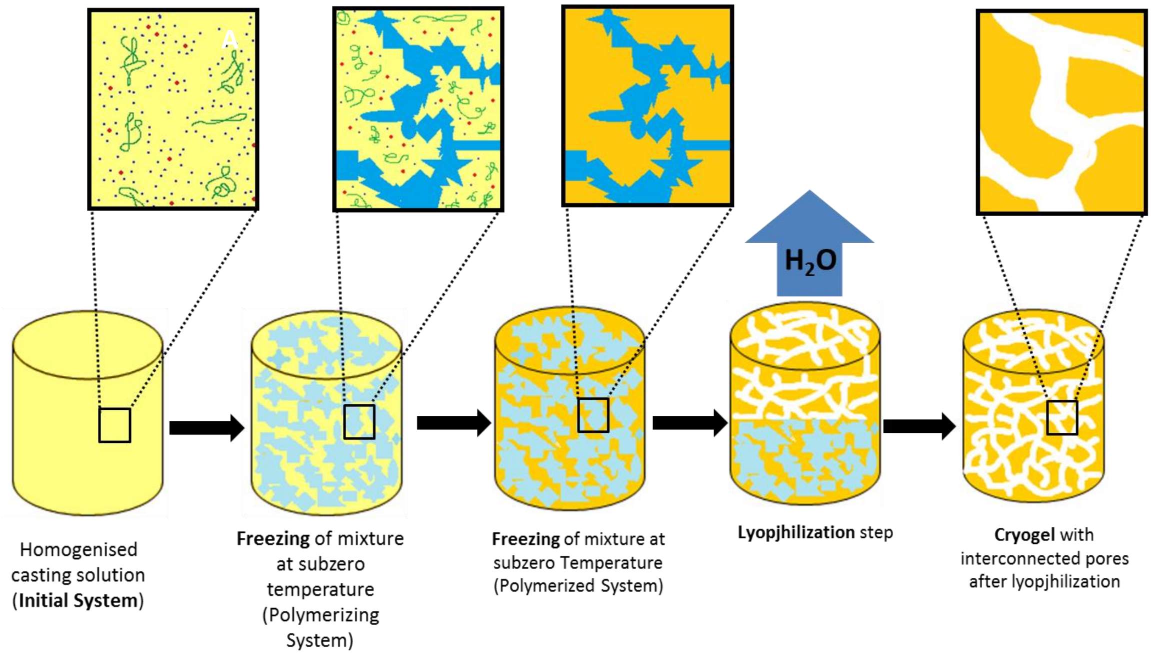
H_2O
Homogenised casting solution (Initial System)
Freezing of mixture at subzero temperature (Polymerizing System)
Freezing of mixture at subzero Temperature (Polymerized System)
Lyopjhilization step
Cryogel with interconnected pores after lyopjhilization

Figure 3.3. – Cryogelation process: The initial system comprising a reaction mixture rich on gel-forming units is frozen; despite looking as a whole firm block, the system is essentially heterogeneous containing an unfrozen liquid micro-phase (UFLMP) together with crystals of frozen solvent; the gel-forming units concentrated in UFLMP allows cryo-concentration occurance with gel formation; solvent acts as porogen leaving cavities when sublimated; the surface tension between solvent and gel phase guarantees the round smooth shape of pores. Green ribbons represent polymers, blue dots represent solvent molecules and the red ones represent the low-molecular weight solutes (e.g. monomers, initiators). Schem based on[142,143].

Thus it can be stated that freezing is a determinant step in the preparation of porous structures with controllable pore morphologies, making freeze-drying a technique that creates tunable porogenic ice templates that left interconnected pores when water is sublimated.

The temperatures and time of freezing was proven to be applicable and adequate for all casting solutions, once -20°C and -80°C temperatures are located below literature reported temperatures, ensuring adequate casting freezing[9,27]. This is corroborated by qualitative and quantitative characterization of prepared monoliths.

In respect to the average time any solution may remain at subzero temperatures, it is defined by the degree of supercooling and heterogeneous nucleation sites available[140,139]. The 24h of cryotropic conditions time seemed to be enough due to macro and microscopic morphology of materials upon monolith sectioning (Figure 3.4.).

Finally the sublimation of water solvent under vacuum and at approximately -45°C allowed the formation of macroporous structures (Figure 3.3.) with in principle highly interconnected pore channels: ice crystals, acting as in situ porogens growing next to each other until they meet at a certain point the sides of other crystals, lead to a more or less robust ice scaffold structure that disappears during sublimation, and leaves a system of interconnected pores inside the cryogel[144]. In fact the casting solutions concentrations of minimum 2% and maximum 6.7% enhances this effect contributing to produce a highly interconnected open pore 3D structure (water vol.% is a tuning parameter)[145,144].

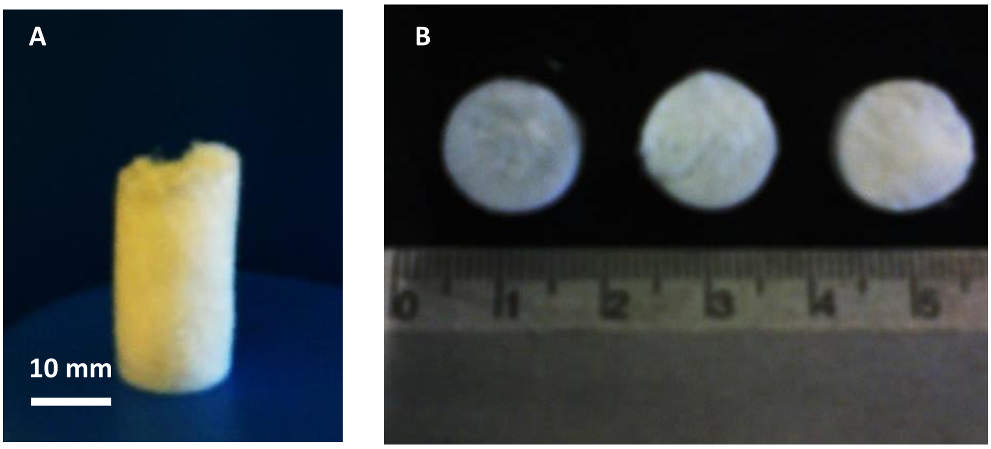

Figure 3.4. - Whole dextran-based monolith (A) and the three samples in which it was sliced (B).

3.3. Monoliths Architecture and Analysis of its Properties through Characterization

3.3.1. Materials Employed: an Overview

In order to elect the most promising monoliths for the mentioned application it was imperative the accomplishment of a series of measurements. In fact the screening of the various proposed materials was made through stability tests, porosity and water flux measurements, and finally macro-scale mechanical compression experiments at dry and hydrated state. Those analyses were made in order to select the three most promising monolithic candidates, from a total of twenty three prepared from some initially elected potential materials.

The prospective bulk materials include the natural polymers chitosan, dextran and agarose (Figure 3.5.).

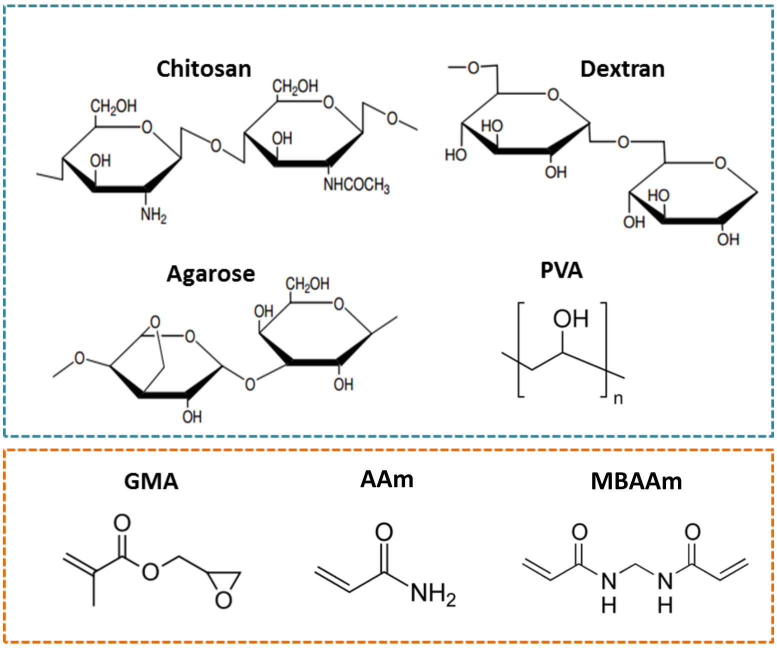

Figure 3.5. – Polymers (blue) and monomers (orange) used in monoliths preparation towards a novel, green and virus purifying support.

Through the usage of these natural materials, monoliths prepared assured a highly hydrophilic surface, not only crucial for the allowance of a reversible adsorption, a requirement in bioseparation processes, but also allowance of low protein adsoption and provision of low unspecific binding. The richness of hydroxyl groups on the surface of prepared monoliths is the responsible for this character, also allowing for the availability of enough functional groups where ligands can be inserted for specific modifications of that surface[146,147]. To the mentioned advantages joins the biodegradability, biocompatibility, ready availability and inexpensive ease of processing. Thus countless advantages led to the election of natural polymers as bulk materials. To the stated benefits joins the commercial availability or lab developing of monoliths mainly based on silica, acrylamide or methacrylates[6,3,19]; and the series of commercial products for chromatographic applications that are already based on modified natural polymers. This situation makes it easier for the market to accept natural-monoliths[147].

However, hydrophilic natural-polymers originate soft structures with poor mechanical properties for chromatography purposes[4]. For that reason, and in order to thwart this reality, it was decided to add a crosslinker agent (e.g. MBAAm) to the casting, or even blend it with synthetic polymers and monomers like poly(vinyl alcohol), acrylamide and/or glycidyl methacrylate. One problem that accompanies this pathway is the increasing in the hydrophobicity of the support as well as the non-specific adsorption. This reinforces why, after this monoliths screening, the elected supports have to be tested without any chemical modification on its surface towards the target; allowing the inspection for this non-specific adsorption of virus and also host cell proteins, once the work goal is the purification of virus with maximum recovery, titer concentration and purity. Beyond helping on the achievement of pretended mechanical and swelling properties, chemical crosslinking of polymers, generally, translates itself on a reduction in degradation rate (covalent bonds and entanglements between polymer chains give rise to a more enclosed hindered network structure, more difficult to disrupt)[148].

According to the literature either the crosslinker or the monomers used in PVA and chitosan, agarose and dextran-based monoliths (i.e. MBAAm or AAm, GMA, respectively) unlikely form covalent bonds with the stated polymers at the reaction conditions employed (cryo-conditions in presence of APS/TEMED)[149,150]. Instead they probably polymerize and imprison the polymeric chains in certain points (e.g. chitosan, C/P, C-G and P-G monoliths (Table 3.3.)), i.e. probably when the monomers/crosslinker are present in very low quantities; or entangle and imprison globally the polymer chains (e.g. agarose and dextran-based monoliths). This probably happens once a free radical polymerization reaction generally ends when two polymerizing ends find each other[151]. The later scenario takes place generally when monomers quantity is significative towards polymer. See Figure 3.6..

An interpenetrating polymer network (IPN) can be defined as a blend of two or more linear or branched polymers in a network structure, in which no less than one is synthesized and/or crosslinked in the immediate attendance of the other(s); moreover the networks are at least partially entangled, however not covalently bonded to each other, thus leading to the impossibility of separation of the networks without breaking chemical bonds[152,153]. On the other hand, while a full-IPN comprises only crosslinked chains independent from each other but entangled in each other, the other type of IPN, semi-IPN, corresponds to a non-reacting polymer entrapped by a crosslinked polymer or co-polymer network entangled in the polymer[153]. This leads to the conclusion that in case of P-G and C-G structures they constitute a semi-IPN, once the structures seems to be similar to Jain *et al.* ones[149]. In case of agarose and dextran, once there is no crosslinking, just an entangling synthesized copolymer that closes upon itself imprisoning the base polymer, it should probably be included into the IPN category. Indeed no covalent binding is likely to occur between polymer backbone and crosslinker molecule, only polymerization of crosslinker.

Table 3.3. – Monoliths prepared for screening tests accompanied by the respective monomeric/polymeric ratios.

Materials	Proportions %(w/w)	Concentrations %(w/w)	Freezing Temperature (°C)	Monolith Denomination
Chitosan	100	2.9	-20 and -80	C2.9%
		2.0	-20 and -80	C2%
Chitosan/Polyvinyl Alcohol	50:50	2.9	-20 and -80	C/P(50:50)
	33:67		-20 and -80	C/P(33:67)
Chitosan-Glycidyl methacrylate	89:11	2.9	-20 and -80	C-G
Polyvinyl Alcohol-Glycidyl methacrylate	79:21	3.3	-20 and -80	P-G(79:21)
	89:11	2.9	-20 and -80	P-G(89:11)
Acrylamide-N,N'-Methylenebisacrylamide*-Glycidyl methacrylate	78:17:5	3.1	-20	AAm-MBAAm3.1%
		6.5	-20	AAm-MBAAm6.5%
Agarose- Acrylamide - Glycidyl methacrylate	56:7:37	4.5	-20	A-AAm-G(56:7:37)
	58:12:30	5.4	-20	A-AAm-G(58:12:30)
Dextran-Acrylamide-Glycidyl methacrylate	56:7:37	4.5	-20 and -80	D-AAm-G(56:7:37)
	49:14:37		-80	D-AAm-G(49:14:37)
	58:12:30	5.4	-20 and -80	D-AAm-G(58:12:30)
	52:17:30		-80	D-AAm-G(52:17:30)
Polyvinyl Alcohol	100	2.9	-20 and -80	P100%

* N,N'-Methylenebisacrylamide (MBAAm) is used not only as a crosslinker but also as a monomer.
"/" denotes a blend
"-" denotes a copolymerization

The preparation of monoliths using as only composites GMA and the hydrophilic monomers acrylamide, MBAAm to give form to a natural-polymer non-based monolith seems to be a pertinent choice, due to the macropores such a structure can be composed of ($\leq 10^5$ nm), and the possibility of comparison towards natural monoliths[9,154]. This structure should comprise a closed network of copolymers, once all monomers covalently bind to each other and the two reactive ends of MBAAM molecule guarantee crosslinking between chains.

Hydrophilic poly(vinyl alcohol) was blended with the hydrophobic glycidyl methacrylate, once the produced structure is thought to have a reasonable hydrophilic character with uniform pores. The monolith prepared is a semi-IPN, once PVA is probably interpenetrated by the polymerizing GMA monomers (crosslinked by MBAAm) that form a polymeric network of poly(GMA) entangling and imprisoning PVA. This weak chemical character of the structure renders unnecessary the chemical crosslinking of PVA with the so used cytotoxic glutaraldehyde, which implies non-uniformity of the obtained matrix[155]. The pure and sole physical crosslinking (only H-bonging, Van der Walls, coulombic, dipole–dipole, hydrophobic interactions or crystallites[156]) can also be avoided.

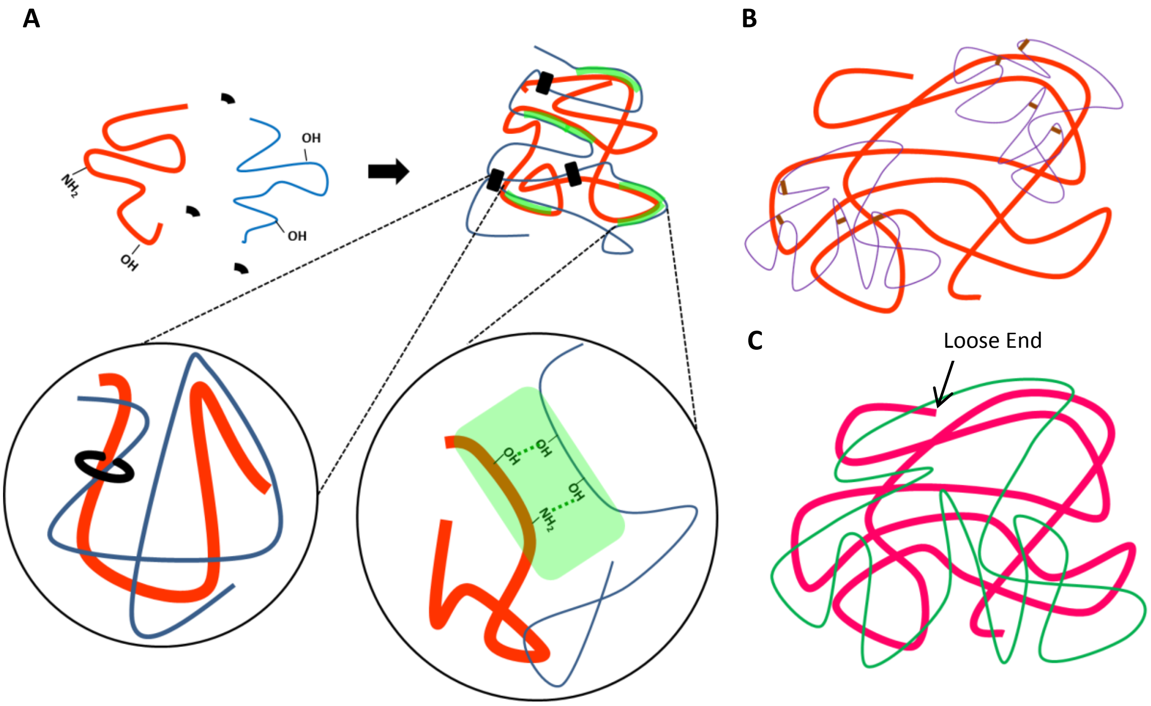

Figure 3.6. – Polymer scale arrangement of composites into monoliths. Structure of chitosan blended with PVA monolith (C/P) (A). Hydrogen bonds are established between polymer chains; and MBAAm polymerizes and imprisons the H-bonding stabilized chains improving. Structure of semi-IPN C-G monolith (B). Here MBAAm crosslinks poly-GMA imprisoning chitosan at some regions. Structure of agarose and dextran-based monoliths (C) where the closed (no loose ends) AAm-GMA copolymer entangles and imprisons agarose/dextran. Orange ribbon represents chitosan; blue ribbon represents PVA molecule; black piece represents MBAAm monomer; black ribbon represents polymerized MBAAm imprisoning H-bonding stabilized C/P chains; green shadow highlights the H-bonding. Purple chains represent poly-GMA; brown sticks represents intra-chain covalent bonds. Pink chain represents agarose/dextran; green chain represents poly(AAm-GMA) chains.

Actually this type of crosslinking is biologically advantageous, once no toxicity is granted to the final monolith due to the presence of moieties potentially obliterators of biocompatibility[157,155]. They can be achieved through repetitive freeze-thaw cycles in aqueous solution, in which crystalline clusters are created functioning as junction zones, or complex coacervation (ionic interactions), etc.[158,155]. However, although the formed cryogels present stability at room temperature for even months, these type of crosslinks alone[159] present poorer mechanical and thermal stability when compared with the chemical crosslinks[158]. The annexation of polymerizable functionalities onto the polymer backbone is also a way to avoid the utilization of crosslinkers, as the addition of unsaturations enables the reticulation of modified polymer chains. GMA was reported to be widespread utilized for the addition of methacryloyl groups on PVA backbone through a transesterification reaction in DMSO[155,160,161].

Indeed it is noteworthy that it is broadly reported in the literature the utilization of both PVA and GMA together, however only for PVA modification. This could be performed as an alternative to the prepared P-G monolith of this work. However that modification of PVA can be thought to imply a slightly more hydrophobic character to final monolith, due to the loss of glycidol group and consequent decrease on oxygen atoms in comparison to poly(GMA) formation[162,163]. Moreover as the purpose of this research work is the pursuit of a green and sustainable support the utilization of organic solvents is a way to be as much as possible avoided.

Furthermore poly(vinyl alcohol) chemical resistance, physical properties, biocompatibility, water solubility, biodegradability and low cost are very attractive stimulating the preparation of monoliths including this synthetic polymer[164,27]. That is why it was blended with chitosan.

Chitosan is a cationic polymer resultant from alkaline deacetylation or enzymatic degradation of chitin (after cellulose the most abundant polysaccharide)[6]. With a backbone comprising β(1→4)-glucosamine and N-acetyl-D-glucosamine residues in different relative proportions, it has proven to be biologically renewable, antimicrobial, biodegradable, biocompatible, non-antigenic, non-toxic, biofunctional, and sensitive towards changes in pH.. Mechanical properties of chitosan-based materials have also been an engine for the interest in its usage[165,27,137]. Chitosan was also copolymerized with GMA forming a semi-IPN structure. In fact by combining synthetic and natural polymers in either IPN or semi-IPN systems, both support physical and biocompatibility properties can be enhanced[155].

Agarose, an algal polysaccharide have been selected due to its high chemical stability over a wide pH and temperature range, hydrophilicity conducting to a significant low non-specific binding of countless proteins and biological molecules, good biocompatibility, and low toxicity, properties responsible for its popularity as a constitutive material on purification/separation supports. Its low mechanical stability limits its usage at relatively high flow rates on HPLC, however with an attractive gravitational flow no pressurized systems need to be used[8].

Regarding dextran it is a water-soluble bacterial exopolysacharide composed mostly by α-1,6-linked D-glucopyranose units and known for its good water-solubility, environmental safety, non-toxicity, bioavailability and high biocompatibility[165].

3.3.2. Monoliths Characterization

Once any proposed monolith is going to be applied under hydrated conditions all the studies performed at this state are deeply crucial and very enlightening. The working pH range is not certain so, and also to test the biodegradability of the supports, monolith rods were placed at different pHs and studied for two weeks. Despite their distinction through classification standards they all origins hydrogels, so all samples presented swelling properties with a significant water uptake[156]. Indeed “reticulation degree” seemed sufficiently high once, in general, all polymeric matrices were verified to be insoluble in water (though swellable in it)[166]. Monoliths that qualitatively presented more water uptake capacity were C2.9%, C3% and dextran-based monoliths, independently from the preparation temperature. This is a good hint once the more water uptake capacity the more virus containing cellular crude extract can access the binding sites on the support. However dextran monoliths disintegrated after three days (prepared at -20°C) or five days (prepared at -80°C) at all pHs (Table 3.4.).

Table 3.4.– Stability Tests performed at pH3, 7 and 11 with different monoliths prepared at -20°C/-80°C. Monoliths were macroscopically analysed during fourteen days.

Monolith	pH 3			pH 7			pH 11		
	3 days	5 days	14 days	3 days	5 days	14 days	3 days	5 days	14 days
P-G (79:21) -80°C		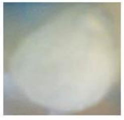			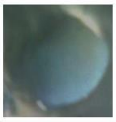				
P-G (79:21) -20°C		-	-			-			-
Aam-MBAAm 3.1% -20°C			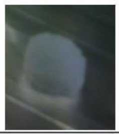					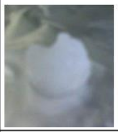	
A-AAm-G (56:7:37) -20°C			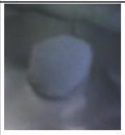						
D-AAm-G (52:17:30) -80°C	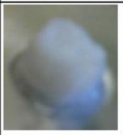		-	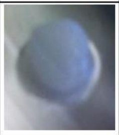		-	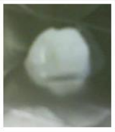		-

P-G monoliths frozen at -20 °C also had the same behaviour, except P-G(79:21)-80. Indeed this behaviourism lead to a 15 minutes enlargement of the reticulation time of first prepared dextran-based monoliths, in order to allow a better arrangement/stabilization of composites before freezing and see if the problem was caused by reaction time. Thus according to the results (easy disintegration upon tweezers mechanical disturbance) the time extension seemed to be insignificant. However the reduction on freezing temperature from -20°C to -80°C seemed more appropriate. However the soft structures achieved were considered not suitable for the purpose of the work (same was valid for P-G monoliths).

The remaining supports frozen at both temperatures were stable. Some photographs of the progressive behaviour of chitosan-based monoliths are pictured at Table 3.5..

All monoliths developed in this work, besides being cryogels – macroporous structures with interconnected pores ranging from several to hundreds of micrometers, allowing easy permeability for biomacromolecules[49] – they also constitute hydrogels. These structures, can be classified into chemical or physical gels, if the chains are hold together by covalent bonds, or otherwise by hydrogen bonds, Van der Waals forces or physical entanglements, respectively[167]. Still they can be termed: i) permanent at a given set of experimental conditions, if they involve covalent bonds or strong physical bonds; ii) reversible, if they involve weak physical interactions formed from temporary associations between chains[158].

Table 3.5.– Stability Tests performed at pH 3, 7 and 11 of different chitosan-based monoliths prepared at -20°C. Monoliths behaviour was analysed during fourteen days, having the first picture being taken at day three.

Monolith	pH 3			pH 7			pH 11		
	3 days	9 days	14 days	3 days	9 days	14 days	3 days	9 days	14 days
C 2.9% -20°C						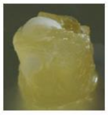			
CP (50:50) -20°C				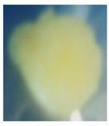		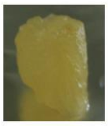			
CP (33:67) -20°C		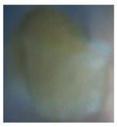			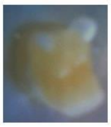		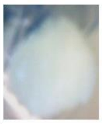		
CG -20°C	-	-		-	-		-	-	

All structures produced constitute physical gels with a minor chemical character, and should be non-permanent once only physical entanglement between chains probably takes place. Moreover they all have degradable polymer backbones, except AAm-MBAAm monoliths, once polyacrylamide is not biodegradable neither is the synthetic small monomer/crosslinker MBAAm, and C-G, due to crosslinking between poly(GMA) chains.

Despite the implementation of a non-degradable crosslinking agent on chitosan-based monoliths, its low content in casting solution (5.6%(w/w) with respect to the polymers and/or monomers mass) allows the formation of a sufficient open mesh that should allow an accelerated chemical degradation.

The retaining capability of produced hydrogels is possible due to its insolubility (provided by the entangled arrangement between chains), and is related to the polymer-water interactions or hydrophilic groups amount on the surface of support, depending also on the crosslinking density. This leads to retaining capacities ranging from ~10% up to thousands of times its dry weight, always maintaining its structure[167]. An increase on hydrophilic groups' content implies higher water retention by the matrix, while an increase on crosslinking density entails a lower swelling equilibrium, due to a decrease in the hydrophilicity and reduction in stretchability provided by a rise on polymeric mesh constraints.

Chitosan is a polymer known to have the ability to respond to pH changes in surrounding environment by protonation/deprotonation of its amine groups ($pKa \approx 6.3$)[168]. Thus chitosan-based monoliths must present changes in their swelling ability according to the external environment. The remaining monolith specimens due to the absence of ionizable groups in their molecular structures at any pH buffer they should not present any structural changes upon pH variation[169]. As some chitosan-based monoliths were copolymerized or blended with other monomers and polymers, dynamic swelling assays were performed to access some information about structures produced.

Through Figure 3.7. it can be observed that all chitosan-based monoliths prepared at -20°C change its structure for different H^+ concentrations in solution. They all present slightly swelled structures at pH7 and relaxed, voluminous, highly swelled frames at pH5. At low buffer pHs (<pK_a of chitosan), like pH5, there is a transfer of H^+ to the $-NH_2$ groups distributed all over chitosan chains ionizing them to $-NH_3^+$. According to Donnan theory this results in displacement and accumulation of counterions (A^-)[1] inside the hydrogel, creating an osmotic pressure gradient between the inside and outside, forcing water entrance into the system. The positive charges generated, also create electrostatic repulsion forces, which contribute to the expansion of gel mesh[169]. However as cryogels swell and matrix enlarges the osmotic pressure declines, and elastic retraction forces provided by the imprisoned mesh increases[158,169].

---

[1] A^- refers to the basic specie from the acid/base solution equilibrium $AH \leftrightarrow A^+ + H^+$

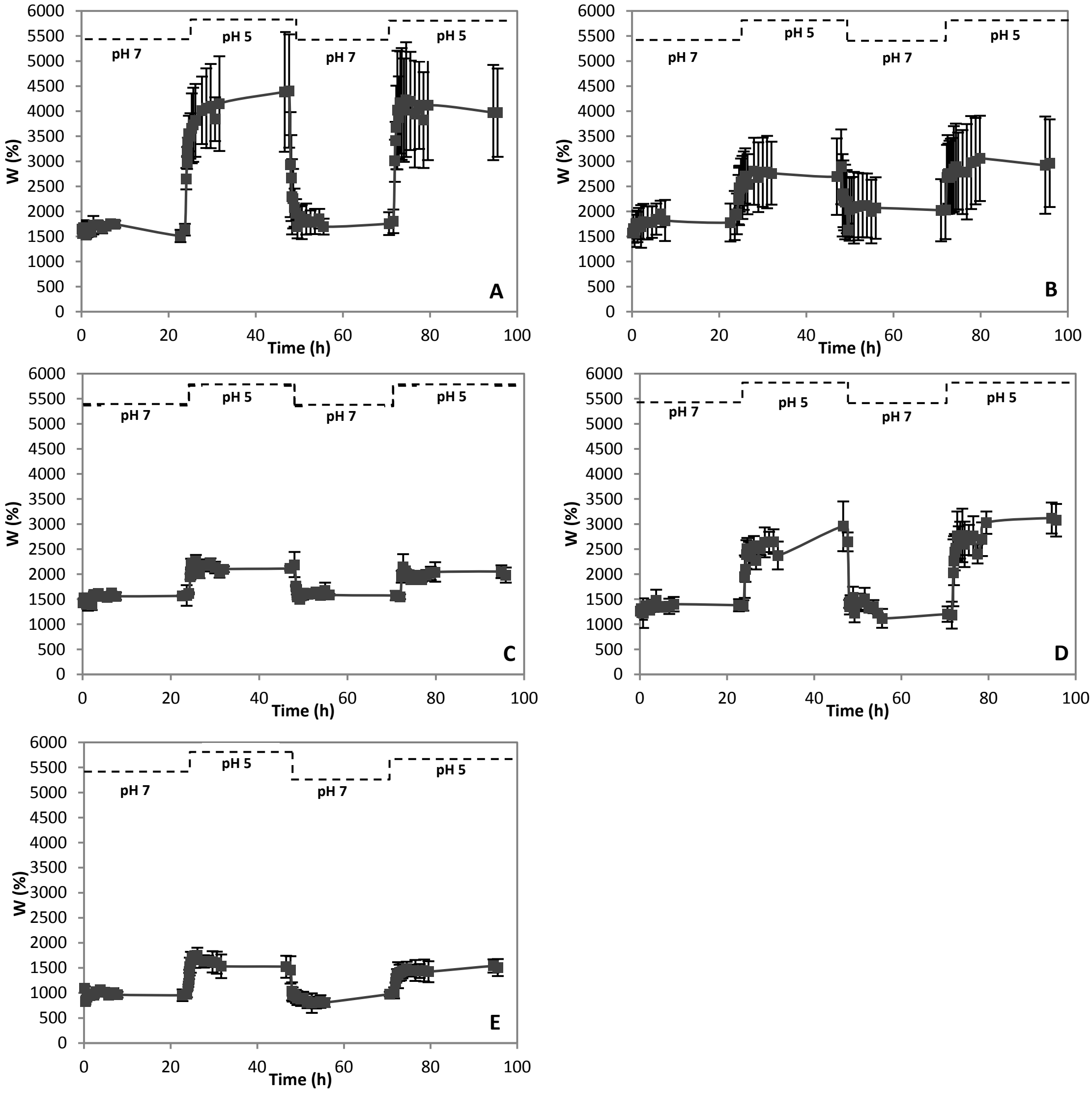

Figure 3.7. – Cyclical swelling analysis: variation of percent swelling degree (W) with time (t). Each monolith (frozen at -20°C) is alternately plunged into two different pH buffers (pH7 and 5) over time. C2.9% (a); C2% (b); C-G (c) C/P(50:50) (d); C/P(33:67) (e). All samples are presented in duplicate.

The eventual balance of these two opposing forces is reflected in the plateaus observed for all plots, few hours after buffer plunge. When the samples are placed in pH7 buffer the originally charged groups of chitosan lose charges losing also their attraction for counter-ions. Thus net osmotic pressure difference between inside and outside environments decrease and monoliths shrink.

It can be observed that monoliths swelled very fast (it could be observed even with naked eye) reaching its final swollen state in few minutes. Furthermore it can be concluded that all chitosan-based monoliths have pH memory once plateau values at same pH are approximately the same.

Analysing carefully the first swelling plateau at pH7 C2% presents a slightly higher equilibrium swelling comparing to C2.9%. Chitosan with its high molecular weight chains leads to viscous casting solutions, that will originate smaller crystals, smaller pores and thicker walls; thus a reduction on polymer concentration should and seems to result in larger pores with thinner struts allowing an easier matrix expand, and so higher W(%)[27]. Moreover the higher amount of imprisoner (MBAAm) in C2% limits even more the swelling ability. Regarding C-G, C/P(50:50) and C/P(33:67) all present lower and decreasing values comparing to C2.9%; this reflects the reduction on the hydrophilic portion (number of ionic groups decreases together with number of counter-ions inside the hydrogels, producing a reduced osmotic pressure that confines cryogel swelling) by increasingly adding PVA or GMA over only chitosan[170,171].

Conversely at pH5, C2% presents a lower swelling degree (W(%)) than C2.9% (2500% against 4000%, respectively). This is probably explained by the higher density of imprisoner in C2% monolith against C2.9%. In C2.9% the concentration of polymer in solution is 30mg/mL whereas in C2% the concentration was decreased to 20mg/mL, but the concentration of imprisoner for both formulations was 1.7mg/mL. The higher the crosslinker density, the higher the resistance of the material to volume enlargement during water uptake[171]. In case of chitosan/PVA blends and chitosan copolymerized with GMA the W% value is also lower than the one held by C2.9%. Probably what occurs is that the network freedom to swell is compromised not only by a decrease on ionic groups, but also by an improvement on mechanical properties. This results in an increment on elastic contraction forces exerted by the hydrogel towards water entrance[27,172]. Indeed a growing chitosan:PVA ratio seems to result in a more constrained swelling. Analysing closely C-G, its equilibrium swelling jump is shorter in comparison to the C/P. This is probably explained by the viscoelastic properties of PVA[173].

Figure 3.8. plots the swelling dynamics of chitosan-based monoliths prepared at -80°C. Looking to the pH5 and 7 both equilibrium swelling plateaus, the results show a reduction for all monoliths. This seems to be caused by the smaller sized pores, with probably more compact walls (stiffer materials as proved by Table 3.6. versus Table 3.7.). These compact walls with closer and tighter polymer segments should reduce the access of water to bulk material with consequent limitations on swelling behaviour. Moreover the distance between crosslinks within the cryogel frame becomes shorter constraining the expansion[174]. Indeed a larger pore architecture has been already involved in lower swelling degrees[175,176]. This reduction on swelling upon freezing temperature reduction is a slight one, probably due to the high surface area provided by small pores.

Chitosan 100% cryogels seem to present the highest W(%) and C/P(33:67) the lowest, probably because of its higher rigidity due to PVA content. A rise is observed in the second pH 5 plateau for C2.9% and C2% reflecting probably the poor elasticity of 100% natural monolith, stretching forward but not completely back.

In both Figures 3.7. and 3.8. it is notorious a general progressive rise on the swelling degree. This is possibly explained by the gradual hydration over time, with progressive expansion and relaxation of polymer chains. Maybe a cooperative action of network relaxation and water diffusion in addition to flow of water through pores[174]. Probably this picture would be different if the study was performed at pH~3 and 9 instead of pH5 and 7 respectively, where the osmotic pressure gradient would be so maximum[169]. The higher value for the first pH5 plateau on C/P(33:67) prepared at -80°C in comparison to its counterpart prepared at -20°C can be related with the higher surface area of the monoliths prepared at lower temperatures, a variable that seems to surpass all the others[154].

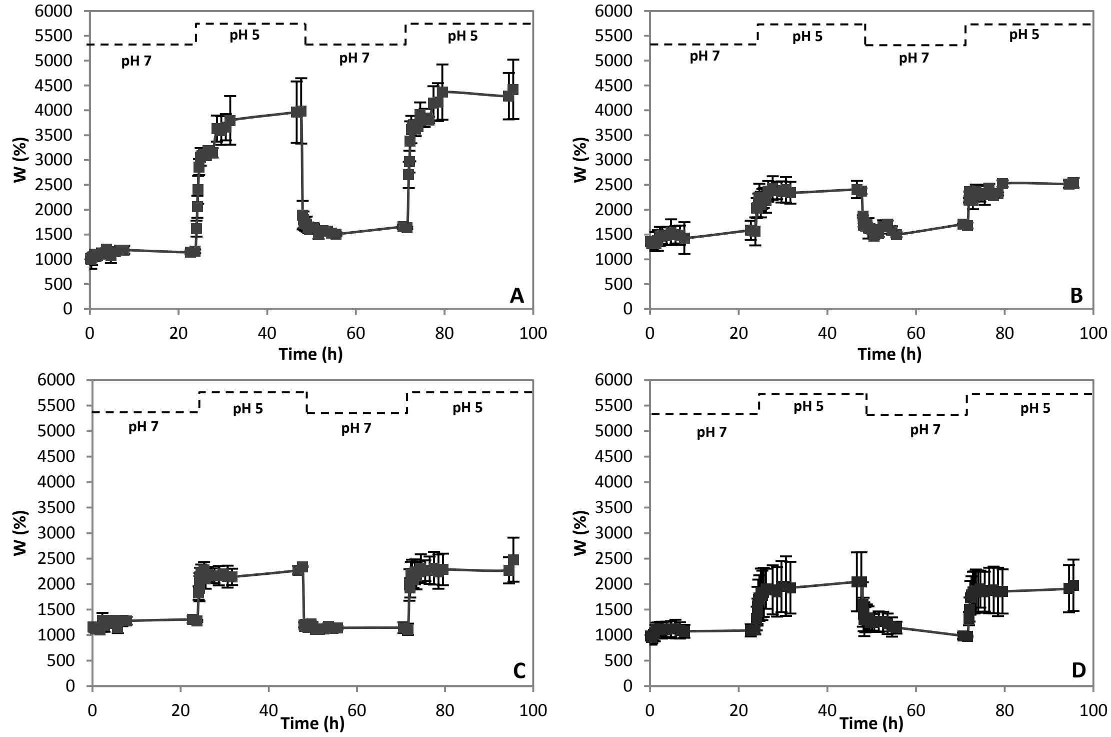

Figure 3.8. – Variation of percent swelling degree (W) with time (t). Each monolith (frozen at -80°C) is alternately plunged into two different pH (pH 7 and 5) solutions over time (t). C2.9% (a); C2% (b); C/P(50:50) (c); C/P(33:67) (d). All samples are presented in duplicate.

According to Table 3.6. all monoliths prepared were, as expected, highly porous (≥83%). When composites concentration is raised to 6.5% the porosity seems to be approximately maintained (88±4 for AAm-MBAAm3.1% against 83±5 for AAm-MBAAm6.5%). However comparing these results to the compressive modulus data we can detect that Archimedes displacement method was non-sufficiently accurate for measuring porosity. Measuring porosity by weighing the mass loss of a certain displacement liquid renders the technique restricted by accuracy to weight that mass loss and by displacement liquid chosen. Moreover the volume measurement with a ruler increases significantly that inaccuracy. In this work the displacement liquid elected was ethanol, once it can enter the pores easily without network swelling or shrinkage[177]. However due to its vapour pressure at 20°C (44.6 mmHg[178]) maybe 2-propanol (33 mmHg[179]) could be an alternative[180]; other methods could also be employed (mercury intrusion porosimetry[27,137], physical gas adsorption, inverse size-exclusion chromatography). Indeed porosity mirrors the stiffness of a material[181,27], in which a lower void volume fraction should imply a higher resistance to equipment claws motion (higher compressive modulus), i.e. a stiffer monolith. Thus a higher compressive modulus associated with a lower porosity was expected from AAm-MBAAm6.5%. The highest compressive modulus of dry and wet AAm-MBAAm6.5% against AAm-MBAAm3.1% shows the influence of a closer mesh on the rigidity of the matrix. A closer network should result from thicker struts[136,174], that in turn should accrue from a higher casting concentration, resisting more to the opposing destructive force of equipment claws.

Table 3.6. – Morphological and mechanical properties of all monoliths prepared at -20°C. All data was obtained from duplicated measurements (in case of water flux measurements each one of the two samples was measured three times).

Monolith	*$T_{Freezing}$ (°C)*	*Porosity[a] (%)*	*Water Flux ($L.m^{-2}h^{-1}$)*	*Compressive Modulus (kPa)*	
				Dry	*Hydrated*
C2.9%	-20	89±3	79±1	1.5±0.4	0.4±0.1
C2%		91±2	n.a.[b]	2.6±0.1	0.6±0.1
C/P(50:50)		94.6±0.3	151±43	3.8±0.1	0.7±0.3
C/P(33:67)		93±3	72±24	4.3±1.0	0.2±0.04
C-G		93±1	209±18	3.7±0.2	1.9±0.1
A-Am-G(56:7:37)	-20	95±1	307±63	1.76±0.05	0.61±0.04
A-Am-G(58:12:30)		95±1	265±44	5.0±0.1	0.77±0.05
AAm-MBAAm3.1%	-20	88±4	23±11	1.6±0.1	0.6±0.1
AAm-MBAAm6.5%		83±5	14±8	2.4±0.1	0.7±0.3
P-G(79:21)	-20	91.8±0.3	7±1	1.8±0.1	0.6±0.02
P-G(89:11)		93±1	14±1	1.2±0.2	0.9±0.2
D-AAm-G(56:7:37)	-20	94.7±0.5	148±48	0.8±0.1	0.25±0.03
D-AAm-G(58:12:30)		95±2	90±16	0.49±0.05	0.3±0.01

[a] Porosity values obtained through Archimedes Principle

[b] Value impossible to measure, maybe due to wall rupture, as consequence of their thin thickness

Regarding water flux through monoliths it mirrors the effects of main architectural properties on mass transportation[182]; it reflects the combination of five important parameters on monoliths: porosity; pore size, shape and distribution; interconnectivity; fenestration size and distribution; and orientation of pores[183]. Thus assuming interconnectivity maintenance, the decrease in porosity, and probably pore and fenestration size (caused by the thicker struts of increased feed concentration) may decrease the water flux value[183,184], as it can be slightly seen comparing AAm-MBAAm3.1% and AAm-MBAAm6.5%. The so low global water flux values of AAm-MBAAm monoliths may be originated by the so closed network comprising them (high concentration of crosslinker[185]), that leads to minor space between network chains available to accept the free water, and so they have tendency to be bound to surface polymer chains (low hydration). The closed mesh may even jeopardize pore interconnectivity[136] (small fenestrations or poor connection due to the higher casting viscosity) despite the high porosity value[183]. Li 2003;Kemppainen 2010;

In case of P-G monoliths, in P-G(79:21) only GMA content was raised in comparison to its resembling P-G(89:11), leading to a higher casting concentration and a higher imprisoning polymer concentration (Table 3.3.). Lower porosity and flux as well as higher compression modulus were expected and obtained. However as water flux is a reflection of countless architectural monolith features, the so low global water flux value must be related to the fragile character shown on stability tests, that probably conducts to a collapsed structure with an emphasized tortuosity (result of preclusion offered to fluid flow by the structure internal architectute[186]). According to information accessed the wet compression modulus may present a high value. It should be explained once again by its deformed/sloppy structure that retains the water that should be expelled during uniaxial compression; once retained and as it is uncompressible the water insert bias on the final values.

In dextran-based monoliths from D-AAm-G(56:7:37) to D-AAm-G(58:12:30) the GMA concentration was maintained constant but dextran and acrylamide concentrations were raised in the same proportion. The increase in casting concentration (Table 3.3.) should lead to, as P-G monoliths, a lower porosity, higher dry and wet compressive modulus and lower water flux, from D-AAm-G(58:12:30) against D-AAm-G(56:7:37). Water flux values were confirmed, however porosity values seems unchanged and therefore probably compromised by referred inaccuracy of used method. In respect to dry compression modulus the strange value of D-AAm-G(56:7:37) and D-AAm-G(58:12:30) could maybe be explained by the increment in the less rigid monomer constitutive of the coiling imprisoning copolymer, i.e. acrylamide , rendering the increment in concentration not significant in terms of stiffness improvement.

The GMA maintenance with increment in acrylamide and base polymer was also accomplished on agarose-based monoliths. Once more porosity seems to be maintained between specimens (A-AAm-G(56:7:37), A-AAm-G(58:12:30)) with water flux decreasing with increasing concentration. However dry and wet compression moduli increase significantly from A-AAm-G(56:7:37) to A-AAm-G(58:12:30). The ~1% increment on composites concentration seems to be enough to significantly alter monolith properties. Maybe the difference between agarose and dextran-based monoliths lies on the natural polymer itself: upon cooling, agarose chains are known to form helical fibres that assemble into supercoiled structures with 20-30 nm radii[187]; and they seem to constitute branch lacking quasi-rigid linear fibers with lengths dependent on polymer concentration, explaining the very low concentration need for its gelation and the high shear modulus of the gels, in comparison to that of a gel gathered from a flexible chain[188] (like dextran[189]).

Comparing C2% and C2.9%, the former which has a lower concentration is expected to present a lower casting viscosity, consequent larger pore size and thinner struts, which imply higher porosity and lower compression modulus. The also consequent lower surface area should origin a higher water flux. Porosity and dry compressive modulus check. However the same is not true for water flux and wet compression modulus, which was probably caused by increased coiling imprisoning monomer concentration, whose effect is just noticed at hydrated state, reinforcing swelling analyzes. This higher imprisoning monomer concentration reduces the effects of higher polymer concentration, and also leads to narrow spaces between the polymer chains limiting free water acceptance. Thus water molecules (not free) have tendency to bind polymer chains, enhancing resistance to solute diffusion (lower water flux)[174].

The copolymerization of chitosan with GMA or PVA seems, as expected to improve chitosan mechanical properties. Against expectations the porosity also increased, this maybe happened because the increase in mechanical strength drift from the materials themselves and not from the thickening of struts. In fact it should be related with a larger pore size caused by a reduction on casting viscosity[27]; possibly also explaining the increased water flux. However for C/P(33:67) despite the higher porosity the water flux seemed to even drop. Maybe the problem is the PVA content, probably insufficiently hydrophylic to grant the water flux desired for the application[190]. Just decreasing freezing temperature a whole set of new and different materials were produced.

Generally speaking, Table 3.7., as well as Table 3.6., shows lower compression moduli for wet specimens than for dry ones. This could be explained by the mobility of network chains upon hydration. These values are very important once the monolith is going to be applied in its hydrated state. However the compression moduli for monoliths prepared at -80°C increased. This is probably related to the formation of more compacted and rigid materials[191]. What could have happened is that the isotropic cellular pore morphology, as a result of rapid ice crystals growth, scatters the unidirectional pressure in every direction, rendering it more difficult to be damaged when compressed. Conversely the anisotropic pore architecture that should characterize monoliths prepared at -20°C (due to ice crystals growing along the direction of the temperature gradient) should present lower compressive modulus once the stress tends to concentrate around the channels of the scaffold with crossed fibers raising the risk of destruction[191,192]. Indeed this results support swelling measurements.

Table 3.7. – Morphological and mechanical properties of all monoliths prepared at -80°C. All data was obtained from duplicated measurements (in case of water flux measurements each one of the two samples was measured three times).

Monolith	$T_{Freezing}$ (°C)	Porosity (%)	Water Flux ($L.m^{-2}h^{-1}$)	Compressive Modulus (kPa)	
				Dry	Wet
C2.9%	-80	91±3	69±8	4.1±0.9	1.8±0.3
C2%		90±3	16±0	1.9±0.5	0.8±0.1
CP50:50		91.0±0.4	74±21	10.1±1.1	1.7±0.3
CP33:67		90±4	4±1	10.5±2.3	1.0±0.3
C-G		91.0±0.3	188±39	6.7±2.2	1.29±0.05
P/G(79:21)		85±4	15±5	2.6±0.6	n.a[b]
P/G(89:11)		83±4	2±1	3.1±1.7	n.a
D/AmG(56:7:37)		95.5±0.3	3±0	0.60±0.04	n.a
D/Am-G(49:14:37)		95±3	13±5	1.4±0.5	n.a
D/Am-G(58:12:30)		89±4	49±12	0.8±0.1	1.0±0.3
D/Am-G (52:17:30)		96.4±0.4	26±1	1.0±0.2	0.88*

[a] Porosity values obtained through Archimedes Principle

[b] Value impossible to measure, maybe due to crumble of structure.

*No quantified error due to just one measurement

However in cases where porosity lowers, this parameter may help in this compression moduli increase. The shorter distance between coiling imprisoning fractions maybe also contribute to the higher modulus, once this shortening should make the monolith more rigid restricting the relaxation of polymer chains with negative influence on water flow[174].

Lowering freezing temperature to -80°C seems, as expected, to have decreased the average pore size[27], once water flux values are very low in comparison to Table 3.6. Assuming maintenance of porosity, the higher surface area produced by the minor pore size is known to increase the friction force between fluid and material, hindering the water flow[183]. C-G has not only the higher value from Table 3.7., its value is very close from its -20°C resembling. This can be caused by the imprisoning hydrophobic polyGMA formed, that somehow facilitates crystal growth. Maybe its presence helps not only in the reduction of casting viscosity (that by itself contributes to larger pores), but also in the easier exclusion of entangled copolymer from the frozen solvent (due to its hydrophobicity), giving rise to larger ice crystals and consequently larger pores improving water flux. It is noteworthy that the larger pores formed at -20°C probably causes larger fenestrations that helps improve permeability.

Regarding porosity, it can increase or diminish with freezing temperature, it depends on the materials constitutive of monoliths[193]. Porosity seemed to exert no effect on compression modulus, once for almost equal porosities between monoliths (Table 3.7.) the compressive moduli varies slightly between them but deeply comparing to their counterparts prepared at a higher temperature.

By maintaining casting concentration and playing with freezing temperature the structures produced (within the same polymer basis) seems to be, once more, different among each other. Comparing C2.9% and C2% maybe the thicker walls of the former, again, give the monolith a higher stiffness. The higher water flux is probably related to these mechanical properties that avoid structure collapsing with increase on tortuosity. Comparing C-G, C/P(50:50) and C/P(33:67) with C2.9% it seems like the minor distance between imprisoning chains accentuates PVA and GMA effect through higher compression modulus.

P-G monoliths from Table 3.7. present a lower porosity than those on Table 3.6., associated with lower pore size that should have diminished the water flux. Although the dry compression modulus reflects more stiffness, when hydrated the real properties of the support arose and the compression modulus was not possible to measure due to water retention in the support (possible pore collapse).

Regarding dextran monoliths the mechanical properties seemed to be improved by increasing acrylamide amount, and decreasing freezing temperature, maybe because with smaller pores the imprisoning copolymer effect is enhanced.

It is noteworthy that each characterizing parameter studied (swelling, porosity, etc.) for each support results from an interplay between, pore size, shape, volume and orientation, fenestrations size, interconnectivity and materials used (concentration, nature), so a deeper study in prepared monoliths is highly demanded to fully understand its behaviour.

Hereupon it seems that the most promising and suitable monoliths to continue the work were A-AAm-G(58:12:30), CP(50:50) and C-G prepared at -20°C, due to their attractive flow, mechanical properties and stability.

Due to influence of hydrated state analyses on applicability of monoliths the elected supports were subject of another analysis. According to swelling kinetics (**Figure 3.9.**) the rate of water uptake showed little difference between specimens. All monoliths swelled up to 80-90% in half a minute reaching some sort of equilibrium. These similar values can be explained by the similar porosity and pore size. However in case of agarose monolith compressive modulus seemed to exert no effect on water flow into the monolith reflecting maybe an independence of water diffusion from polymer segments relaxation[174].

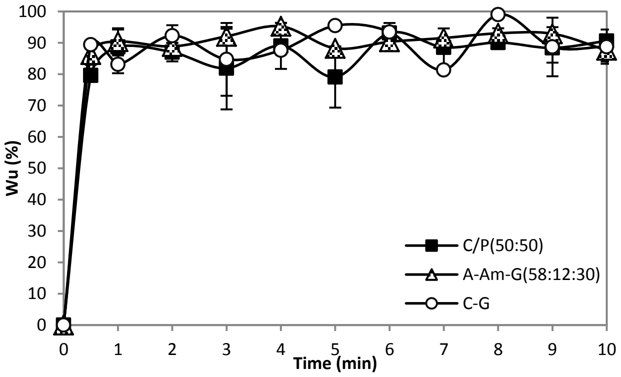

Figure 3.9- Swelling kinetics of A-AAm-G(58:12:30), C-G and C/P(50:50).

3.3.3. Magnetic Field Responsive Monoliths

Chemical co-precipitation was the elected method to synthesize the superparamagnetic iron oxide nanoparticles (MNPs) due to its cost-effectiveness and simplicity. The superparamagnetic nanoparticles synthesized presented, as expected, a large hydrodynamic diameter of 655±35 nm, consistent with the literature values[86,87]. The polydispersity value 0.7 is high and so the particles synthesized are not homogeneous. Regarding zeta potential (-2.69±0.21V) it evidenced a negative surface for the particles at pH5.6 as already noticed[86,87].This low value explains the large hydrodynamic diameter determined, once the not stabilized bare MNPs tend to aggregate and form larger clusters..

Magnetic-field sensitive monolithic cryogels (hybrid monoliths) in which MNPs are dispersed and incorporated were developed. These ferro-cryogels combine the magnetic properties of particles and the elastic properties of the cryogel. Moreover the biocompatibility of MNPs does not compromise the applicability of monoliths in question[87]. The embedding of MNPs onto the monoliths renders them spongier and seems to confer them some additional robustness and elasticity (Figure 3.10.). Morphologically on a macroscopic level all monoliths are comparable to the non-magnetic ones in terms of wetting rates and geometrical preservation of shape upon complete hydration over 24h. Some characterizations were performed in order to ascertain if native monoliths morphological and mechanical properties are maintained or not. Table 3.8. shows that for all specimens the MNPs embedding seems to first cause little decrease (24/46 mg/mL) and then a slightly increase (51/67 mg/mL) in porosity values. This close values probably reflect the good distribution of the particles, forming low aggregates due to stabilization by the polysaccharides. Maybe the decreasing value reflects the preference of the particles to remain on surface of pores (higher surface area), which when in higher concentrations due to some attraction they migrate faster for the interior of struts during crystallization. However MNPs leaching in ethanol during porosity measurements can be a possibility, so further studies on the matter should be done to exclude this possibility.

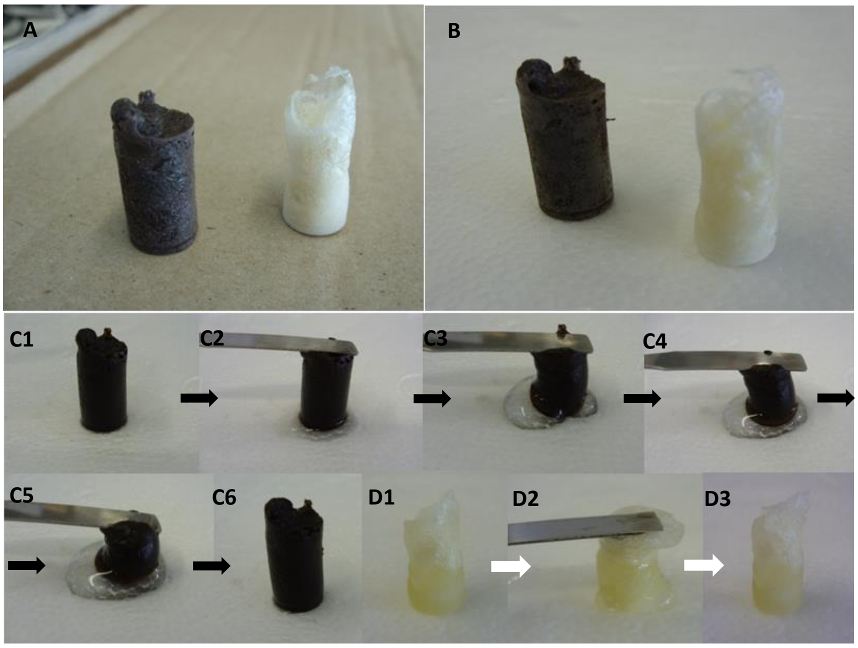

Figure 3.10.- Digital pictures from C-G monoliths: dry monolith embedding MNPs (A, on the left) and native monolith (A, on the right); hydrated magnetic monolith (B, on the left) and native monolith (B, on the right); sequential squeezing of hydrated magnetic monolith (C1-6) and native monolith (D1-3). Both recover its original shape after deformation.

Once more, due to the high porosity and consequent interconnectivity of the monolithic networks, no pressure was necessary to make water flow through the support, so measurements were performed at 1atm (25°C). Upon hydration 25mg/mL magnetic C/P(50:50) presented a more fragile character than the other supports, and maybe enough to cause some pore collapse and consequent tortuosity increase with pore closure. This may have led to the immeasurable flux under gravitational force; little pressure needed to be applied. In case of C-G and Ag-AAm-G(58:12:30) it seems that the MNPs embedding causes an increase in the water flux. An increase that reveals itself astonishing for C-G when the MNPs concentration in the casting solution is raised (1620±377 $L.m^{-2}.h^{-1}$). This probably happens once hydrated C-G presents a decrease in compressive modulus when MNPs concentration in solution is raised, conferring the support enough elasticity to endure such a high water flux. However the same is not verified for Ag-AAm-g(58:12:30) maybe due to some pore obstruction caused by the MNPs leaching corroborating the porosity value.

Analysing globally the compressive modulus surprisingly it seems that for both dry and hydrated states the increasing of MNPs concentration is followed by a decrease in moduli values.

Table 3.8. – Morphological and mechanical comparison between non-magnetic and magnetic monoliths with MNPs at two different concentrations for each specimen. All data was obtained from duplicated measurements (in case of water flux measurements each one of the two samples was measured three times). M_C/P(50:50) denotes magnetic C/P(50:50), the same is true for the others.

Monolith	*[MNPs] (mg/mL)*	*Porosity*[a] *(%)*	*Water Flux (L.m^{-2}.h^{-1})*	*Compressive Modulus (kPa)*		*Average Pore Size Diameter (µm)*
				Dry	*Wet*	
C/P(50:50)	-	94.6±0.3	151±43	1.5±0.3	0.7±0.3	33±9
M_1_C/P(50:50)	25	90.7±0.2	n.a.	0.8±0.6	0.2±0.05	n.a.
M_2_C/P(50:50)	51	93±1	-	-	-	-
C-G	-	93±1	209±18	3.2±0.3	1.9±0.1	111±31
M_1_C-G	25	92.1±0.4	224±32	0.7±0.2	0.3±0.01	154±54
M_2_C-G	51	95±1	1620±377	-	0.09±0.01	-
Ag-AAm-G(58:12:30)	-	95±1	265±44	2.4±0.1	0.7±0.05	34±8
M_1_Ag-AAm-G(58:12:30)	46	92±1	324±1	0.9±0.3	0.4±0.2	54±16
M_2_Ag-AAm-G(58:12:30)	67	92.8±0.5	247±19	-	0.1±0.05	-

[a] Porosity Measured through Archimedes Method

Apparent density takes into account the whole monolith volume whereas true density takes into account only the composites volume. Thence there is a discrepancy between these values for all specimens (Table 3.9.). It was also noticed that both apparent and true densities for dry state monoliths are several times lower than for hydrated ones. This is explained by the huge water uptake ability of the three specimens.

Dry and hydrated state non-magnetic monoliths have also different apparent densities between specimens reflecting the macroscopic observations: C/P(50:50) and C-G present similar and slightly shrinked structures contrasting to Ag-AAm-G(58:12:30), with reflections in their hydrated volume. Thus Ag-AAm-G(58:12:30) despite its higher hydrated volume, its superior mass endows it with higher apparent density. The same was verified between magnetic monoliths.

As expected the true densities present higher values (same mass but polymers volume instead of whole rod volume). It seems that the water uptake capacity is slightly higher for C/P(50:50) and C-G both magnetic/non-magnetic monoliths (ratio of hydrated and dry true density) going against the conclusions drawn through compressive modulus, where to the stiffer materials less water uptake is expected. In case of native monoliths the lower hydrophilic/hydrophobic composites ratio of Ag-AAm-G(58:12:30) possibly explains uptake value. On the other hand the presence of particles could have reduced global charge inside the cryo-monolith (due to interactions between –NH_3^+ and –O^- of MNPs), and the less charge attracts less water molecules into monolith that swells less). Moreover due to MNPs presence probably the water binding the surface chains and MNPs finds itself hindered to penetrate walls. The H-bonding established between the polysaccharide and the particles could have slightly diminished the water necessity for solvation of the molecules.

As expected, the relative density of dried monoliths was significantly lower than the hydrated ones. As in elastomeric cellular solids[194], prepared monoliths should vary its relative density proportionally to compressive modulus. It is verified only in hydrated state, maybe due to volume measurements associated errors. The relative density independence from porosity reinforces the independence of compression modulus from porosity verified on Table 3.8..

The high and similar total pore volume explains the high and similar porosities of scaffolds, either magnetic or non-magnetic and between specimens. These high values, together with high elasticity of modified matrices, can explain the high permeabilities. In case of Ag-AAm-G(58:12:30) the total pore volume decreases when it is modified. Maybe a thickening of walls accompanied by an enlargement of pores explains it.

Table 3.9. – Pore volume and density values for magnetic and non-magnetic (native) monoliths. All data was obtained from duplicated measurements. M_C/P(50:50) denotes magnetic C/P(50:50), the same is true for the others.

Monolith	*[MNPs] (mg/mL)*	*Apparent Density x10^3 (g/cm3)*		*True Density x10^{-1} (g/cm3)*		*Relative Density x10^{-3} (g/cm3)*		*Total Pore Volume (cm^3/g support)*	
		Dry	*Wet*	*Dry*	*Wet*	*Dry*	*Wet*	*Dry*	*Wet*
C/P(50:50)	-	87±18	713±110	28±5	668±215	1.48±0.41	10.8±1.9	8±2	1.3±0.2
M_C/P(50:50)	25	96±6	1015±94	36.2±0.5	801±4	0.96±0.18	8.4±1.3	8±1	0.9±0.1
C-G	-	71±6	782±12	33±4	533±8	0.92±0.02	8.8±1.4	11±1	1.09±0.02
M_C-G	25	72±11	883±152	37.2±0.9	548±27	0.46±0.01	5.9±1.8	11±2	1.0±0.2
Ag-AAm-G (58:12:30)	-	78.6±0.5	1084±49	75±5	835±296	0.30±0.07	4.8±0.2	11.38±0.01	0.8±0.1
M_Ag-AAm-G (58:12:30)	46	100±4	1003±47	91±7	998±40	0.32±0.08	3.0±0.6	8.9±0.5	0.90±0.04

To a higher total pore volume is associated a higher stiffness (chitosan-based monoliths). This fact could be explained by an increase of pores together with the influence of materials (PVA, GMA).

The swelling ratio in deionized water after 10 minutes was: 8.0±0.4 (Ag-AAm-G(58:12:30)), 10.8±0.2 (M_Ag-AAm-G(58:12:30)), 17.5±0.5 (C-G), 13.7±1.1 (M_C-G), 17.7±0.1 (C/P(50:50)) and 18.1±1.4 (M_C/P(50:50)). Despite Ag-AAm-G(58:12:30) pore volume and elasticity it has the least adsorption capacity, probably due to its lower hydrophilic/hydrophobic composites ratio. The lower values of C-G magnetic/native in comparison with C/P(50:50) magnetic/native should be related to the former minor elasticity. Comparing with Figure 3.8., despite the water uptake capacity, Ag-AAm-G(58:12:30) adsorption rate seems to be the lowest of the three specimens.

The response of magnetic monoliths to four different magnetic-flux densities (0.25T, 0.50T, 0.53T and 1.5T) (Figure 3.11.) was tested. Matrix distortion/recovery was monitored for 30 minutes. When superparamagnetic materials are posed in a magnetic-field gradient, forces act on the magnetic entities and due to the strong interactions between them and polymers segments, the monolith moves as a sole unit. It was verified that shape distortion was relatively fast (varying with specimen and magnetic-flux density) as well as its vanishing when the external magnetic field was applied and removed, respectively (Figure 3.12.).

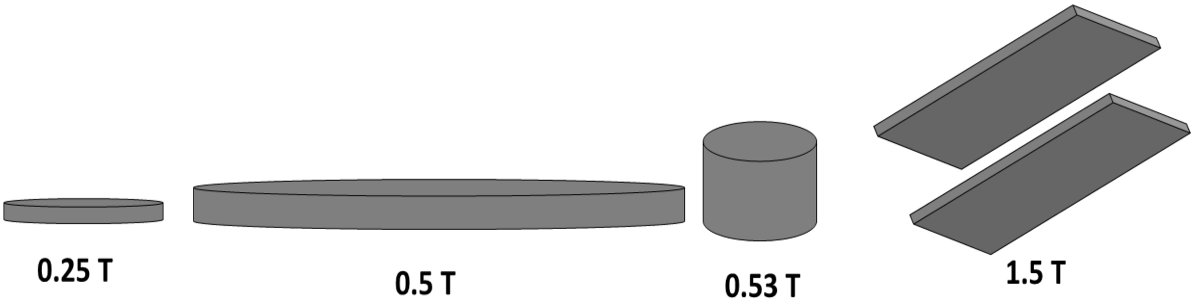

Figure 3.11. – Permanent magnets used for field response testing.

In fact the measurements performed in the centre (data not shown) or edges of the magnet shown a variation: monoliths response was more evident when placed near the edges.

Generally, all monoliths presented a faint response when placed on a 0.25T magnet and a clearest one when placed over a 0.53T magnet. The clearest response at 0.53T magnet over 1.5T is maybe related with the monolith position on the latter magnet and its geometry: the two rectangular magnets configuration (attractive or repulsive) dictates where the maximum flux density is located[195] and in case of attractive magnets the maximum is settled near the centre not where the monolith was placed; on the other hand the low height-to-length ratio that diminishes the axial component of the flux density rendering flux density quiet non-uniform inside magnet (both along its axis and across its length)[196] probably enhances the bad monolith position; despite the relatively high error bars.

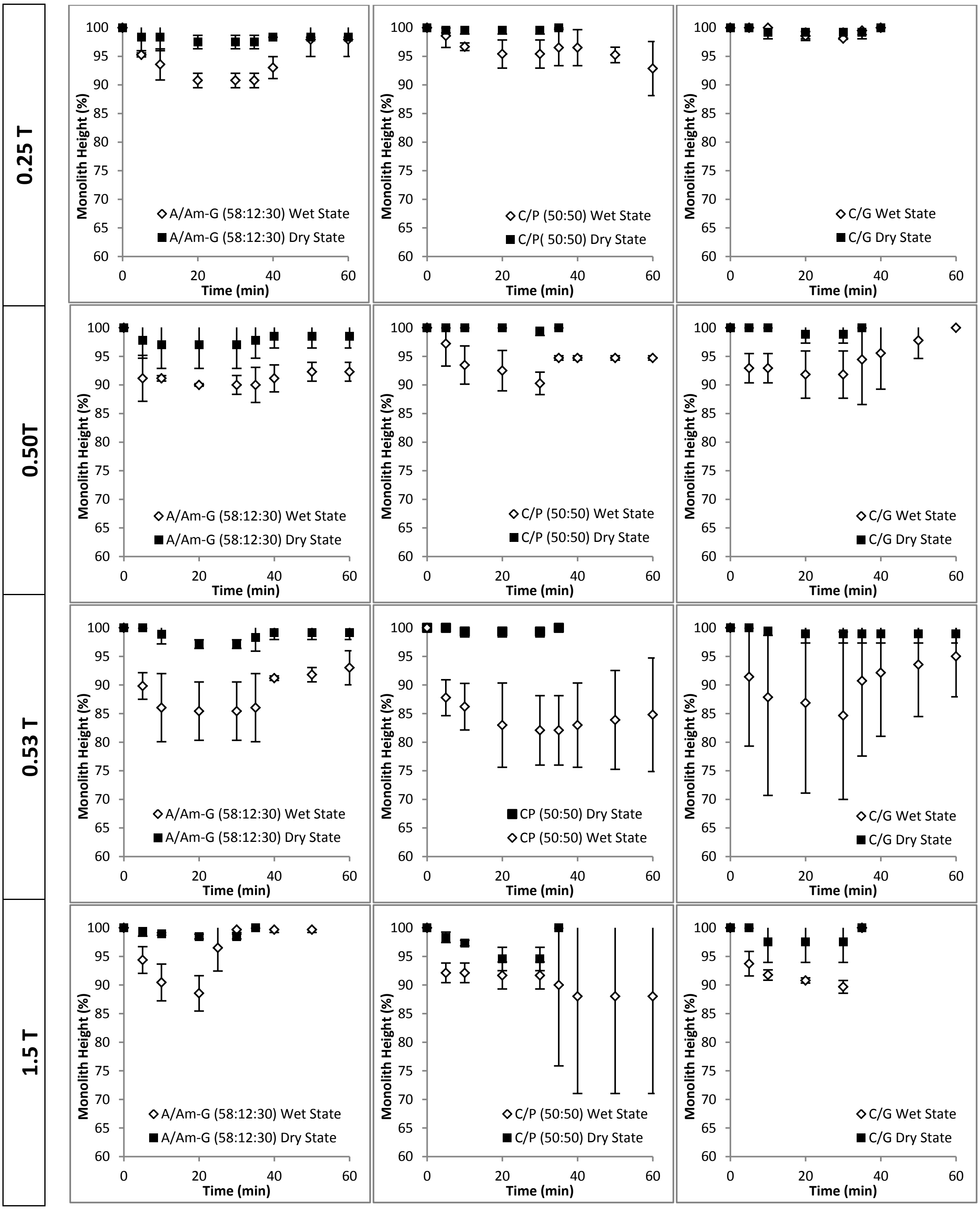

Figure 3.12.– Magnetic-field response of Agarose (A-AAm-G (58:12:30)) and chitosan-based monoliths (C/P (50:50), C-G) to different magnetic-flux densities: 0.25T, 0.50T, 0.53T and 1.5T. The first five points plotted no each graph corresponds to deformation under external magnetic-field, the following five corresponds to matrix behaviour after external field removal (when reached the initial length no more points were plotted). Data was obtained from duplicated measurements.

Regarding high response to field C/P(50:50) seems to give the most prominent one. However in accordance to macroscopic analysis and results from Tables 3.8. and 3.9. the fragile character of magnetic C/P(50:50) was unmasked again. Comparing Ag-AAm-G(58:12:30) and C-G, despite the former enhanced response it seems that for 0.50T and 0,53T fields 30 minutes were not sufficient for its total recovery.

The stiffer monolith (C-G) seemed the one that faster recovers its initial height and the less stiff (C/P(50:50)) is the one that slowly recovers its initial height (not recover at all in the 30 minutes) or even collapse. This reinforces that results are in accordance to previous characterizations.

For a deeper and final morphological analysis both magnetic and non-magnetic monoliths microstructure was analysed by SEM (Figure 3.13.). It was noticed that freezing and lyophilization processes produced an open pore microstructure provided with a high degree of interconnecting channelling. Non-magnetic monoliths exhibited a smooth surface contrasting with the rough coarse-grained like surface regarding magnetic ones. For magnetic C-G and Ag-AAm-g(58:12:30) the microscopy revealed a uniform distribution of MNPs throughout the matrices with MNPs embedded within the walls, confirming pore volume data. This reflects the effectiveness in MNPs stabilization by the materials. However the same was not verified for magnetic C/P(50:50), in which some clumps or segregations were observed, probably as a result of MNPs aggregation as happened elsewhere[197]. Even the cutting stage for analysis can explain the clusters observed (fragile structure destruction). Freezing temperature tunes average pore size, originating large pores at -20°C that fends MBAAm coils; this together with a probably not so stabilized chitosan/PVA physical blend, could probably explain non-uniform MNPs stabilization. A slightly decrease on average pore size, as well as loss on pore architecture definition was verified for C/P(50:50). This phenomenon should be a result of aggregates formation that probably took place before/during freezing, thus compromising pore size definition by freezing temperature. Those observations corroborate the mechanical and physical information from Tables 3.8. and 3.9..

In turn an increase on wall thickness for Ag-AAm-g(58:12:30) was not enough to reduce water flow, instead a significant increment was verified when MNP were embedded; probably due to pore enlargement. This increase in the pore size with gross porous morphology maintenance could be an MNPs enhancement effect on ice crystal formation. Regarding magnetic C-G pore size and shape heterogeneity increased.

It seems that fenestrations size is reduced in all supports when MNPs are embedded, explaining probably the obtained porosities.

Comparing non-magnetic supports the smoothest surface belongs to C-G, the other supports present some roughness, probably arising from dendritic morphologies of ice crystals.

Regarding pore architecture on non-magnetic monoliths it was observed that the most viscous casting solutions (C-G) presented more oval pores (semi-spherical) in contrast to the more uniform pore structures (equiaxed) from C/P(50:50) or Ag-AAm-g(58:12:30). C-G high compression meduli can be attributed to its thick walls.

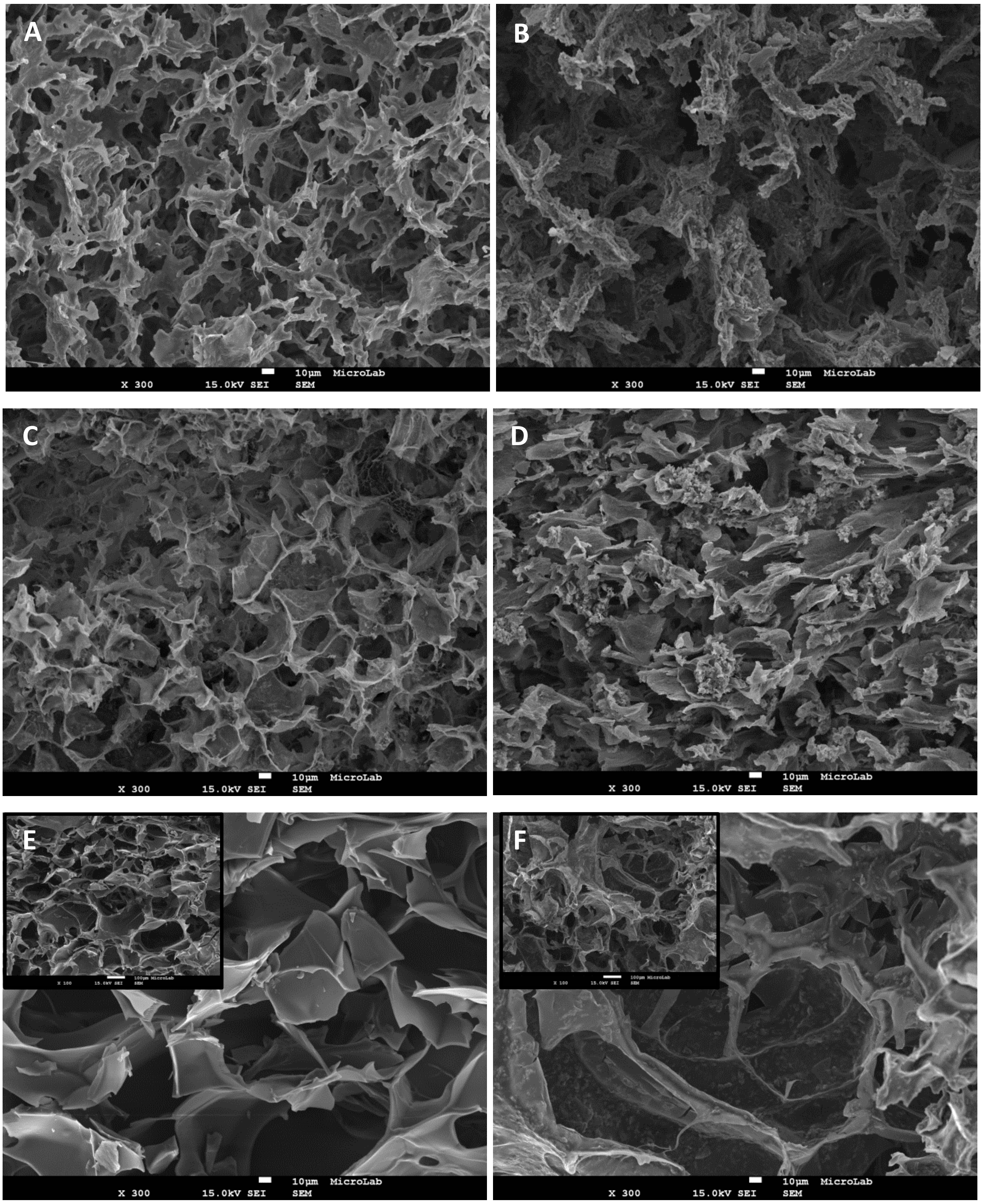

Figure 3.13. – SEM micrographs of non-magnetic (A,C,E) and magnetic (B,D,F) chitosan and agarose-based monoliths at x300 magnification: Ag-AAm-G(58:12:30) corresponds to A and B; C/P(50:50) to C and D; and C-G to E and F. For C-G monoliths a micrograph with lower magnification (x100 (left) x150 (right)) is shown.

Looking at a different region of native C/P(50:50) monolith (zoomed in Figure 3.14.) it was noticed the presence of polymeric suspended strings. This can probably be explained by freezing kinetics, where entrapment of small fractions of polymer blend within ice crystals (in the form of dendrites) can happen. MNPs presence can probably favour this phenomenon by innate aggregation tendency, which vanishes with total freezing.

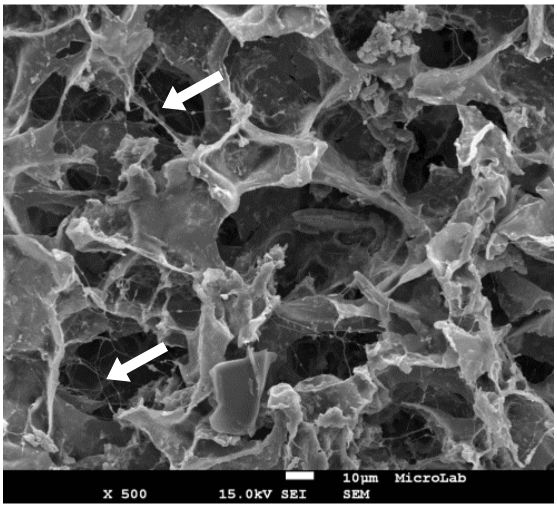

Figure 3.14. – SEM micrograph of C/P(50:50) native monolith at a magnification of x500. Notice the peculiar pendant polymer strings.

3.4. Testing for Non-Specific Binding of Ad5

The promising features of the analysed supports only render them viable if non-specific binding between it and Ad5 is negligible. In order to investigate this key parameter and validate the monoliths as potential chromatographic supports for adenovirus purification, screening tests were performed with the non-functionalized prepared supports. With a 1.45×10^{11} TP/mL virus loading obtained results are summarized on Table 3.10.. It is noteworthy that other previously prepared and discontinued monolithic supports were also tested.

Analysing monoliths prepared at -20°C, the results are very interesting once magnetic monoliths were the ones presenting the highest recovery values (71-81%), i.e only ~20% of viral particles were retained in the network. It is noteworthy that screening assays on magnetic monoliths were not conducted in the presence of an external magnetic field, even though there performance is still attractive. This superior performance could be explained by the determined and observed increase in elasticity and average pore size, at least for M_C-G and M_Ag-AAm-G(58:12:30). In case of M_C/P(50:50), as expected, a gravimetric flow was not achieved, however applying a slightly pressure with a plunger a good recovery was achieved proving that apparent fragile support can handle some pressure without significant collapsing with virus entrapment.

Table 3.10. – Comparative analysis of different monolithic supports for recovery of adenovirus vectors.

Monolith	*$T_{Freezing}$ (°C)*	*Modification with MNPs*	*Gravitational Flow*	*Recovery Yield (TP^a,%)*
M_C/P(50:50)	-20	✓	✗	77±2
C/P(50:50)	-20	✗	✓	57*
M_C-G	-20	✓	✓	81±5
C-G	-20	✗	✓	71*
M_ Ag-Am-G(58:12:30)	-20	✓	✓	71*
Ag-Am-G(58:12:30)	-20	✗	✓	49±1
C-G	-80	✗	✓	84*
M_C/P(50:50)	-80	✓	✓	81±7
C/P(50:50)	-80	✗	✓	79±2

[a] TP=Total adenoviral particles

*No quantified error due to just one measurement

The viral faction that remained into the support seems to be entrapped by the polymeric matrix once previews assays with the supports using an elution buffer 20 mM Tris 2M NaCl pH8.0 resulted in no additional virus recovery.

As adenovirus have an average diameter of 60-110 nm[114,113,115]; commercial monolith channels for adenovirus purification varies between 1-5µm[5]; and the average pore size of non-magnetic monoliths prepared at -20°C was between 33±9 µm (C/P(50:50)) and 111±3 µm (C-G); the two monoliths prepared at -80°C presenting the highest water flux values were also tested (Table 3.7.). Their performance seems to be improved even compared to magnetic monoliths produced at -20°C (84% recovery). However from all monoliths prepared at -80°C only C-G seems to be promising according to Table 3.7. data.

The overall recovery values were very promising once the support is not functionalized, and when a ligand is surface immobilized the access of the virion to the monolith wall is deeply reduced due to steric hindrance.

3.5. Concluding Remarks

Cryotropic gelation processing of materials followed by lyophilization was the strategy adopted, in order to procure a green, relatively robust, mechanically and chemically stable monolithic support for viral particles purification. Indeed the methodology employed was successful for the obtainment of supermacroporous monoliths.

In a first approach a whole screening of different combinations of distinct materials, and at two different temperatures was attempted. It could be concluded that physical blending of polymers and co-polymers together with the MBA proved to be a new, greener and efficient way to produce robust, insoluble, stable monoliths with attractive gravitational flow. That is, the usage of minimal quantities of a generally reported crosslinker molecule not as a crosslinker but instead as an entangling imprisoning polymer/co-polymer allows the preparation of a green (cryogelation of naturally sourced polymers followed by liophilization) macroporous structure falling into monoliths category of chromatographic supports. However to corroborate the latter, FTIR analysis should be performed.

Despite some structures present attractive properties being potentially applicable, others fell short of expectations. The conflict between optimizing porosity and maximizing mechanical performance was not successful for dextran-based, PVA and chitosan alone. However we believe that further optimizations mainly for dextran-based structures (in terms of its blending with other more rigid polymers, usage of lower molecular weight natural sourced polymers, or even change the nature/amount of imprisoning polymer) could give rise to a potential and efficient structure for virus purification. Molecular weight of synthesized polymers can be tuned through initiators concentration plyaing[198]. Smaller the chains higher the crystallinity of gel and stronger the mechanical properties.

It could be concluded that blending/copolymerizing chitosan with PVA/GMA, respectively, had improved significantly chitosan-based monoliths mechanical performance and gravitational flow properties.

Monoliths processed at higher temperatures presented in general higher permeabilities, porosities, and swelling capacity, however lower stiffness character.

It was found that according to the aims of work, the evaluation of morphological, mechanical and physico-chemical properties identified C-G, Ag/AAm-G(58:12:30), and C/P (50:50), processed at -20ºC, as the most promising supports.

After election of most promising materials, the magnetic modification was executed and the novel materials were characterized.

It seemed that these new monoliths present different properties from respective resemblants like higher flow rates, and lower mechanical properties, thought to be caused by cooperative and concerted approximation of particles due to its innate attraction.

Then magnetic and non-magnetic monoliths were tested towards Ad5 to ascertain the existent of non-specific binding to supports.

Magnetic natural polymer-based monoliths seems extraordinarily promising towards future virus purification, once not only the surface area is expanded but also the non-specific binding values were the lowest ones, with minimum and maximum recoveries of 71% and 81%, respectively. Thus magnetic C-G was assumed as the potentially best candidate for further development of ligand functionalized monoliths.

However, since MNPs embedding into monoliths induced increased flows, high porosity and robustness maintenance, and due to recovery results on monoliths processed at -80°C (84%), changes on C-G pore size should be a wise and even more promising step towards high throughput adenovirus purification.

4 AFFINITY MONOLITHS FOR GFP PURIFICATION

4.1. Introduction

Therapeutic proteins are nowadays considered the main biopharmaceuticals[199], and despite many non-proteinaceous biomolecules development, therapeutic proteins seems to keep constituting the fastest-growing cantle among all pharmaceuticals[106,107,199].

No universal protocol is available to purify recombinant proteins[102]; however affinity chromatography is a high-throughput, selective and efficient technique, that results in high protein purity products (>90%) in just one step, from complex mixtures of similar molecules[200,102,201]. An absence of appropriate affinity ligands for a broad range of proteins, and the difficult development of a generic protocol for protein purification (due to its variety), renders tag fusion to target protein a very appealing strategy to achieve the desired capture and purification, with consequent reduction of purification steps. Moreover, fusion to a reporter protein seems to ease recombinant proteins production[201].

GFP (Green Fluorescent Protein) is considered one of the broadest investigated and exploited proteins in areas as biochemistry and cell biology[202]. So taking advantage of GFP fusion to proteins to purify the target protein can reveal itself a broad and efficient mean of purification.

GFP was first isolated from the bioluminescent jellyfish *Aequorea Victoria*[203]. It is a 27-29 kDa protein that comprises 238 amino acid residues folded into a 11 β-sheet barrel-like structure, with an α-helix running through the centre and little distorted helical portions that stopples the barrel ends providing an unusual protective environment for three residues (Ser65, Tyr66, and Gly67) of that α-helix, that form a fluorophore[204,205]. The chromophore results from the covalently rearrangement of referred residues during GFP folding process together with oxidation by molecular oxygen, in a post-translational intramolecular autocatalytic cyclization reaction[204]. GFP is very stable, being resistant to several proteases, detergents, pH 5.5-12.6 environments, temperature (T_m=78°C), organic salts, chaotropic agents (8M urea), photobleching, or even pressure[204,206]. Moreover it presents low-toxicity, allows its easy detection in cell suspensions avoiding cell lysis, and contributes to minor burden of host cells due to its fairly small molecular weight[204,206]. Once recombinant GFP was shown to be expressed in countless species, from bacterial *E. coli* to animals or plants, passing throw fungi, it has been widely used in multiple assays, in many areas of science and medicine[203,204]. This pronounced versatility, together with its large two-photon absorption, and its harmless character when fused to proteins (no function alteration[204]) renders GFP an appealing candidate in applications such as tag/reporter or indicator. Regarding tagging applications GFP fluorescence mirrors gene expression levels or sub-cellular placements, by exposing domains/proteins to which

GFP is fused. This allows imaging biochemistry inside cells, visualise chromosome and protein dynamics in vivo, etc. As an indicator, GFP can be used to analyze protein-protein interactions, pH, metal or calcium concentrations by post-translational modulation of its fluorescence[204,203].

This renders GFP *"one of the most useful tools in modern science and medicine"*[207], that revolutionized our prospects over biological imaging.

Due to its extensive usage, countless reports on GFP purification methodologies arise, comprising: affinity character, hydrophobic interactions, size-exclusion and ion-exchange chromatography, phase partitioning, organic solvent extraction, and salt and metal precipitation, occasionally applied in combination[208]. Some reported affinity systems comprise: 6-his tag fused GFP towards NiII[209]; anti-GFP antibodies[202]; and even a GFP-binder 16kDa protein derived from a llama heavy chain antibody, binding GFP with high affinity and specificity[210].

Immunoaffinity chromatography that requires biological ligands usage such as monoclonal antibodies seems to be the most popular strategy[102]. However, biological ligands commonly tend to present high target specificity and binding capacity, together with high costs, low stability and life-span[102]. Conversely the economic structural ligands comprise low selectivity or tend to be leached, committing final product purity. The stable, re-usable, and robust biomimetic ligands (synthetic), can join the best of both worlds: economy and selectivity[102,211].

Recently, a novel biomimetic ligand towards GFP, ligand A4C7, was developed by Pina *et al.*[102] and was successfully tested on agarose beads. It can yield similar recoveries and purities, and can surpass the limitations of the previously mentioned methods. In another recent work Barroso *et al.*[27] developed novel chitosan-based monoliths suitable for antibody purification. This chapter presents the results from the combination of ligand A4C7 with referred chitosan-based monoliths, to create affinity systems for cost-effective purification of GFP-fused proteins.

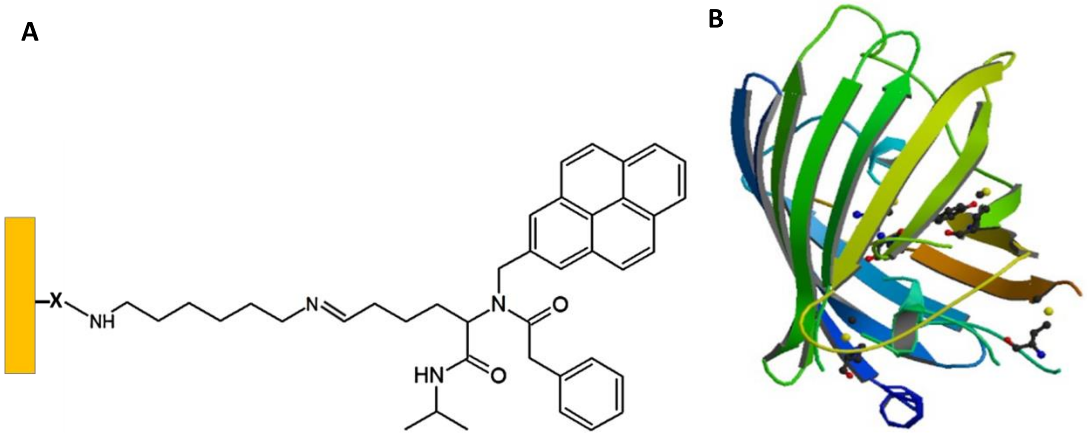

Figure 4.1. – Scheme showing ligand A4C7 coupled to chitosan-based monolith surface (A), and structure of GFP (PDB I.D.: 1ema) (B).

4.2. Results and Discussion

4.2.1. GFP Expression and Production

The plasmid containing the gene that encodes for GFP (pET-21c[2]) was captured (transformation) and amplified in NZY5*α* cells , chemically competent cells suitable for high efficiency transformation[212]. pET-21c expression vector containing an ampicillin resistance gene was introduced to the NZY5*α* *E. coli* cells that incorporates it making it part of its own genetic material. Then cells were cultivated on LB agar plates with antibiotic to denounce the ones that acquired the foreign DNA, as the cells without pET-21c lysed. The latter isolation of plasmid DNA for further transformation allowed the determination of its final concentration and purity through standard spectroscopic analysis (Figure 4.2.).

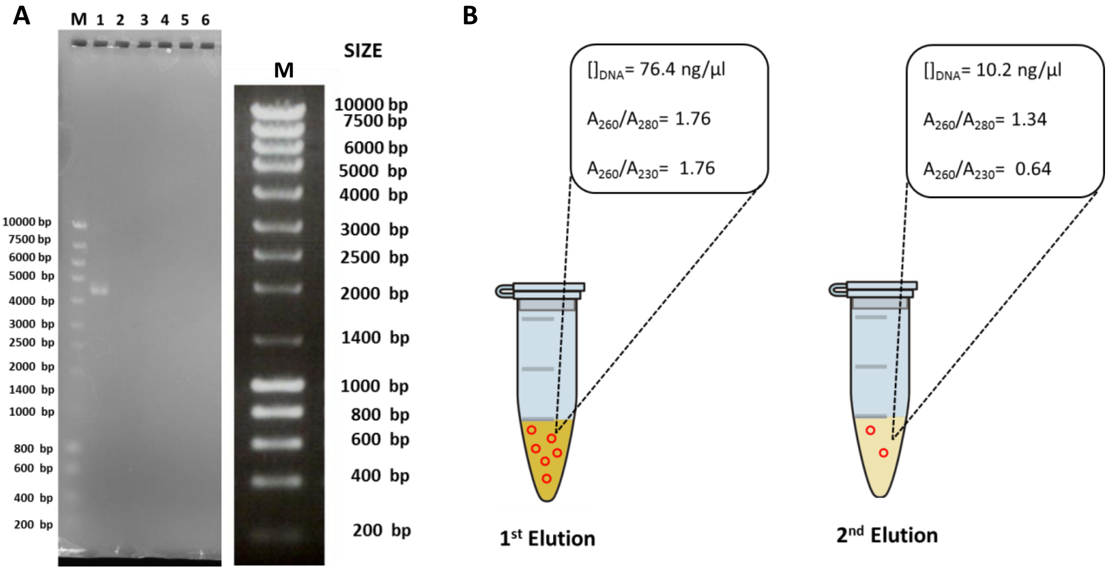
A
M 1 2 3 4 5 6
10000 bp
7500 bp
6000 bp
5000 bp
4000 bp
3000 bp
2500 bp
2000 bp
1400 bp
1000 bp
800 bp
600 bp
400 bp
200 bp
M
SIZE
10000 bp
7500 bp
6000 bp
5000 bp
4000 bp
3000 bp
2500 bp
2000 bp
1400 bp
1000 bp
800 bp
600 bp
400 bp
200 bp
B
[]DNA= 76.4 ng/µl
A260/A280= 1.76
A260/A230= 1.76
[]DNA= 10.2 ng/µl
A260/A280= 1.34
A260/A230= 0.64
1st Elution
2nd Elution

Figure 4.2. – pET-21c isolation and purification was successfully achieved as agarose gel electrophoresis (0.8%(w/v) agarose, stained after running) can prove (A): marker, 1st elution, 2nd elution (lanes 1, 2, 3 from left to right). First and second elutions recovered through NZYminiprep kit for DNA purification were quantified and analysed by NanoDrop spectrophotometer (B).

As expected, the first elution presented the highest pDNA concentration and purity.

---

[2] pET-21c is a widely used system developed for the cloning and expression of recombinant proteins in E. coli. For the purpose of this work pEt-21c was subcloned by Geneart™ to include a GFP encoding gene. However this created vector keeps the same denomination throughout this work

The large scale expression of GFP was performed in *E.coli* BL21(DE3) competent host cells, using first eluted DNA. Indeed the target gene initially cloned and established in NZY5α cells (non-expression host), was then transformed into BL21(DE3) cells (expression host) for further GFP expression. This strategy aims to avoid plasmid instability caused by the production of proteins potentially toxic to the host cell, being achieved once non-expression host lacks T7 RNA polymerase gene[213].

The large scale production of GFP was accomplished at the optimal conditions determined on small scale studies for a tagged GFP protein: induction with 1mM IPTG when OD_{600nm} ranged between 0.6-0.8 at 37 °C and 210 rpm[102]. Induction extension was 18h. During expression, growth and GFP production were monitored by fluorescence and optical density measurements (OD_{600nm}) (Figure 4.3.).

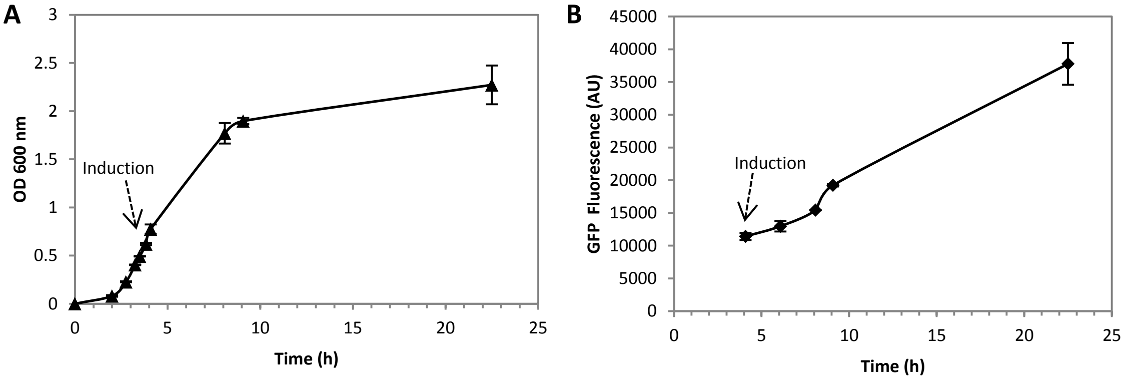

Figure 4.3. – Monitoring of Cells growth and GFP expression through OD_{600nm} (A) and fluorescence intensity measurements (B), respectively. A correlation between phenomena can be seen (conversion of nearly all cell's resources towards GFP gene expression[213]).

In order to qualitatively determine the relative amount of GFP in different time periods an SDS-PAGE analysis was performed (Figure 4.4.). However, to directly compare the amount of GFP produced at different times after induction, the loaded samples at different induction times were normalized to a final optical density of 1.2. Comparing GFP band in lane 6 (18h) and the other lanes, the former seems darker, thicker and more defined.

After GFP overproduction, its extraction from intracellular medium required its harvesting and mechanical lysing. A subsequent fractionation through two different steps of centrifugation took place and allowed cell debris and membrane fragments to be cleared. A clarified soluble extract could be obtained. The samples collected during fractionation stage were further analysed by SDS-PAGE and fluorescence (Figure 4.5.). Once finished fractionation stage GFP content was also evaluated by BCA assay.

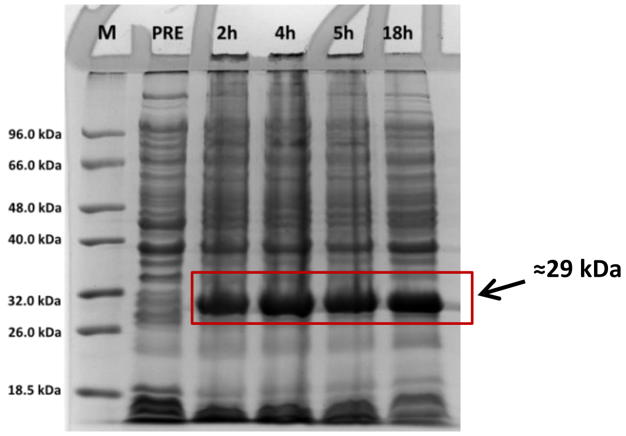

Figure 4.4. – Time course SDS-PAGE gel (12.5% acrylamide gel stained with Coomassie Blue R-250). GFP mass production can be visualized. M represents protein marker; PRE corresponds to sample collected at $t_{induction}$=0; all following lanes matches the GFP profile at different times of induction (2h, 4h, 5h and 18h). The band of GFP is expected to be placed at ~29 kDa[102,205]. The loading volume of each sample was normalized to a constant specific optical density value (1.2).

Fluorescence values rose intensively when cells were lysed and fractionated, probably due to fluorescence unmasking by cell debris removal.

GFP presence on centrifugation pellet is explained by contamination of wells, due to fluorescence results, and knowledge of GFP solubility in PBS[102].

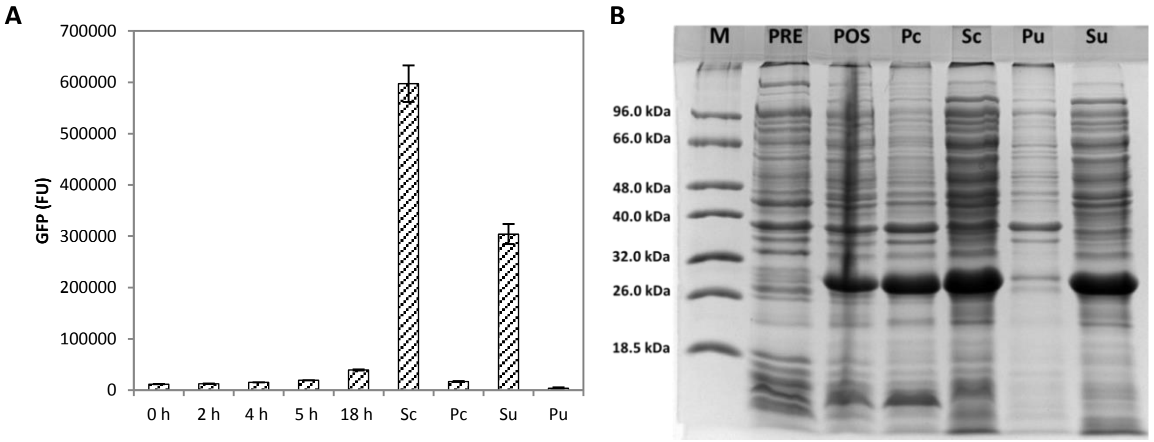

Figure 4.5. – Fluorescence monitoring during induction time and fractionation (A): 0h-18h represents the time after induction; Sc corresponds to supernatant obtained after centrifugation; Pc to pellet obtained after centrifugation; Su to supernatant obtained from ultracentrifugation; Pu to pellet obtained from ultracentrifugation. Cellular fractionation analysis by SDS-PAGE was performed (B): M represents protein marker; PRE corresponds to sample collected just before induction; POS corresponds to sample collected after 18h induction.

The fluorimetric and BCA assays to quantify the amount of GFP produced over the total protein revealed a 10.8% GFP content (1.11±0.42 mg/mL) in total clarified soluble crude extract (10.6±3.43 mg/mL) against 13% GFP from a previous work[102].

4.2.2. Preparation of Affinity Monolith towards GFP Purification

Monoliths based on a 50:50 %(w/w) chitosan:PVA blend prepared at -80°C (NC), with and without the incorporation of magnetic nanoparticles, have been prepared based on Barroso *et al.*[27] work. Both magnetic and native chitosan-based monoliths were activated with argon (Ar) plasma treatment in order to subsequently add amine free groups at its surface. The amination step was accomplished using 1,6-diaminohexane, and was crucial as it guarantees the insertion of a spacer-arm. It pulls away the ligand from matrix and alleviates steric hindrance, to facilitate an efficient binding between protein and ligand. Besides it has already been used in monoliths for a ligand comparable in size[27].

In plasma surface treatment the polymeric monolith is exposed to a low-temperature, low-pressure glow discharge. A partially ionized gas (free electrons, atomic, molecular, ionic, and free-radical species) named plasma is formed as a result of a certain gas imprisonment in a vacuum chamber and its subjection to an electric field. In turn this new-born highly reactive species interact with monolith surface modifying it[214,215].

Generally, plasma treatment is a fast and solvent free approach which allows surface modification through the introduction of chemical species, without creating any hazardous by-products. The capacity to retain the bulk material properties constant while surfaces are modified is crucial to the success of this technique[215,27]. Besides it is known to reduce non-specific protein adsorption[216].

Argon inert gas was chosen once plasmas generated in pure Ar leads to the creation of surface free radicals that can be used for cross-linking or grafting [215]. Its relatively low cost[217] and radical survival for several days make its application advantageous in comparison to ammonia plasma treatment[214].

Regarding the surface density of amine groups the experimental values obtained can be compared to the ones from the literature (Table 4.1.). Despite the highest efficiency of non-thermal plasma activation with amination reaction performed outside plasma chamber, and considering the high error bar associated with traditional epoxy activation route, the results of amination density by non-thermal plasma treatment with direct amination inside chamber were fairly satisfactory.

Table 4.1. – Comparative analysis on the efficiency of amination through three different approaches: traditional preliminary epoxyactivation, non-thermal plasma treatment followed by amination out-of-chamber, and non-thermal plasma with direct amination inside chamber. MC denoted for magnetic non-functionalized monolith and NC for non-magnetic non-functionalized monolith.

Monolith	*Epoxy Activation Followed by Amination*	*Plasma Activation with Amination Reaction Outside Chamber*	*Plasma Activation with Amination Reaction Inside Chamber*
	$[NH_2]$ x10 (µmol/gsupport)	*$[NH_2]$ x10 (µmolg/support)*	*$[NH_2]$ x10 (µmolg/support)*
MC	-	-	14±1
NC	23±7[a]	175±5[a]	20.4±0.3

[a] Values obtained by Barroso *et. al*[27]

The epoxyactivation route comprised the reaction of epichlorohydrin with surface free -OH groups. This results in a dependence of the surface amination extension on density and availability of OH groups, and thus on method efficiency. During plasma treatment there is a creation of countless potentially reactive free radicals, beyond those created from polymers functional groups on the monolith surface. So the number of amination sites rise, explaining the higher amination yield. In case of amination outside chamber the surface activated monolith is plunged into an amine solution (1,6-diaminohexane) allowing the contact of the radicals with a great amount of amine. However in case of direct amination inside chamber, the 1,6-diaminohexane is dragged into the chamber to the discharge zone, by taking it to vapour phase. Due to low 1,6-diaminohexane vapour pressure (0.12 mm Hg at 25°C[103]) and boiling point only at 204-205°C[103] (work temperature was ≥160°C), dragged amines might not have been sufficient to cover all formed radicals. This could have favoured a blocking effect by symmetrical 1,6-diaminohexane (both sides can equally react with nearby radicals), rendering amination not so effective as the former. Another possibility can be the presence of oxygen in the amine vapour that inhibits the reactions[217]. The power applied could be raised or the time of experiment could be extended, however it was verified that there is tendency for monolith degradation. A solution could be the improvement of system isolation (allowing O_2 privation and a rise on temperature), or optimization of operating pressure[218]. It is noteworthy that outside chamber amination (post-plasma irradiation grafting) takes more time (≈24h) than inside chamber amination (double plasma treatment) (only 33 minutes).

4.2.2.1. Monolith Functionalization and Characterization

Ligand A4C7, an affinity ligand created by Dr. Ana Pina[102], and based on a Ugi-scaffold was synthesized through a Ugi reaction, a multicomponent reaction between four distinct compounds: an aldehyde, an amine, an isocyanide and a carboxylic acid[102,219,220]. It is a chemical sustainable reaction, simple, atomically economic, cost-efficient, and convergent, in which the overall reaction yield trends to be maximized with minimal number of steps involved[102,221].

In order to perform the Ugi reaction on the monoliths a preliminary test on monolith stability and MNPs leaching (in case of magnetic supports) was performed at typical Ugi reaction conditions (48h assay in 100%(v/v) methanol at 60°C, 220 rpm). No MNPs leaching was verified and both magnetic and non-magnetic monoliths preserved their integrity.

The synthesis of ligand A4C7 was performed directly onto the solid support (step by step) employing NC compatible solvents and a 5x excess of starting materials.

Chitosan-based monoliths were firstly modified with glutaraldehyde and the success of this step was confirmed by the silver mirror test (Figure 4.6.). According to the visualized results it can be concluded that aldehyde was successfully attached to the solid phase monolith. No mirror was obtained in either of the negative controls but a shiny clear sliver mirror was obtained in both magnetic and non-magnetic monoliths (ML and NL respectively).

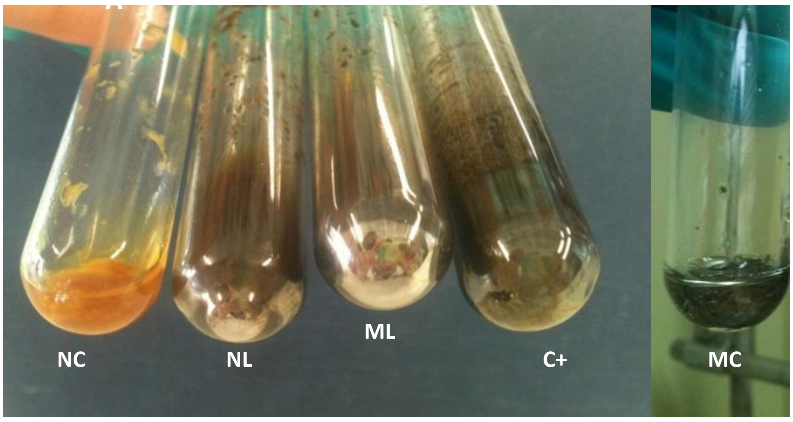

Figure 4.6. – Silver mirror test on aldehyde functionalized monoliths: non-magnetic and non-functionalized monolith (NC, negative control); non-magnetic and functionalized monolith (NL); magnetic and functionalized monolith (ML); Glutaraldehyde as positive control (C+); and magnetic and non-functionalized monolith (MC, negative control) (from left to right).

Then A4C7 synthesis was completed by addition of remaining components to the system. As the ligand comprises a polycyclic aromatic hydrocarbon (pyrene), the success of the reaction could be confirmed by fluorescence microscopy observations (Figure 4.7.). Controls and functionalized samples were visualized (after regeneration) through fluorescence microscopy and fluorescence could be observed only on monoliths where the four components of the Ugi reaction were present (1 sec exposure).

To monitor monolith bulk properties before and after ligand attachment, several parameters were measured and analysed (Table 4.2.). In case of non-magnetic and non-functionalized monolith (NC), the compressive modulus values are comparable with those previously reported[27] Comparing both NC and MC (magnetic and functionalized monolith), they present similar porosities, however the latter shown an increase in water flux, and a minor compression modulus. In case of both magnetic (ML) and non-magnetic functionalized monoliths (NL) they present decreased porosities when compared with their non-functionalized counterparts. ML and NL also present higher water fluxes and higher compressive modulus in dry state.

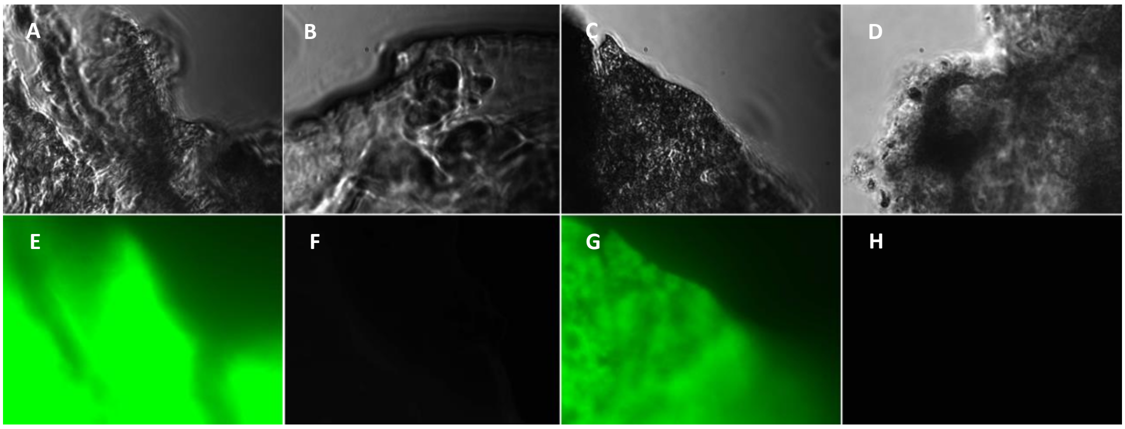

Figure 4.7. – Pyrene presence at the surface of NL and ML monoliths: non-magnetic monolith functionalized with A4C7 (NL) (A,E); non-magnetic and non-functionalized monolith (NC) (B,F), magnetic monolith functionalized with A4C7 (ML) (C,G), magnetic non-functionalized monolith (MC) (D,H) (from left to right). Pictures were taken on the fluorescence microscope under bright field filter (A,B,C,D) and fluorescence filter (E,F,G,H) at x40 magnification. All supports were regenerated before analysis.

However in dry state ML and NL seemed more brittle than native counterparts, explaining the compressive modulus. It is noteworthy that ligand functionalization seems to approximately maintain bulk rigidity/elasticity of both magnetic and non-magnetic supports, something that does not happen in case of ligand 22/8 based on a triazine scaffold[27]. Average pore size diameter is in accordance to mercury porosimetry values for NC (53±5 μm), and MC presents larger pores than the former.

SEM micrographs, allowed further elucidation of the internal morphology of prepared matrices (Figure 4.8.). The large and semi-spherical pores of NC monolith are mantained when MNPs are embedded. Approximately uniform distribution of macropores into polymer network is visible; however pore size increases, possibly explaining the raise in water flux. MNPs on MC surface seems relatively well distributed, however a peculiar pattern, resembling the suspended strings of Figure 3.14., is found on pores surface. That curious pattern observed, together with the whole pore, resemble the negative of several little rough staked columns[222], that when in ice form were connected to each other. They look like hanging networks near pores surface. Freezing kinetics could be an explanation and MNPs probably enhance the phenomenon (see chapter 3).

Table 4.2. – Morphological and mechanical properties of functionalized and non-functionaliized monoliths. All data was obtained from duplicated measurements (in case of water flux each one of the two samples was measured three times).

Monolith	*Porosity (%)*	*Water Flux ($mL^{-1}h^{-1}$)*	*Average Pore Size Diameter (μm)*	*Compression Modulus (kPa)*	
				Dry	*Wet*
ML	88±1	708±74	n.a[a]	1.12±0.30	0.65±0.03
MC	93±1	164±44	76±24	2.02±0.20	0.64±0.01
NL	89±1	779±36	n.a. a	2.09±0.69	0.97±0.18
NC	93.2±0.5	85±7	48±13	5.09±1.1	0.75±0.09

[a] n.a.: Measurement impossible to perform due to technique applied.

SEM image reinforces the possibility of ligand coupling onto monolith. Pores apparently obstructed had lost its initial shape and rigidity, however flow properties were enhanced. The same is valid for ML that seems to present narrower pores, probably explaining its lower water flux when compared to NL, i.e. smaller the pores lower the water flow due to increase on surface area, however the inclusion of MNP create ups-and-downs on the surface contributing even more to the surface area increase.

Magnetite crystals obtained by co-precipitation (diameter 5-20 nm), with high surface area and strong surface forces tend to form clusters. A way to counteract this trend is stabilizing them by adding surfactants or coating them with polymers[223]. The embedment of particles into the monolith is a way of coating the particles.

However with destruction of the matrix structure during axial compression, particles could not only be pushed against each other but also be exposed. This could promote MNPs aggregation alleviating clamps load over the network, and impart virtual elasticity to the support explaining compressive modulus of magnetic monoliths from this section and chapter 3.

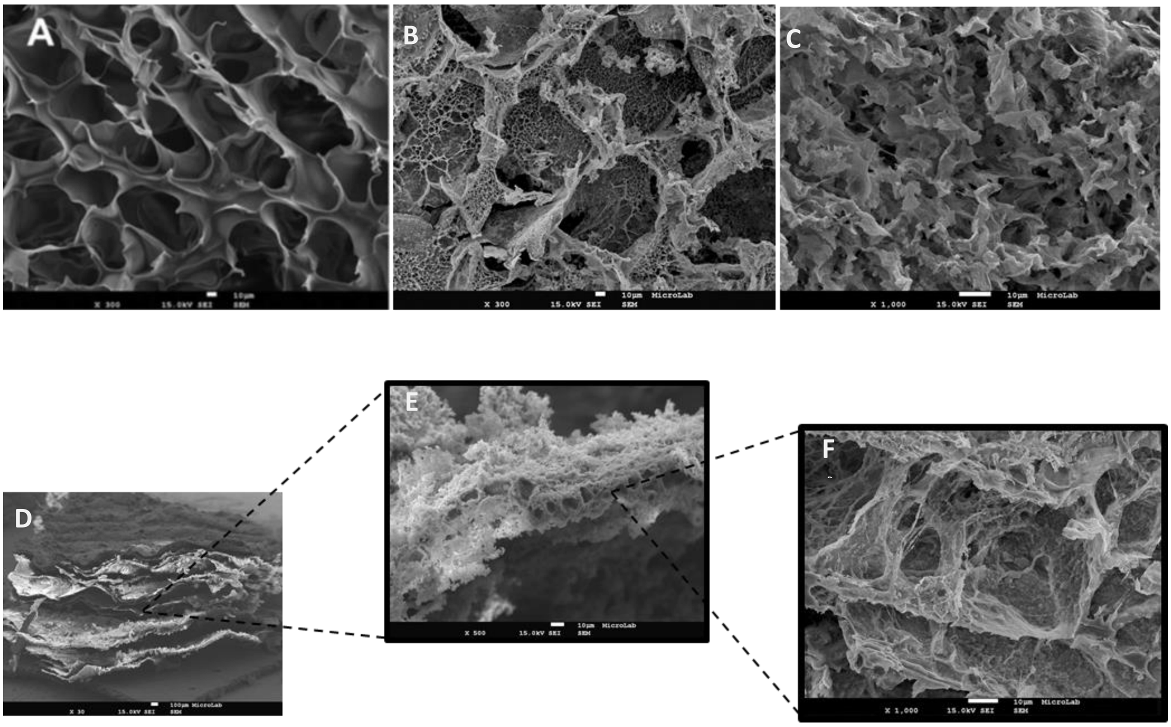

Figure 4.8. – SEM micrograph of NC monolith with x300 magnification kindly provided by Barroso et al.[27] (A), MC monolith with x300 magnification (B), NL monolith with x1000 magnification (C), and ML monolith with several magnifications: x30 (D), x500 (E) and x1000 (F).

Macroscopically, the colour change denounces the microscopic modification of monoliths surface. The shape and bulk dimensions are maintained, however a little shrinkage is observed with modification progression (Figure 4.9.).

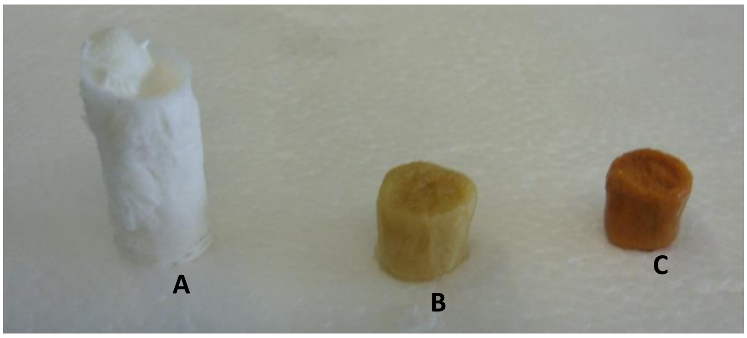

Figure 4.9. – Visual comparison between stages of monolith surface modification. C/P(50:50)80 native just lyophilized monolith (A), after aldehyde functionalization (B), after A4C7 solid-phase synthesis (C) (from left to right).

To monitor the magnetic response towards external magnetic field exposure, ML was placed above a 1.5T permanent magnet and its response was monitored for 1h

(Figure 4.10.). The monolith shrinkage has to guarantee the maintenance of pores micro-architecture, which has major effects on matrix properties and performance.

The 1.5T magnetic flux seems suitable enough for further screening tests, once the objective of field application is to induct little vertical shrinkage, in order to help target molecule expulsion during elution step or undesired molecules expulsion during regeneration step (column cleaning toward re-usage).

It was verified that before any surface modification the dry MC presented almost negligible response recovering immediately its initial height upon magnetic-field removal. The deformation was more pronounced in hydrated state, however the recovery was fast (~10 min). Upon amination with plasma technology and aldehyde coupling, the hydrated C/P (50:50)80 reduced significantly its elasticity. After stability test in 100%(v/v) MeOH during 48h, the monolith C/P(50:50)80 presented again a more flexible character.

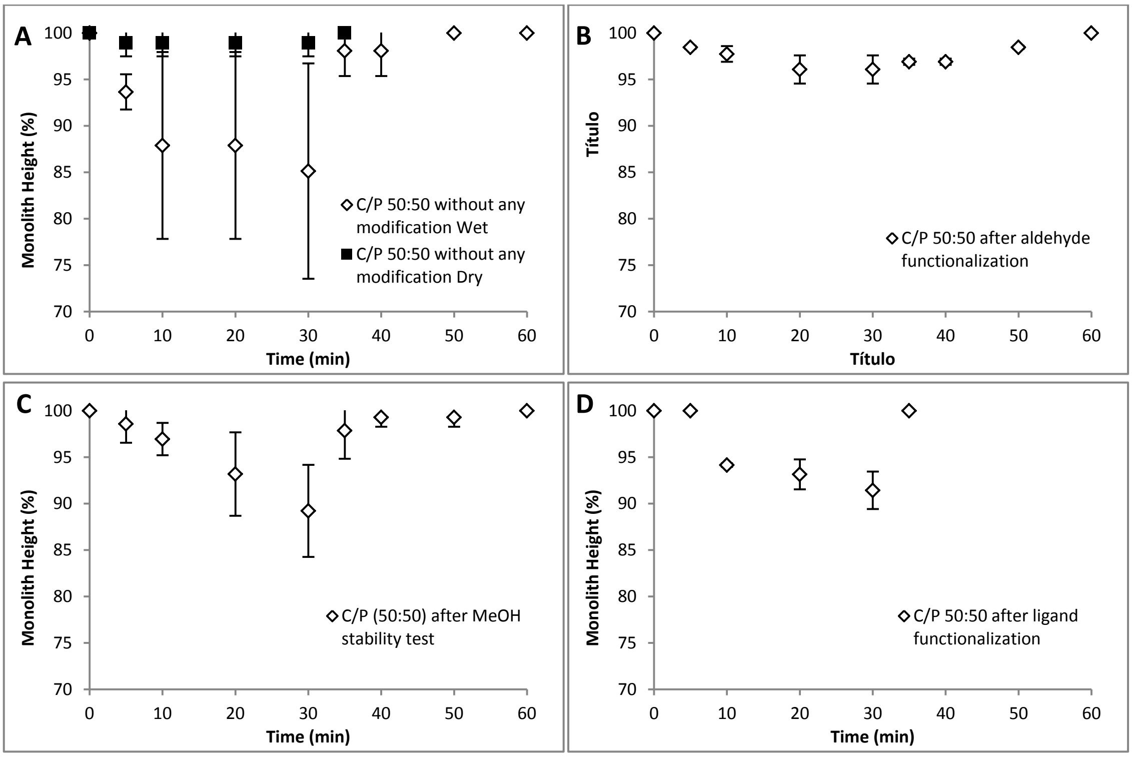

Figure 4.10. – Magnetic-field response of magnetic C/P (50:50)80 monolith at various modification stages at its dry (square) and wet states (diamond): without any modification (A); after aldehyde functionalization (B); after stability test in 100%(v/v) MeOH during 48h (C); C/P(50:50)80 after A4C7 functionalization. First five points plotted no each graph corresponds to deformation under external magnetic-field (1.5T), the following five corresponds to matrix behaviour after external-field removal (when reached the initial length no more points were plotted). Data obtained from duplicated measurements.

This might be related with molecular polarity: when aldehyde is functionalized on monolith surface, the carbon chain of amine cannot be properly solvated by water molecules, though when C/P(50:50)80 is soaked in MeOH these molecules are more suitable for the 6-carbon chains stabilization conferring additional material flexibility upon field response.

When C/P(50:50)80 is functionalized with A4C7 and thoroughly washed with a cocktail of solutions (final solution 20%(v/v) aqueous ethanol) the capacity to field-response decreases due to the rigidity imposed by A4C7 coupling, balanced with ethanol molecules present (EtOH less polar than MeOH or water).

4.2.2.2. Evaluation of Affinity Monoliths for GFP Purification

Screening tests with GFP crude extract (GCE) were performed using the best elution conditions tested by Dr. Ana Pina[102], i.e under alkaline conditions such as 0.1M glycine-NaOH pH9 with (E1) and without (E2) 50% ethylene glycol.

The leaching of ligand A4C7 from the monoliths ML and NL was tested at both elution conditions (Figure 4.11.). This was performed because A4C7 and GFP absorb and emit fluorescence at equal wavelengths, and because ethylene glycol is known to induce perturbations in the GFP fluorescence through ligand leaching, inducing bias on the results[102].

It is verified that elution with E1 buffer caused no A4C7 leaching whereas elution in the presence of ethyleneglycol (E2) caused negligible ligand leaching comparing with the scale of fluorescence of obtained GFP samples .

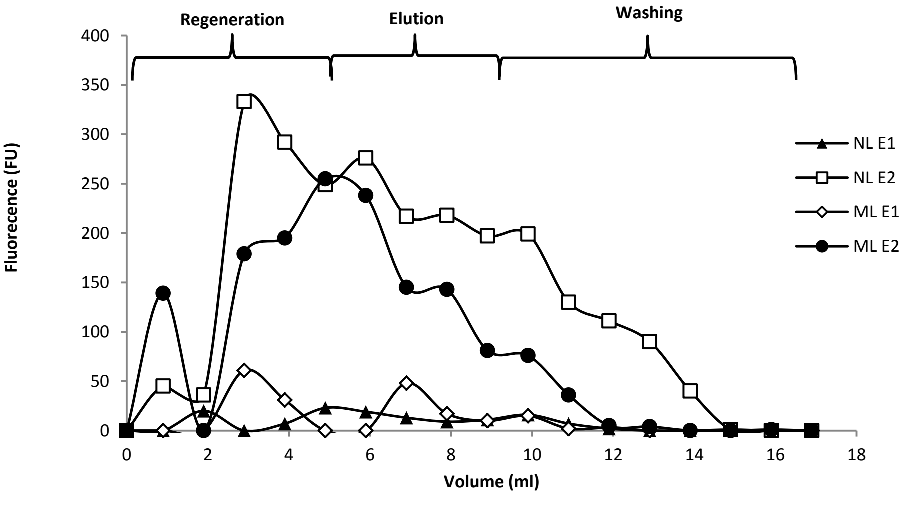

Figure 4.11. – Ligand Leaching assays. A4C7 leaching for NL and ML monoliths at 0.1M glycine-NaOH pH 9 (E1) and 0.1M glycine-NaOH pH 9, 50%ethylene glycol (E2).

Beyond the two elution conditions two binding conditions were also tested in GCE screenings. The two binding conditions were: pH~9 and pH 7.4. According to Figure 4.12. (A) the low selectivity of A4C7 for binding GFP seems to be confirmed[102]. Moreover the binding percentage was significantly low, once the maximum GFP binding was 20%. Curiously both functionalized and non-functionalized monoliths had approximately the same values.It seemed that the majority of GFP, together with great part of protein, was expelled from the column in the flow-through and washes, for both control and functionalized monolith (data not shown).

By changing the binding conditions to a higher pH it seems that a higher amount of GFP bound to the support (Figure 4.12 (B)); however the amount of total bound protein also increased and control samples continued to bind almost the same as the functionalized ones. In pairs columns ML and NL, MC and NC were expected to bind similarly. ML and NL seem to bind same amount of GFP and total protein at each pH; however MC seems to differ from NC, binding more GFP at pH7.4. The magnetic monoliths surface lacework (Figure 4.8.) can probably increase GFP binding capacity of support, a probable meaningless feature when it comes to shrinked monolith at pH9, once the same behaviour is not observed.

Once chitosan pI is 6.3[168], it presents little or even zero charge above 6[224]; and GFP pI is ~5[206] so either at pH7.4 and pH~9 it presents a negative charge. The ligand is neutral at pH7.4[102] and at pH9. Once it is known that aromatic rings can act as H-bond acceptors (can also establish hydrophobic interactions[206]), carbonyl and -NH moieties from ligand can operate as H-bond acceptor and donor respectively, and due to Figure 4.11., it seems like the predominant interactions between ligand-GFP and C/P(50:50)80-GFP are H-bonding.

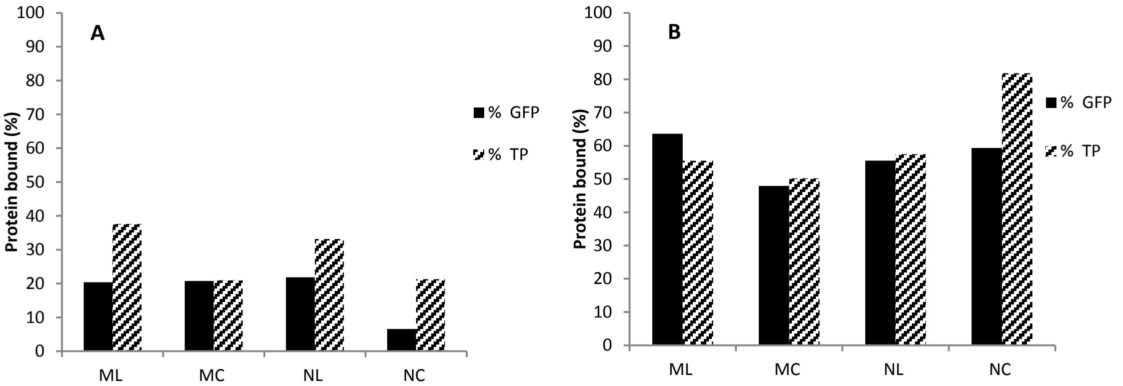

Figure 4.12. – Selectivity of ligand A4C7 towards GFP at different pH values: pH7.4 (A) and pH9 (B). Results refer to a batch system where the protein is incubated with the support for 15 minutes. TP denotes for total protein.

Although it was previously verified that, at the tested conditions, A4C7 affinity ligand was not very selective for binding GFP, it shown considerable potential to selectively recover the small protein[102]. In this work it seems that only the first statement was verified. Indeed regarding the elution stage of chromatography, no selectivity towards GFP recovery was verified. All bound protein is retained in the matrix, no GFP nor any total protein was eluted for both buffers tested. Even regeneration step was not successful in expelling proteins from the polymeric network. Against expectations the 50%(v/v) ethylene glycol did not result in significant additional GFP recovery. As a polarity reducing agent, and consequently a hydrophobic interactions disruptor, ethylene glycol binds to hydrophobic sites of desired protein reducing hydrophobic interactions between ligand-target pair[225]. Then if GFP binding happens, E2 condition should have eluted more GFP than E1 one.

The high GFP concentration values verified in washing steps (data not shown) corroborate Figure 4.12. charts, in which less binding corresponds to more GFP concentrated washed samples.

Preliminary tests were performed in order to ascertain if the presence of an external magnetic flux density have any effect on solution flow through column (Table 4.3.). Results showed a little increase, faced as promising, once no damage is intended to be induced in the support during field application. Internal structure damage not only alters support morphological and mechanical properties, but also can entrap the molecules avoiding its outlet from column. As error bars intersect themselves more samples need to be tested in order to confirm these preliminary results.

As Table 4.3. results were gathered through already tested (screening) columns the lower values obtained (compared to Table 4.2.) seems to corroborate the entrapment of protein inside column. However the large error bars, probably due to natural polymers-based materials propensity to have batch-to-batch variations, shows that more measurements are necessary to corroborate the apparent tendency.

Table 4.3. – Flow analysis through ML monolith after different times of exposure. Monolith is kept inside magnet during different periods of time. All data was obtained from duplicated measurements (in case of water flux each one of the two samples was measured three times**).**

Time of Magnetic Field Exposure (min)	*Water Flux x10 ($Lm^{-2}h^{-1}$)*
without exposure	41±7
0	45±8
10	51±9
20	53±7

It is noteworthy to refer that, during screening assays, the swollen monoliths filled the chromatographic column tightly with no by-pass of liquid noticed when magnet was or not applied.

Due to minor binding verified during 15 minutes batch system, and in order to ascertain if those low values had their probable origin in time of binding established or in the ligand itself, screening assays were performed in batch system for 60 minutes and in continuum. The studies had proceeded with magnetic monoliths in order to try to guarantee protein elution. Elution condition E1 was elected to proceed due to ethylene glycol proneness to introduce bias on total protein recovery values.

As expected the batch system enhances both specific and non-specific protein binding (Figure 4.13.). However the results were not encouraging once the control monolith continues binding the same as the functionalized one, which is also confirmed by SDS-PAGE analysis (Figure 4.14.).

A4C7 Ugi-based ligand synthesis was performed for the first time in a monolith, a solid phase distinct from the widely studied agarose beads. To this joins all intrinsic solid-phase organic synthesis drawbacks, including the trouble in translating the solution-phase environment of workaday organic synthesis to the heterogeneous solid-phase dimension, and the chitosan-based monoliths few studies comparing to agarose beads.

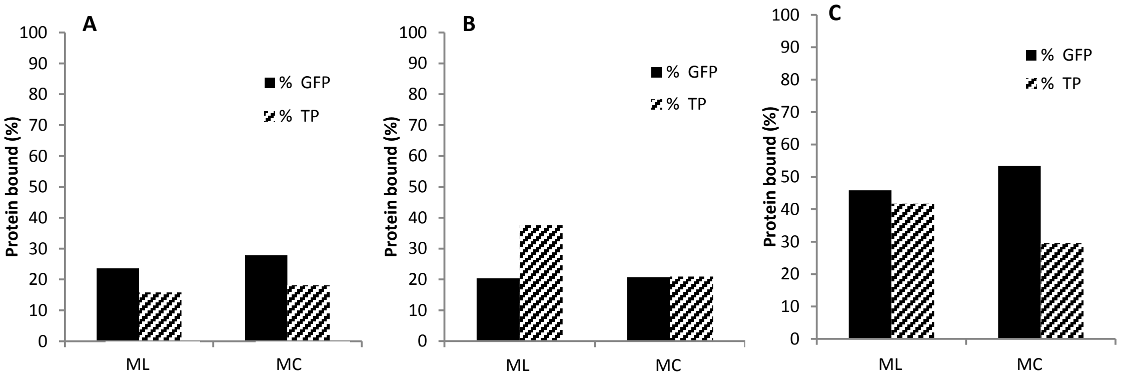

Figure 4.13. – Selectivity of A4C7 towards GFP at different times of incubation: 0 minutes or continuous system (A), 15 minutes (B) and 60 minutes (C) batch system. Binding condition: pH7.4.

Solid phase organic synthesis (SPOS) is generally associated with: heterogeneous reaction conditions (nonlinear kinetics); irregular distribution and/or accessibility of chemical reaction; and solvation issues[226]. Due to difficult analytical characterization of intermediate by-products and impossible purification from those by-products that covalently bind C/P(50:50)80, we are not certain about what has been synthesized at C/P(50:50)80 surface[227]. Moreover limitations can be associated to the polymeric matrix: modest loading capacity, restrict mechanical stability or non-suitable reagents infiltration due to hydrophilicity of support.

Monoliths are extremely advantageous when it comes to macromolecules like viruses and cells, and it was shown to be applicable on hIgG purification as well[27]. However hIgG have 150-170 kDa and GFP only 27-29kD and the capacity diminishes with decreasing molecular weight. Fouling of monolith by non-specific binding, pore obstruction by residual material, or steric hindrance by inadequate ligand synthesis are also possibilities.

High selectivity is mainly required when working with crude feedstocks; otherwise the impurities block the available surface for adsorption of the product. So having in mind solid-phase synthesis drawbacks, probably the surface-functionalized compound does not present the desired selectivity.

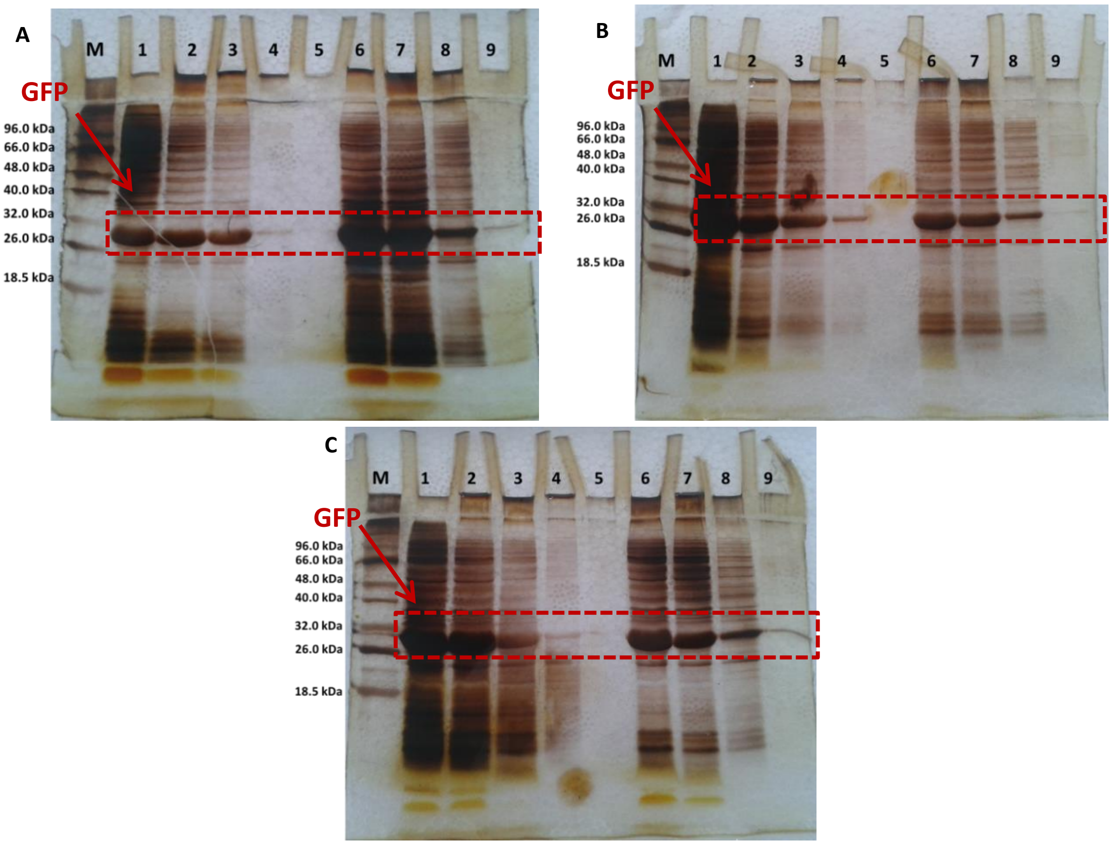
A
M 1 2 3 4 5 6 7 8 9
GFP
96.0 kDa
66.0 kDa
48.0 kDa
40.0 kDa
32.0 kDa
26.0 kDa
18.5 kDa
B
M 1 2 3 4 5 6 7 8 9
GFP
96.0 kDa
66.0 kDa
48.0 kDa
40.0 kDa
32.0 kDa
26.0 kDa
18.5 kDa
C
M 1 2 3 4 5 6 7 8 9
GFP
96.0 kDa
66.0 kDa
48.0 kDa
40.0 kDa
32.0 kDa
26.0 kDa
18.5 kDa

Figure 4.14. – SDS-PAGE analysis of GFP screening on magnetic functionalized (ML) monoliths: Continuum assay (A); 15 minutes batch assay (B); 60 minutes batch assay (C). M corresponds to protein marker and lanes 1, 2, 3, 4, 5, 6, 7, 8, 9 denotes for: loading, flow-through, 1st wash, 2nd wash and 1st elution for ML and loading, flow-through, 1st wash, 2nd wash and 1st elution for MC, respectively. GFP bands position (~29kDa) is highlighted. The gel was silver stained.

The elution performed under external 1.5T magnetic-field was not successful: the support retains the proteins. The time of exposure to external magnetic-field, in which the monolith was only placed into permanent magnet when elution began, and not before elution, precluded any effect. This seems to happen this way once, yet with no magnet, the regeneration step presented little outlet of GFP suggesting that the chromatographic column should be placed into the magnet sooner, and maybe left there for regeneration step (data not shown).

Moreover the method used for MNPs synthesis, co-precipitation, is sometimes characterized by aggregation, poor crystallinity with consequent low saturation magnetization values, and early ion oxidation before precipitation, what disturbs the physical and chemical properties of MNPs[228]. This can contribute to a lower response of the particles embedded on monoliths.

It was verified that after screening assay the monolith presented a decreased rigidity, probably caused by previous shrinkage. However despite the slower recovery verified, the monolith restores its initial height ensuring thus its physical capacity to be subjected to another screening assay if necessary (Figure 4.15.).

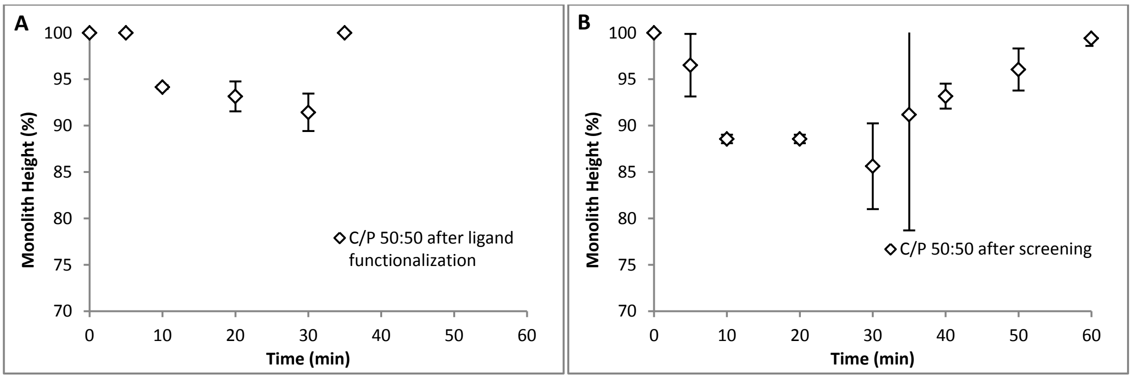

Figure 4.15. – Magnetic-field response of ML monolith before and after screening assay.

4.4. Concluding Remarks

Direct amination of monolith surface inside plasma chamber proved to be a green, safe, fast and reliable methodology. However optimization of the system is imperative in order of it to display its full potential.

Monoliths C/P(50:50)80 were surface functionalised to allow in situ synthesis of ligand A4C7, which has been previously shown to allow GFP purification in agarose chromatographic systems. It was observed that ligand coupling renders the support less elastic while increasing the gravitational flow. Monoliths with the incorporation of magnetic particles respond to external magnetic field and shows potential to elute faster and help column regeneration.

These preliminary studies concerning the development of green monoliths with affinity towards GFP denounce the necessity to optimize Ugi-based ligand synthesis in solid phase monolith platform.

In future studies it should be performed quantitative and qualitative assays to evaluate if there are intermediates formed during SPOS until final product generation. An XPS analysis can be a helpful tool, as the most broadly used surface analysis technique, involving fine simplicity in usage and data interpretation. Optimization regarding total characterization of binding thermodynamics, elution and regeneration conditions is also imperative. Competitive elution can be a hypothesis, as well as temperature, chelating substances or chaotropic agents.

As to date, no selective synthetic affinity ligand for GFP and GFP-fused proteins purification is available, and monoliths present themselves as suitable tools for minor proteins purification, it is crucial to understand what could have failed in the case study.

It is noteworthy that only an affinity monolithic system (CIM IDA-Cu^{2+}) had been employed on purification of GFP proteins[229]. With a capacity of ≈30 mg/mL the system lead to a purity of ≈90%. The support itself lacks some advantages that can be overcome by natural polymer-based monoliths.

5 GENERAL CONCLUSIONS AND RECOMMENDATIONS FOR FUTURE WORK

Environmentally friendly cryotropic gelation combined with freeze-drying proved to be a reliable method for processing naturally sourced polymeric macroporous structures with biocompatibility, low footprint and high flow-rates sparing pressure usage or only requiring negligible pressures.

A review on the literature concerning chemistry of the compounds (polymers, monomers, initiator and catalyst) employed to perform the reactions lead to the conclusion that it is very likely that the structures produced comprise a mix of interactions. That is, the pre-formed polymer chains interact with each other physically by H-bonding, and the monomers AAm, MBAAm and/or GMA polymerize probably forming little/medium imprisoning polymerized chains entangling the physically interacting pre-formed chains, and holding together the 3D matrix. The temperature conditions applied to the system seems to disallow the covalent linkage between those monomers and –OH and/or $-NH_2$ groups of the pre-formed polymer chains. However this theory must be proved by further looking on the arrangement of molecules composing the monolithic matrices, to prove the inexistence of covalent linkages between formed and pre-formed chains. A FTIR analysis should be helpful. Anyway this probable behaviour between chains seems to be insufficient for the structural stability of Dextran-AAm-GMA, and PVA-GMA monoliths. Even though the "reticulation" involved in this work seems not to be a conventional one, it would be interesting to evaluate the reticulation degree[230]. The execution of degradability tests for the chosen supports with agarase and lysozyme respectively would be also interesting.

Through monoliths characterization it was possible to conclude that their properties depend on a whole set of variables: the nature of composites, proportion and concentration on casting solution; with implications on porosity, pore distribution, size and tortuosity, interconnectivity, fenestration size and distribution, pore uniformity and consistency throughout all support.

The produced monolithic structures were highly permeable, chemically and mechanically stable with exception of Dextran-AAm-GMA, PVA-GMA and P100%. These structures crumbled easily in solution when mechanically disturbed with a tweezers, regardless of pH environment. The increase on P100% crosslinker (maleic acid) or its substitution with boronic acid, and the addition of a crosslinker in case of the other specimens could be attempted, however as the objective of the work is a biodegradable support, maybe it is wiser in a future approach to combine dextran polymer with other polymers like chitosan, gelatine or gum Arabic (preferably with lower molecular weights). Another possibility could be the execution of a series of freeze thaw cycles (to obtain strong physical bonds)[144]. An increase on mechanical properties can also be attempted by playing with initiator pair TEMED/APS concentration (concentration increase corresponds to the formation of a more rigid structure)[198]. However, heterogeneous structures can be obtained[231].

Glass transition temperature measurements of candidate monoliths should be interesting once mechanical properties can be adjusted with temperature.

MNPs embedding and entrapment in the monolithic network is technically practicable and straightforward, and seem to induce larger pores formation, increased water flux and more pronounced elasticity in the supports. In addition the presence of MNPs buried within the polymeric matrix allows support deformation and recover cycles helping purification assays. Furthermore the exposed MNPs at the surface help to balance the surface area. As different combinations of materials were used for the MNPs embedding approach, and the quantities employed were based in previous works performed in our lab concerning chitosan/PVA monoliths frozen at -80°C, additional studies should be made regarding the limitations on the amount of nanoparticles that can be added to prepared materials, due to the polarity incompatibility between embedded nanoparticles and polymerization mixture[48]. TEM analysis would also be interesting to confirm if MNPs are either buried or exposed on the monolithic surface in a uniform fashion or not[77].

Regarding GFP and Ad5 sizes, and obtained results, maybe a decrease on freezing temperature is a wise step on future developments. Hypercrosslinking could also be a smart strategy in case of GFP purification. It is a newly developed approach proven to enhance the efficacy of polymeric monoliths for small-molecules separation, that comprises a post-preparation modification allowing the maintenance of original pores and porosity with the preparation of an additional extensive network of smaller pores, and consequent substantial boost on surface area[232,51]. However, to guarantee the preparation of a biodegradable material with minimal footprint, biodegradability tests should be performed. Thus an even more attractive approach could be the preparation of a double-continuous macroporous network via sequential freezing–thawing, that guarantees good mechanical properties[233].

Stability tests over CG frozen at -80ºC, and C/P(50:50)80 with and without A4C7 should be executed. Chops of each specimen should be submerged for 12h into solutions normally used during cleaning-in-place procedures.

It is important in future developments to evaluate quantitatively the conservation of virus infectivity.

Optimizations regarding the synthesis of the synthetic ligand on monolith platform are imperative in order to create an ideal stationary phase for GFP purification, competitive towards the well-established agarose beads. If this stage is achieved with success it would be interesting to perform the scale-up screening between the ligand and GFP in an automated system.

In order to allow future processing of larger volumes of analytes in this type of attractive devices, it would be interesting to perform scale-up studies on natural polymers-based monoliths. However according to research realized and results obtained only lab scale disposable supports should be attainable (industrial scale seems unlikely due to mechanical properties of natural polymers-based supports).

Supercritical fluid (CO_2) technology should be an alternative and promising platform for natural monolith preparation, due to homogeneous pore tuning (narrow pore size distribution) with expulsion of unreacted species, and attractive energetic costs[79].

6 REFERENCES

1. P. Gagnon, in *Encyclopedia of Industrial Biotechnology*, ed. M. Flickinger, JohnWiley & Sons, 2009, vol. m, pp. 1–20.

2. A. Podgornik and N. Krajnc, *J. Sep. Sci.*, 2012, **35**, 3059–3072.

3. S. Hajizadeh, Lund University, 2012.

4. A. Jungbauer, *J. Chromatogr. A*, 2005, **1065**, 3–12.

5. P. Gagnon, *Bioprocess Int.*, 2008, **6 (Suppl.**, 24–30.

6. T. Barroso, A. Hussain, A. Roque, and A. Aguiar-Ricardo, *Biotechnol. J.*, 2013, **8**, 671–681.

7. F. Plieva, I. Savina, S. Deraz, J. Andersson, I. Galaev, and B. Mattiasson, *J. Chromatogr. B*, 2004, **807**, 129–137.

8. S. Sun, Y. Tang, Q. Fu, X. Liu, W. Du, L. Guo, and Y. Zhao, *J. Sep. Sci.*, 2012, **35**, 893–900.

9. P. Arvidsson, F. Plieva, V. Lozinsky, I. Galaev, and B. Mattiasson, *J. Chromatogr. A*, 2003, **986**, 275–290.

10. F. Svec, *LC-GC Eur.*, 2010, **23**, 272–277.

11. R. Arrua, M. Strumia, and C. Igarzabal, *Materials (Basel).*, 2009, **2**, 2429–2466.

12. F. Svec, *J. Chromatogr. A*, 2010, **1217**, 902–924.

13. A. Podgornik, S. Yamamoto, M. Peterka, and N. Krajnc, *J. Chromatogr. B*, 2013, **927**, 80–89.

14. P. Gagnon, R. Richieri, S. Zaidi, and F. Aolin, *Validated Biosyst.*, 2007.

15. A. Jungbauer and R. Hahn, *J. Chromatogr. A*, 2008, **1184**, 62–79.

16. W. Johnson, Y. Makame, and L. Mkayula, *Tanzania J. Nat. Appl. Sci.*, 2011, **2**, 238–250.

17. P. Gagnon, 2009, 1–43.

18. A. Podgornik, M. Barut, M. Peterka, and A. Štrancar, in *Biopharmaceutical Production Technology*, ed. G. Subramanian, WILEY-VCH Verlag GmbH & Co. KGaA, Weinheim, Germany, 2012, pp. 333–375.

19. A. Nordborg and E. Hilder, *Anal. Bioanal. Chem.*, 2009, **394**, 71–84.

20. V. Orr, L. Zhong, M. Moo-Young, and C. Chou, *Biotechnol. Adv.*, 2013, **31**, 450–465.

21. K. Saunders, A. Ghanem, W. Boon Hon, E. Hilder, and P. Haddad, *Anal. Chim. Acta*, 2009, **652**, 22–31.

22. F. Svec and A. Kurganov, *J. Chromatogr. A*, 2008, **1184**, 281–295.

23. F. Svec, *J. Chromatogr. B*, 2006, **841**, 52–64.

24. M. Talebi, University of Tasmania, 2013.

25. Y. Wei, X. Huang, R. Liu, Y. Shen, and X. Geng, *J. Sep. Sci.*, 2006, **29**, 5–13.

26. L. Liu, S. Yu, S. Yang, P. Zhou, J. Hu, and Y. Zhang, *J. Sep. Sci.*, 2009, **32**, 2752–2758.

27. T. Barroso, A. Roque, and A. Aguiar-Ricardo, *RSC Adv.*, 2012, **2**, 11285–11294.

28. A. Trauner, M. Bennett, and H. Williams, *PLoS One*, 2011, **6**, 1–6.

29. D. Forcic, M. Brgles, J. Ivancic-Jelecki, M. Santak, B. Halassy, M. Barut, R. Jug, M. Markušić, and A. Strancar, *J. Chromatogr. B*, 2011, **879**, 981–986.

30. P. Arvidsson, F. Plieva, I. Savina, V. Lozinsky, S. Fexby, L. Bülow, I. Galaev, and Mattiasson, *J. Chromatogr. A*, 2002, **977**, 27–38.

31. C. Aydoğan, F. Yılmaz, and A. Denizli, *J. Sep. Sci.*, 2013, **36**, 1685–1692.

32. S. Williams, M. Eccleston, and N. Slater, *Biotechnol. Bioeng.*, 2005, **89**, 783–787.

33. H. Yavuz and A. Denizli, *Int. J. Biol. Macromol.*, 2011, **48**, 577–582.

34. R. Bakry, G. Bonn, D. Mair, and F. Svec, *Anal. Chem.*, 2007, **79**, 486–493.

35. E. Vlakh and T. Tennikova, *J. Sep. Sci.*, 2013, **36**, 1149–1167.

36. F. Svec, *Electrophoresis*, 2006, **27**, 947–961.

37. J. Krenkova and F. Svec, *J. Sep. Sci.*, 2009, **32**, 706–718.

38. E. Vlakh, A. Novikov, G. Vlasov, and T. Tennikova, *J. Pept. Sci.*, 2004, **10**, 719–730.

39. J. Kingsbury, S. Garber, J. Giftos, B. Gray, M. Okamoto, R. Farrer, J. Fourkas, and A. Hoveyda, *Angew. Chemie*, 2001, **113**, 4381–4386.

40. J. Tripp, T. Needham, E. Ripp, B. Konzman, and P. Homnick, *React. Funct. Polym.*, 2010, **70**, 414–418.

41. T. Rohr, C. Yu, M. Davey, F. Svec, and J. Fréchet, *Electrophoresis*, 2001, **22**, 3959–3967.

42. S. Ilic-Stojanovic, L. Nikolic, V. Nikolic, S. Petrovic, M. Stankovic, and I. Mladenovic-Ranisavljevic, *Facta Univ. Ser. Physics, Chem. Technol.*, 2011, **9**, 37–56.

43. T. Garg, O. Singh, S. Arora, and R. Murthy, *Crit. Rev. Ther. Drug Carrier Syst.*, 2012, **29**, 1–63.

44. I. Galaev, M. Dainiak, F. Plieva, R. Hatti-Kaul, and B. Mattiasson, *J. Chromatogr. A*, 2005, **1065**, 169–175.

45. Z. Altun, C. Skoglund, and M. Abdel-Rehim, *J. Chromatogr. A*, 2010, **1217**, 2581–2588.

46. D. Allen and Z. El Rassi, *Electrophoresis*, 2003, **24**, 3962–3976.

47. Z. Walsh, B. Paull, and M. Macka, *Anal. Chim. Acta*, 2012, **750**, 28–47.

48. R. Arrua, M. Talebi, T. Causon, and E. Hilder, *Anal. Chim. Acta*, 2012, **738**, 1–12.

49. T. Henderson, K. Ladewig, D. Haylock, K. McLean, and A. O'Connor, *J. Mater. Chem. B*, 2013, **1**, 2682–2695.

50. A. Namera, A. Nakamoto, T. Saito, and S. Miyazaki, *J. Sep. Sci.*, 2011, **34**, 901–924.

51. A. Nordborg, E. Hilder, and P. Haddad, *Annu. Rev. Anal. Chem.*, 2011, **4**, 197–226.

52. R. Bandari, W. Knolle, A. Prager-Duschke, H.-J. Gläsel, and M. Buchmeiser, *Macromol. Chem. Phys.*, 2007, **208**, 1428–1436.

53. C.-C. Liu, Q.-L. Deng, G.-Z. Fang, H.-L. Liu, J.-H. Wu, M.-F. Pan, and S. Wang, *Anal. Chim. Acta*, 2013, **804**, 313–320.

54. K. Liu, P. Aggarwal, J. Lawson, H. Tolley, and M. Lee, *J. Sep. Sci.*, 2013, **36**, 2767–2781.

55. C. Bisjak, S. Lubbad, L. Trojer, and G. Bonn, *J. Chromatogr. A*, 2007, **1147**, 46–52.

56. C. Yao, L. Qi, G. Yang, and F. Wang, *J. Sep. Sci.*, 2010, **33**, 475–483.

57. S. Yu, F. Ng, K. Ma, F. Ng, J. Zhao, and S. Tong, *J. Appl. Polym. Sci.*, 2011, **120**, 3190–3195.

58. Z. Walsh, P. Levkin, V. Jain, B. Paull, F. Svec, and M. Macka, *J. Sep. Sci.*, 2010, **33**, 61–66.

59. Z. Altun, L. G. Blomberg, and M. Abdel-Rehim, *J. Liq. Chromatogr. Relat. Technol.*, 2006, **29**, 1477–1489.

60. M. Grasselli, E. Smolko, P. Hargittai, and Á. Sáfrány, *Nucl. Instruments Methods Phys. Res. Sect. B*, 2001, **185**, 254–261.

61. Á. Sáfrány, B. Beiler, K. László, and F. Svec, *Polymer (Guildf).*, 2005, **46**, 2862–2871.

62. Y.-P. Zhang, X.-W. Ye, M.-K. Tian, L.-B. Qu, S.-H. Choi, A. Gopalan, and K.-P. Lee, *J. Chromatogr. A*, 2008, **1188**, 43–49.

63. P. Krajnc, N. Leber, D. Stefanec, S. Kontrec, and A. Podgornik, *J. Chromatogr. A*, 2005, **1065**, 69–73.

64. R. Arrua, T. Causon, and E. Hilder, *Analyst*, 2012, **137**, 5179–5189.

65. F. Plieva, I. Galaev, and B. Mattiasson, *J. Sep. Sci.*, 2007, **30**, 1657–1671.

66. C. Viklund, A. Nordstro, K. Irgum, F. Svec, and J. Fre, *Macromolecules*, 2001, **34**, 4361–4369.

67. J. Hasegawa, K. Kanamori, K. Nakanishi, T. Hanada, and S. Yamago, *Macromol. Rapid Commun.*, 2009, **30**, 986–990.

68. G. Yang, L. Bai, C. Yan, Y. Gu, and J. Ma, *Talanta*, 2011, **85**, 2666–2672.

69. X. Li, M. Zhou, M. Turson, S. Lin, P. Jiang, and X. Dong, *Analyst*, 2013, **138**, 3066–3074.

70. E. Byström, C. Viklund, and K. Irgum, *J. Sep. Sci.*, 2010, **33**, 191–199.

71. R. Bandari, W. Knolle, and M. Buchmeiser, *J. Chromatogr. A*, 2008, **1191**, 268–273.

72. C. Peskoller, R. Niessner, and M. Seidel, *J. Chromatogr. A*, 2009, **1216**, 3794–3801.

73. A. M. Nguyen, A. Nordborg, A. Shchukarev, and K. Irgum, *J. Sep. Sci.*, 2009, **32**, 2619–2628.

74. Y. Xin, T. Fujimoto, and H. Uyama, *Polymer (Guildf).*, 2012, **53**, 2847–2853.

75. F. M. Plieva, H. Kirsebom, and B. Mattiasson, *J. Sep. Sci.*, 2011, **34**, 2164–2172.

76. J. Krenkova, F. Foret, and F. Svec, *J. Sep. Sci.*, 2012, **35**, 1266–1283.

77. D. Connolly, S. Currivan, and B. Paull, *Proteomics*, 2012, **12**, 2904–2917.

78. K. Yao, J. Yun, S. Shen, L. Wang, X. He, and X. Yu, *J. Chromatogr. A*, 2006, **1109**, 103–110.

79. T. Barroso, Faculdade de Ciência e Tecnologia - Universidade Nova de Lisboa, 2014.

80. M. Wu, R. Wu, Z. Zhang, and H. Zou, *Electrophoresis*, 2011, **32**, 105–15.

81. Y. Ueki, T. Umemura, J. Li, T. Odake, and K.-I. Tsunoda, *Anal. Chem.*, 2004, **76**, 7007–7012.

82. T. Zhu and K. Row, *J. Sep. Sci.*, 2012, **35**, 1294–1302.

83. E. Vlakh and T. Tennikova, *J. Sep. Sci.*, 2013, **36**, 110–127.

84. T. Desmet, R. Morent, N. De Geyter, C. Leys, E. Schacht, and P. Dubruel, *Biomacromolecules*, 2009, **10**, 2351–2378.

85. K. Tetala and T. van Beek, *J. Sep. Sci.*, 2010, **33**, 422–438.

86. I. Batalha, A. Hussain, and A. Roque, *J. Mol. Recognit.*, 2010, **23**, 462–471.

87. S. Santana, Universidade Nova de Lisboa - Faculdade de Ciência e Tecnologia, 2011.

88. R. Sabaté, R. Barnadas-Rodríguez, J. Callejas-Fernández, R. Hidalgo-Alvarez, and J. Estelrich, *Int. J. Pharm.*, 2008, **347**, 156–162.

89. L. Silva, Universidade Nova de Lisboa - Faculdade de Ciências e Tecnologia, 2008.

90. T. Barroso, M. Temtem, A. Hussain, A. Aguiar-Ricardo, and A. Roque, *J. Memb. Sci.*, 2010, **348**, 224–230.

91. A. Tripathi and A. Kumar, *Macromol. Biosci.*, 2011, **11**, 22–35.

92. Q. Loh, C. Choong, D. Oxon, M. Hons, and C. Mimmm, *Tissue Engeneering Part B*, 2013, **19**, 485–502.

93. F. O'Brien, B. Harley, I. Yannas, and L. Gibson, *Biomaterials*, 2005, **26**, 433–441.

94. O. Okay, *Prog. Polym. Sci.*, 2000, **25**, 711–779.

95. G. Khang, *Handbook of Intelligent Scaffolds for Tissue Engineering and Regenerative Medicine*, Chonbuk,Korea, First., 2012.

96. I. Ruiz, É. Hermida, and Baldessari, *J. Phys. Conf. Ser.*, 2011, **332**, 1–11.

97. V. Rajal, D. Thompson, B. Kildare, S. Tiwari, B. Mcswain, and S. Wuertz, *Management of Pathogens Associated with Storm Water Discharge: Methodology for Quantitative Molecular Determination of Viruses, Bacteria And Protozoa*, 2005.

98. WHO, *Int. Pharmacopoeia*, 2013.

99. Novagen, *Bacterial Protein Expression - Catalog 2009/2010*, 2008.

100. Nanodrop Technologies, *ND-1000 Spectrophotometer V3.5 User's Manual*, 2007.

101. S. Magdeldin, *Gel Electrophoresis - Principles and Basics*, InTech, Rijeka,Croatia, 2012.

102. A. Pina, Faculdade de Ciência e Tecnologia - Universidade Nova de Lisboa, 2013.

103. TCI America, *MSDS - 1,6 Diaminohexane*, 2005.

104. F. Johannsen, G. Levinskas, R. Ben-Dyke, and G. Hogan, *Fundam. Appl. Toxicol.*, 1987, **9**, 504–511.

105. J. Highsmith, *Biologic Therapeutic Drugs: Technologies and Global Markets*, 2013.

106. B. Bain and J. Shortmoor, *Pharm. Technol.*, 2010, **34**, 38–45.

107. PhRMA, *Medicines in development: Biologics*, 2013.

108. P. Pattnaik, *Merck Millipore*, 2013, 1–26.

109. N. Moran, *Nat. Biotechnol.*, 2012, **30**, 807–809.

110. Global Industry Analysts, *PRWeb*, 2012, 1–3.

111. S. Ginn, I. Alexander, and M. Edelstein, *J. Gene Med.*, 2013, **15**, 65–77.

112. N. Tatsis and H. Ertl, *Mol. Ther.*, 2004, **10**, 616–629.

113. C. Volpers and S. Kochanek, *J. Gene Med.*, 2004, **6**, S164–S171.

114. D. Prazeres and J. Santos, in *Pharmaceutical Sciences Encyclopedia*, ed. S. C. Gad, John Wiley & Sons, Lisbon, Portugal, 2010, pp. 1–36.

115. E. Burova and E. Ioffe, *Gene Ther.*, 2005, **12**, S5–S17.

116. W. Russell, *J. Gen. Virol.*, 2009, **90**, 1–20.

117. J. Vellinga, S. Van der Heijdt, and R. Hoeben, *J. Gen. Virol.*, 2005, **86**, 1581–1588.

118. C. Martín, *Viruses*, 2012, **4**, 847–877.

119. C. Peixoto, T. Ferreira, M. Sousa, M. Carrondo, and P. Alves, *Biotechnol. Prog.*, 2008, **24**, 1290–1296.

120. P. Fernandes, C. Peixoto, V. Santiago, E. Kremer, S. Coroadinha, and P. Alves, *Gene Ther.*, 2013, **20**, 353–360.

121. R. Whitfield, S. Battom, M. Barut, D. Gilham, and P. Ball, *J. Chromatogr. A*, 2009, **1216**, 2725–2729.

122. a M. Duffy, a M. O’Doherty, T. O’Brien, and P. M. Strappe, *Gene Ther.*, 2005, **12 Suppl 1**, S62–72.

123. C. Peixoto, T. Ferreira, M. J. Carrondo, P. Cruz, and P. Alves, *J. Virol. Methods*, 2006, **132**, 121–126.

124. M. a Croyle, D. J. Anderson, B. J. Roessler, and G. L. Amidon, *Pharm. Dev. Technol.*, 1998, **3**, 365–72.

125. F. Schagen, H. Rademaker, M. Rabelink, H. van Ormondt, F. Fallaux, A. van der Eb, and R. Hoeben, *Gene Ther.*, 2000, **7**, 1570–1574.

126. G. Braas, S. Walker, and A. Lyddiatt, *J. Chromatogr. B*, 2000, **743**, 409–419.

127. P. Gagnon, *Genet. Eng. news*, 2006, **26**, 1–4.

128. A. Green, J. Huang, M. Scott, T. Kierstead, I. Beaupré, G.-P. Gao, and J. Wilson, *Hum. Gene Ther.*, 2002, **13**, 1921–1934.

129. D.-S. Lee, B.-M. Kim, and D.-W. Seol, *Biochem. Biophys. Res. Commun.*, 2009, **378**, 640–644.

130. BIAseparations, *Single-step Purification Method for Adenovirus Vectors Using CIMQA Disk Monolithic Column*, 2010.

131. BIAseparations, *Virus Downstream Processing using CIM Monoliths*, 2010.

132. M. Segura, M. Puig, M. Monfar, and M. Chillón, *Hum. Gene Ther. Methods*, 2012, **23**, 182–197.

133. Sartorius, 2013.

134. BIAseparations, 2013.

135. Pall Corporation, 2013.

136. J.-W. Kim, K. Taki, S. Nagamine, and M. Ohshima, *Chem. Eng. Sci.*, 2008, **63**, 3858–3863.

137. V. Correia, M. Coelho, T. Barroso, V. Raje, V. Bonifácio, T. Casimiro, M. Pinho, and A. Aguiar-Ricardo, *Biofouling*, 2013, **29**, 273–282.

138. H. Kirsebom, G. Rata, D. Topgaard, B. Mattiasson, and I. Galaev, *Macromolecules*, 2009, **42**, 5208–5214.

139. C. Clarke, *The Science of Ice Cream*, Royal Society of Chemistry, 2nd edn., 2012.

140. P. Wilson, A. Heneghan, and A. Haymet, *Cryobiology*, 2003, **46**, 88–98.

141. F. O'Brien, *Biomaterials*, 2004, **25**, 1077–1086.

142. A. Kumar, R. Mishra, Y. Reinwald, and S. Bhat, *Mater. Today*, 2010, **13**, 42–44.

143. A. Jungbauer and R. Hahn, *J. Sep. Sci.*, 2004, **27**, 767–778.

144. V. Lozinsky, I. Galaev, F. Plieva, I. Savina, H. Jungvid, and B. Mattiasson, *Trends Biotechnol.*, 2003, **21**, 445–451.

145. S. Deville, *Materials (Basel).*, 2010, **3**, 1913–1927.

146. E. Heftmann, *Fundamentals and Applications of Chromatography and Related Differential Migration Methods Fundamentals and Techniques*, 1992, vol. 51.

147. P. Maharjan, B. Woonton, L. Bennett, G. Smithers, K. DeSilva, and M. Hearn, *Innov. Food Sci. Emerg. Technol.*, 2008, **9**, 232–242.

148. X. Liu, L. Ma, Z. Mao, and C. Gao, *Adv. Polym. Sci.*, 2011, **244**, 81–127.

149. E. Jain and A. Kumar, *J. Biomater. Sci. Polym. Ed.*, 2009, **20**, 877–902.

150. E. Jain, A. Karande, and A. Kumar, *Biotechnol. Prog.*, 2011, **27**, 170–180.

151. University of Southern Mississippi, 2005.

152. L. Sperling, in *Introduction to Physical Polymer Science*, ed. L. Sperling, John Wiley & Sons, 4th edn., 2006, pp. 29–67.

153. J. Berger, M. Reist, J. Mayer, O. Felt, N. Peppas, and R. Gurny, *Eur. J. Pharm. Biopharm.*, 2004, **57**, 19–34.

154. S. Xie, F. Svec, and J. Fréchet, *J. Polym. Sci. Polym. Chem.*, 1997, **35**, 1013–1021.

155. E. Crispim, J. Piai, A. Fajardo, E. Ramos, T. Nakamura, C. Nakamura, A. Rubira, and E. Muniz, *Express Polym. Lett.*, 2012, **6**, 383–395.

156. J. Kopecek and J. Yang, *Polym. Int.*, 2007, **56**, 1078–1098.

157. J. Zhang, in *Gums and Stabilisers for the Food Industry*, eds. P. Williams and G. Phillips, Royal Society of Chemistry, 2010, vol. 15, pp. 420–426.

158. S. Gulrez, S. Al-assaf, and G. Phillips, in *Progress in Molecular and Environmental Bioengineering*, ed. A. Carpi, InTech, 2003, pp. 117–150.

159. K. Kamath and K. Park, *Adv. Drug Deliv. Rev.*, 1993, **11**, 59–84.

160. M. Muscatello and S. Asher, *Adv. Funct. Mater.*, 2011, **1186**, 1–17.

161. E. Crispim, J. Piai, I. Schüquel, and A. Rubira, *e-Polymers*, 2006, 1–18.

162. J. Deng, Q. He, Z. Wu, and W. Yang, *J. Polym. Sci. A Polym. Chem.*, 2008, **46**, 2193–2201.

163. A. Reis, A. Fajardo, I. Schuquel, M. Guilherme, G. Vidotti, A. Rubira, and E. Muniz, *J. Org. Chem.*, 2009, **74**, 3750–3757.

164. P. Aramwit, T. Siritientong, S. Kanokpanont, and T. Srichana, *Int. J. Biol. Macromol.*, 2010, **47**, 668–675.

165. F. Plieva, A. Oknianska, E. Degerman, I. Y. Galaev, and B. Mattiasson, *J. Biomater. Sci. Polym. Ed.*, 2006, **17**, 1075–1092.

166. G. Crini, *Prog. Polym. Sci.*, 2005, **30**, 38–70.

167. K. Pal, A. Banthia, and D. Majumdar, *Des. Monomers Polym.*, 2009, **12**, 197–220.

168. A. Tourrette, in *Surface modification systems for creating stimuli responsiveness of textiles*, ed. D. Jocic, University of Twente, Enschede, 2010, pp. 77–92.

169. S. Gunasekaran, T. Wang, and C. Chai, *J. Appl. Polym. Sci.*, 2006, **102**, 4665–4671.

170. O. Okay, in *Hydrogel Sensors and Actuators*, eds. G. Gerlach and K.-F. Arndt, Springer Berlin Heidelberg, Berlin, Heidelberg, 2010, vol. 6, pp. 1–15.

171. K. Anseth, C. Bowman, and L. Brannon-Peppas, *Biomaterials*, 1996, **17**, 1647–1657.

172. E. Parparita, C. Cheaburu, and C. Vasile, *Cellul. Chem. Technol.*, 2012, **46**, 571–581.

173. N. Kathuria, A. Tripathi, K. Kar, and A. Kumar, *Acta Biomater.*, 2009, **5**, 406–418.

174. S. Jin, F. Bian, and M. Liu, *Polym. Int.*, 2009, **58**, 142–148.

175. J. Wu, Q. Zhao, J. Sun, and Q. Zhou, *Soft Matter*, 2012, **8**, 3620–3626.

176. F. Chiellini and A. Morelli, in *Biomaterials - Physics and Chemistry*, ed. R. Pignatello, InTech, Pisa,Italy, 3rd edn., 2011, pp. 75–99.

177. M. Pezeshki, H. Mirzadeh, and M. Zandi, *Iran. Polym. J.*, 2012, **21**, 191–200.

178. SIGMA-ALDRICH, *MSDS-Absolute Ethanol*, 2013.

179. SIGMA-ALDRICH, *MSDS-Isopropanol*, 2014.

180. I. Ro and I.-C. Kwon, *J. Biomater. Sci. Polym. Ed.*, 2002, **13**, 769–782.

181. Tel-Aviv University, *Porosity*, 249–278.

182. A. Mitsak, J. Kemppainen, M. Harris, and S. Hollister, *Tissue Engeneering A*, 2011, **17**, 1831–1838.

183. S. Li, J. De Wijn, J. Li, P. Layrolle, and K. De Groot, *Tissue Eng.*, 2003, **9**, 535–548.

184. J. Kemppainen and S. Hollister, *Biomaterials*, 2010, **31**, 279–287.

185. J. Huang, X. Wang, and X. Yu, *Desalination*, 2006, **192**, 125–131.

186. T. Karande, J. Ong, and C. Agrawal, *Ann. Biomed. Eng.*, 2004, **32**, 1728–1743.

187. S. Lee and A. Bahaman, in *Gel Electrophoresis - Principles and Basics*, ed. S. Magdeldin, InTech, 2012, pp. 41–56.

188. N. Stanley, D. Bell, P. Blanchard, Y. Brummer, A. Chesson, and D. Coffey, *Food Polysaccharides and Their Applications*, Taylor & Francis Group, Second., 2006.

189. V. Caligur, *SIGMA-ALDRICH BioFiles*, 2008, 17, 1–7.

190. V. Gun'ko, I. Savina, and S. Mikhalovsky, *Adv. Colloid Interface Sci.*, 2013, **187-188**, 1–46.

191. Y. Wang, M. Gawryla, and D. Schiraldi, *J. Appl. Polym. Sci.*, 2013, **129**, 1637–1641.

192. A. Alberich-Bayarri, M. Sánchez, M. Pérez, and D. Moratal, in *Finite Element Analysis*, ed. D. Moratal, Sciyo, Rijeka, Croacia, 2010, pp. 251–265.

193. Q. Hou, D. Grijpma, and J. Feijen, *J. Biomed. Mater. Res. B Appl. Biomater.*, 2003, **67B**, 732–740.

194. B. Harley, J. Leung, E. Silva, and L. Gibson, *Acta Biomater.*, 2007, **3**, 463–474.

195. A.-L. Gassner, M. Abonnenc, H.-X. Chen, J. Morandini, J. Josserand, J. Rossier, J.-M. Busnel, and H. Girault, *Lab Chip*, 2009, **9**, 2356–2363.

196. J. Hawley, *Modeling a cylindrical permanent magnet with a surface charge of magnetic monopoles*, 2012.

197. T.-Y. Liu, S.-H. Hu, T.-Y. Liu, D.-M. Liu, and S.-Y. Chen, *Langmuir*, 2006, **22**, 5974–5978.

198. BIO-RAD, *Electrophoresis - tech note 1156*, 2000.

199. G. Carta and A. Jungbauer, in *Protein Chromatography: Process Development and Scale-Up*, eds. G. Carta and A. Jungbauer, WILEY-VCH Verlag GmbH & Co. KGaA, 2010, pp. 1–55.

200. G. Scriba, in *Molecular Biology in Medicinal Chemistry*, eds. T. Dingermann, D. Steinhilber, and G. Folkers, WILEY-VCH Verlag GmbH & Co. KGaA, 2004, vol. 1383, pp. 211–241.

201. J. Arnau, C. Lauritzen, G. Petersen, and J. Pedersen, *Protein Expr. Purif.*, 2006, **48**, 1–13.

202. R. Zhuang, Y. Zhang, R. Zhang, C. Song, K. Yang, A. Yang, and B. Jin, *Protein Expr. Purif.*, 2008, **59**, 138–43.

203. R. Tsien, *Biochemistry*, 1998, **67**, 509–544.

204. M. Zimmer, *Chem. Rev.*, 2002, **102**, 759–781.

205. M. Ormo, A. Cubitt, K. Kallio, L. Gross, R. Tsien, and S. Remingtont, *Science (80-.).*, 1996, **273**, 1392–1395.

206. W. Ward, in *Green Fluorescent Protein: Properties, Applications, and Protocols*, eds. M. Chalfie and S. R. Kain, John Wiley & Sons, Hoboken, USA, Second., 2006, vol. 47, pp. 39–65.

207. M. Zimmer, *Chem. Soc. Rev.*, 2009, **38**, 2823–2832.

208. G. Peckham, R. Bugos, and W. Su, *Protein Expr. Purificationcation*, 2006, **49**, 183–189.

209. M. Mohamadipoor, M. Habibi Roudkenar, N. Masroori, A. Mohammadi Roushandeh, and S. Saki, *DARU*, 2009, **17**, 60–63.

210. U. Rothbauer, K. Zolghadr, S. Muyldermans, A. Schepers, M. Cardoso, and H. Leonhardt, *Mol. Cell. Proteomics*, 2008, **7**, 282–289.

211. C. Roque, C. Lowe, and M. Taipa, *Biotechnol. Prog.*, 2004, **20**, 639–654.

212. nzytech, *NZY5α Competent Cells - Brochure*, 2013.

213. Novagen, *pET System Manual 11 th Edition*, 2010.

214. K. Siow, L. Britcher, S. Kumar, and H. Griesser, *Plasma Process. Polym.*, 2006, **3**, 392–418.

215. N. Geyter and R. Morent, in *Biomedical Science, Engineering and Technology*, ed. D. Ghista, InTech, 2012, pp. 225–246.

216. H. Mathieu, X. Gao, and D. Balazs, *J. Surf. Anal.*, 2005, **12**, 193–199.

217. P. Chu, J. Chen, L. Wang, and N. Huang, *Mater. Sci. Eng. R*, 2002, **36**, 143–206.

218. March Plasma Systems, *Surface Preparation and Improved Adhesion*, 2001.

219. A. Dömling and I. Ugi, *Angew. Chemie*, 2000, **39**, 3168–3210.

220. S. Marcaccini and T. Torroba, *Nat. Protoc.*, 2007, **2**, 632–639.

221. J. Zhu, Q. Wang, and M. Wang, in *Handbook of Green Chemistry*, ed. P. Anastas, WILEY-VCH Verlag GmbH & Co. KGaA, 12th edn., 2012, vol. 7, pp. 121–157.

222. S. Deville, *J. Mater. Res.*, 2013, **28**, 2202–2219.

223. P. Chang, J. Yu, X. Ma, and D. Anderson, *Carbohydr. Polym.*, 2011, **83**, 640–644.

224. N. Bhattarai, J. Gunn, and M. Zhang, *Adv. Drug Deliv. Rev.*, 2010, **62**, 83–99.

225. C. Lowe and K. Mosbach, *Eur. J. Biochem.*, 1975, **52**, 99–105.

226. H. Han, M. Wolfe, S. Brenner, and K. Janda, *Proc. Natl. Acad. Sci. USA*, 1995, **92**, 6419–6423.

227. A. Porzelle and W.-D. Fessner, *Angew. Chemie*, 2005, **44**, 4724–4728.

228. Wahajuddin and S. Arora, *Int. J. Nanomedicine*, 2012, **7**, 3445–3471.

229. M. Peterka, M. Jarc, M. Banjac, V. Frankovic, K. Bencina, M. Merhar, V. Gaberc-Porekar, V. Menart, a Strancar, and a Podgornik, *J. Chromatogr. A*, 2006, **1109**, 80–5.

230. J. Ratanavaraporn and S. Damrongsakkul, *J. Met. Mater. Miner.*, 2006, **16**, 31–36.

231. Y. Hwang, C. Zhang, and S. Varghese, *J. Mater. Chem.*, 2010, **20**, 345–351.

232. J. Urban, F. Svec, and J. Fre, *Anal. Chem.*, 2010, **82**, 1621–1623.

233. F. Plieva, P. Ekström, I. Galaev, and B. Mattiasson, *Soft Matter*, 2008, **4**, 2418–2428.